`

UNIVERSITY OF CALIFORNIA,
IRVINE

Neural circuit organization and function of hippocampal CA1 and the subiculum

DISSERTATION

submitted in partial satisfaction of the requirements
for the degree of

DOCTOR OF PHILOSOPHY

in Biomedical Sciences

by

Yanjun Sun

Dissertation Committee:
Associate Professor Xiangmin Xu, Chair
Professor Diane K. O'Dowd
Associate Professor David C. Lyon

2017

`

DEDICATION

To

my parents, Huaizhong and Yuzhen,
my wife, Jiaqi,
all my family and friends

"You shall know the truth, and the truth shall set you free."

---- John 8:32

`

TABLE OF CONTENTS

`

LIST OF FIGURES

`

LIST OF TABLES

`

ACKNOWLEDGMENTS

First and foremost, I would like to express my sincerest gratitude to my advisor, Dr. Xiangmin Xu, who has supported me throughout my entire graduate study. This dissertation would not have been possible without his great mentorship and training. His knowledge, diligence, persistence, patience, generosity, and encouragement have been with me during the whole dissertation. He gave me guidance as well as the freedom to explore my own research interests. It has been an extraordinary experience working with him. More importantly, his life attitude and work ethics significantly influenced me and are deeply embedded in my mind. These merits from him shaped my own values and will continue to benefit my future career of being a successful scientist.

I would like to thank Drs. Diane O'Dowd, David Lyon, Todd Holmes, and John Weiss for serving on my dissertation or advancement committees. They provided extremely helpful guidance and suggestions in all aspects of my study. Particularly, I was very pleased to be a member of the HHMI-UCI Professor Program established by Dr. O'Dowd to learn creative pedagogy of teaching undergraduate students. As our graduate study advisor, Dr. Lyon manages the graduate program of the department and trained us with his scientific thinking and kindness. He made us understand how to survive and succeed in graduate school. Special thanks go to Dr. Holmes in helping us editing our manuscripts with his excellent writing skills. Additionally, I thank faculty members who have helped or worked with me during my graduate study. I learned and performed multiple animal behavioral assays in Dr. Marcelo Wood's lab and Dr. Olivier Civelli's lab, and EEG experiments with Dr. Qun-Yong Zhou. I received viruses for my experiments from Dr. Edward Callaway's lab at Salk Institute and Dr. Larry Zweifel at University of Washington, Seattle. Drs. Martin Smith, Diane O'Dowd, and Robert Hunt provide great help on my single-cell RT-PCR project. Dr. Sunil Gandhi's lab helped me with intrinsic optical imaging on my project of visual cortical plasticity. More recently, I learned and adopted the miniscope technique from Dr. Peyman Golshani's lab at UCLA and got help on the data analysis tools from Dr. Qing Nie's lab. In addition, Dr. Douglas Nitz from UCSD helped us on setting up LFP/single unit recordings for our future experiments.

I would also like to thank my lab members who had overlapped with me during my graduate study. Dr. Taruna Ikara, a former postdoc scholar, helped me on the slice electrophysiology experiments with his excellent patch-clamp skills. Dr. Yulin Shi, a former graduate student, made a great contribution on the analysis tools and software development in the lab with his programming expertise. Dr. Nicholas Olivas, a former graduate student, shared a lot of his scientific ideas with me. It's been a great experience working with Dr. Julie Dela Cruz, a former postdoc in the lab, who has excellent managing and organizing skills and helped me interact and network with other people. Special thanks go to Ms. Xiaoxiao Lin, who is a very interesting girl and brings a lot of fun and colorful ideas to our works as well as daily lives. She also helped me a lot with the experiments in my dissertation. It is an unforgettable period of time that I worked with Drs. Walter Francesconi and Fulvia Berton on the stress project. I can still

`

remember some Italian words they taught me. Thank our current postdocs Drs. Christy Itoga and Steven Grieco for their continuous help of my experiments and English writing. I definitely won't forget to thank all of my undergraduate students who helped me with different experiments.

I want to thank my colleagues or collaborators from other labs. Drs. Nayna Sanathara and Lien Wang from Dr. Civelli's lab helped me with behavioral experiments. I have been closely working with Dr. Nian Gong in Dr. David Luo's lab with many different experiments. It has been a wonderful experience working with her and I also learned a lot from her. Drs. Suoqin Jin and Tao Peng from Dr. Nie's lab helped us with data analysis tools with their mathematical expertise.

Please allow me to express my deepest appreciation to my family. My parents Huaizhong Sun and Yuzhen Zhao raised me up and educated me with their endless caring love. They maintain our family in a constant harmonious and creative environment, encourage and support me to do whatever I'm interested in. They instilled in me, since I was a small child, with the principle that I should devote my life to make contributions to mankind and our society. This principle, which is embedded deeply in my mind, continuously guides me in the path of my education. I would definitely like to thank my dearest wife, Jiaqi Cheng, for her persistent support, encouragement, patience, and unwavering love. Her support, both emotionally and financially, along with her trust enabled us to survive a long distance relationship for the past year. I believe this will become a memorable experience in our life journey.

Finally, I would like to acknowledge our funding sources from the National Institute of Neurological Disorders and Stroke (NS078434) and the National Institute of Mental Health (MH105427).

`

CURRICULUM VITAE

Yanjun Sun

Education

2017	Ph.D., Neuroscience, University of California, Irvine
2012	M.S., Biotechnology, University of California, Irvine
2010	B.S., Life Sciences & Biotechnology, Northeast Forestry University, China

Honors and Awards

2016	Public Impact Fellowship, UC Irvine
2016	3rd Place Oral Presentation, Grad Day Symposium, UC Irvine
2015	Associated Graduate Students Travel Grant, UC Irvine
2015	1st Place Poster Presentation, Grad Day Symposium, UC Irvine
2014	Graduate Fellow Award, HHMI-UCI Teaching Fellows Program
2010	Graduate Fellowship, Molecular Biology & Biochemistry, UC Irvine
2008	National Scholarship, Ministry of Education, China
2006 - 2010	Annual Academic Excellence Scholarship, Northeast Forestry University, China

Publications (Journal Articles, * indicates the lead authorship)

Sun Y, Grieco SF, Holmes TC, Xu X. (2017) Local and long-range circuit connections to hilar mossy cells in the dentate gyrus. *eNeuro* 4(2):0097-17

Sun Y, Ikrar T, Davis MF, Gong N, Zheng X, Luo ZD, Lai C, Mei L, Holmes TC, Gandhi SP, Xu X. (2016). Neuregulin-1 (NRG1)/ErbB4 signaling regulates visual cortical plasticity. *Neuron* 92(1):160-173.

Zhou QY, Burton KJ, Neal ML, Qiao Y, Kanthasamy A, **Sun Y**, Xu X, Ma Y, Li X. (2016) Differential arousal regulation by prokineticin 2 signaling in the nocturnal mouse and the diurnal monkey. *Molecular Brain* 9(1):78.

Xu X, **Sun Y**, Holmes TC, Lopez AJ. (2016) Noncanonical

`

connections between the subiculum and hippocampal CA1. *Journal of Comparative Neurology 524(17):3666-3673*.

Xu X, Ikrar T, **Sun Y**, Holmes TC, Francesconi W, and Berton F. (2016) High-resolution and cell-type-specific photostimulation mapping shows weak excitatory versus strong inhibitory inputs in the bed nucleus of the stria terminalis. *Journal of Neurophysiology* 115(6): 3204-16.

Nguyen A*, Dela Cruz J*, **Sun Y***, Holmes TC , Xu X. (2016). Genetic cell targeting uncovers specific neuronal types and distinct subregions in the bed nucleus of the stria terminalis. *Journal of Comparative Neurology* 524(12): 2379-99.

Sun Y, Nguyen A, Nguyen J, Le L, Saur D, Choi J, Callaway EM, Xu X. (2014). Cell-type specific circuit connectivity of hippocampal CA1 revealed through Cre-dependent rabies tracing. *Cell Reports* 7: 269–280.

Haettig J*, **Sun Y***, Wood MA, Xu X. (2013) Cell-type specific inactivation of hippocampal CA1 disrupts location-dependent object recognition in the mouse. *Learning & Memory* 20: 139-146.

Zhang ZW, Zhang LQ, Ding L, Wang F, **Sun YJ**, An Y, Zhao Y, Li YH, Teng CB. (2011). MicroRNA-19b downregulates insulin 1 through targeting transcription factor NeuroD1. *FEBS Letters* 585: 2592-2598.

Publications (Conference Proceedings)

Ikrar T, **Sun Y**, Gong N, Davis MF, Gandhi SP, Xu X. Neuregulin1 (NRG1)/ErbB4 signaling regulates visual critical period cortical plasticity. Program No. 36.27. 2016 Neuroscience Meeting Planner. San Diego, CA: Society for Neuroscience.

Sun Y, and Xu X. Circuit connection and function of the subicular neurons that project to hippocampal CA1. Program No. 838.15. 2016 Neuroscience Meeting Planner. San Diego, CA: Society for

Neuroscience.

Xu X, **Sun Y**, Ikrar T. Excitatory hilar mossy cells are the major local circuit integrators in the dentate gyrus. Program No. 838.11. 2016 Neuroscience Meeting Planner. San Diego, CA: Society for Neuroscience.

Sun Y, and Xu X. Circuit connection mapping of the subicular neurons projecting to hippocampal CA1. Program No. 656.02. 2015 Neuroscience Meeting Planner. Chicago, IL: Society for Neuroscience.

Dela Cruz JAD, **Sun Y**, Xu X. Cell-type specific septal innervation of excitatory and inhibitory hippocampal neurons. 2015 Gordon Research Conference: Excitatory Synapses and Brain Function at Salve Regina University, Newport, RI.

Sun Y, Ikrar T, López AJ, Xu X. Topographical and functional innervation of non-canonical back-projection from the subiculum to hippocampal CA1. Program No. 091.11. 2014 Neuroscience Meeting Planner. Washington, DC: Society for Neuroscience.

Sun Y, Nguyen A, Nguyen J, Le L, Callaway EM, Xu X. Cell-type specific circuit connectivity of hippocampal CA1 revealed through Cre-dependent rabies tracing. Session 3. 2014 Neuronal Circuits Meeting, Cold Spring Harbor, NY.

Sun Y, Nguyen A, Nguyen J, Le L, San Antonio A, Choi J, Callaway EM, Xu X. Cell-type specific circuit connectivity of hippocampal CA1 revealed through Cre-dependent rabies tracing. Program No. 696.05. 2013 Neuroscience Meeting Planner. San Diego, CA: Society for Neuroscience.

Sun Y, Nguyen A, Choi J, Cetin A, Callaway EM, Xu X. Monosynaptic rabies-mediated tracing of local and long-range circuit connections to specific groups of inhibitory neurons in hippocampal CA1. Program No. 705.06. 2012 Neuroscience Meeting Planner. New Orleans, LA: Society for Neuroscience.

`

ABSTRACT OF THE DISSERTATION

Neural circuit organization and function of hippocampal CA1 and the subiculum

By

Yanjun Sun

Doctor of Philosophy in Biomedical Sciences

University of California, Irvine, 2017

Associate Professor Xiangmin Xu, Chair

The hippocampal formation is a brain region that plays critical roles in memory and spatial navigation. A mechanistic understanding of hippocampal circuit organization and function is fundamental for determining how this brain region contributes to memory and cognition. Although the general anatomy and circuit organization of the hippocampal CA1 has been well-studied, most of our understanding of hippocampal circuits comes from the conventional anatomical tracing studies which lack cell-type specificity and quantitative measurements of connectional strengths. New advances in virology and genetics complement traditional approaches and are powerful tools for mapping cell-type-specific circuit connectivity and function. Herein, through a series of extensive studies using cutting-edge viral and genetic techniques, novel hippocampal circuits and their functions are elucidated. In Chapter 1, a Cre-dependent, genetically modified rabies-based tracing system was developed to map local and long-range monosynaptic connections to specific excitatory and inhibitory CA1 neuron types in the mouse. Our data show the different input sources of varying strengths are distributed onto each specific CA1 cell type, providing insight into differential circuit mechanisms of hippocampal functional operations. In Chapter 2, quantitative re-evaluation of intra- and para-hipppocampal input connections to excitatory neurons in different CA1 proximodistal subfields

`

was performed using monosynaptic rabies tracing. The results provide a new topographic circuit basis for functional considerations of CA1-associated memory and cognition. For the studies reported in Chapters 3 and 4, a detailed analysis of synaptic circuit organization and function of the subiculum to CA1 back-projection pathway was performed using state-of-the-art techniques including combinatorial viral tracing, genetically targeted manipulation of neural activity, and behavioral analysis. Building on the results from chapter 1 that provide unambiguous anatomical evidence for non-canonical subicular back-projections to CA1, global circuit input and output connections of CA1-projecting and other subicular neurons were mapped and compared. These studies establish that CA1-projecting subicular neurons are a distinct neuronal group with unique circuit properties within the subiculum. To link circuit mapping to function and behavior, I investigated how DREADDs-mediated inactivation of CA1-projecting subicular neurons modulates spatial learning and memory, and found that inactivating CA1-projecting subicular neurons specifically impairs animal's object location memory. This study has, for the first time, implicated the non-canonical subicular projections in hippocampus-associated spatial memory behavior. Together, this dissertation has provided novel, cell-type-specific anatomical and functional insights for hippocampal CA1 and the subiculum, and addressed the circuit organization and function of the under-appreciated bidirectional connections of subiculum and hippocampal CA1. This study may also lead to a better understanding of the neural circuit mechanisms that underlie hippocampal-related neurological disorders such as Alzheimer's disease.

`

INTRODUCTION

The hippocampus plays very important roles in learning, memory (Scoville and Milner, 1957, Morris et al., 1986, Kim and Fanselow, 1992, Squire and Wixted, 2011), and spatial navigation (O'Keefe and Dostrovsky, 1971, O'Keefe, 1976, Hafting et al., 2005, Moser et al., 2008). The knowledge of hippocampal circuit organization is fundamental for understanding how the hippocampus gives rise to memory and cognitive functions. The general anatomy and circuit connectivity of the hippocampal formation has been extensively studied (Amaral and Witter, 1989, Cappaert et al., 2015). Principal neurons in layer II of the entorhinal cortex (EC) project to granule cells of the dentate gyrus (DG) via the perforant path (Witter, 2007); DG granule cells give rise to distinctive unmyelinated axons which are called mossy fibers and innervate CA3 pyramidal neurons (Amaral et al., 2007); CA3 pyramidal neurons project extensively to CA1 pyramidal neurons via the Shaffer collaterals or CA2 (Chevaleyre and Siegelbaum, 2010, Cappaert et al., 2015). CA1 transfers excitatory information out of the hippocampus either directly to EC or via a dense projection to the subiculum (Amaral and Witter, 1989, Amaral, 1993, Naber et al., 2001). These unidirectional, feedforward circuit connection schemes are important for understanding how the information is being propagated through the hippocampal circuitry. While the “trisynapto-centric” view has been emphasized, there are other circuits that provide alternative pathways for information flow. For example, CA1 and subiculum receive direct excitatory projections from entorhinal layer III through the temporoammonic pathway controlling spatial information processing and temporal association memory (Brun et al., 2002, Kitamura et al., 2014). CA3 recurrent collaterals are believed to serve as the underlying circuits for pattern completion (Knierim and Neunuebel, 2016). CA3 to DG back-projections also play important roles in controlling associative information processing

`

(Scharfman, 2007). More relevant to my dissertation work is that accumulating evidence indicates the existence of non-canonical back-projections from the subiculum to CA1, which potentially contribute to modulation of the hippocampal network oscillations and spiking timing of CA1 pyramidal cells (Jackson et al., 2014, Craig and McBain, 2015a). Functional understanding of a given circuitry requires specific knowledge of how intermingled neuronal types integrate into local and global neural networks. Due to previous technical limitations, cell-type specific circuit organization and function of hippocampal pathways remain to be studied. The goal of this dissertation is to dissect cell-type specific hippocampal neuronal circuit organization and function, with a main focus on hippocampal CA1 and the subiculum. I have used recent technological advancements in genetic cell targeting, molecular and viral tracing, and functional circuit mapping for the proposed experimental work.

In the study described in Chapter 1of this dissertation, I have mapped local and long-range circuit connections to specific excitatory and inhibitory neuron types in hippocampal CA1. I test the hypothesis that functional differences of specific types of hippocampal neurons are largely due to their distinct circuit connections. Compared to the relative uniformity of excitatory neurons, hippocampal inhibitory neurons are diverse in their morphology, axonal targeting, intrinsic physiology, and expression of neurochemical markers (Freund and Buzsaki, 1996, Kepecs and Fishell, 2014). They also show distinct functions in regulating the activity of hippocampal pyramidal cells and contribute differentially to network oscillations and cognition (Klausberger et al., 2003, Murray et al., 2011, Royer et al., 2012). In order to know the circuit connections of each constituent CA1 cell type, I have developed and applied a Cre-dependent, genetically modified rabies-based tracing system to map direct synaptic connections to targeted cell types of hippocampal CA1 in the intact brain (Wickersham et al., 2007b, Wall et al., 2010).

`

Using various Cre-driver mouse lines (Tsien et al., 1996, Monory et al., 2006, Taniguchi et al., 2011), I characterized direct input connections to CA1 excitatory pyramidal cells, mixed inhibitory cell types, parvalbumin (PV)-expressing inhibitory neurons, and somatostatin (SOM)-expressing inhibitory neurons, respectively (Sun et al., 2014). I was able to demonstrate quantitative differences in presynaptic local and distant circuit connections to CA1 targeted cell types and provide insights into differential circuit mechanisms for hippocampal functional operations. In line with rabies tracing experiments, physiological measurements of functional connections in vitro also verified the cell-type specific differences in the intrahippocampal circuit connections (Sun et al., 2014).

In Chapter 2, I test the hypothesis that different place field properties and differential functional memory involvement of hippocampal excitatory neurons in proximal versus distal CA1 (Henriksen et al., 2010, Hartzell et al., 2013, Nakazawa et al., 2016) can be attributed to the differential circuit inputs from topographically organized projections of intra- and para-hippocampal regions. Most of the previous studies characterized the hippocampal topographic circuit organization using conventional chemical tracers and investigated the projection patterns relying on the anterograde axonal labeling (Steward, 1976, Amaral and Witter, 1989, Ishizuka et al., 1990, Tamamaki and Nojyo, 1995). Although these studies have provided the circuit basis for interpreting physiological and functional studies, there are caveats that we should be aware of. First, the existence of axonal projections in a specific brain region does not necessarily mean these labeled axons indeed innervate neurons in that place. Second, they are not able to provide a perfect quantitative and comparative result across different animals, as it is hard to determine how many neurons take up the tracer around the injection site. Therefore, as the CA1 functional cell types, place cells for example, are likely a subset of CA1 excitatory pyramidal neurons

`

(Moser et al., 2008), it is worthwhile to re-evaluate the topographic organizations specifically for CA1 pyramidal cells. By using the same Cre-dependent rabies tracing technique (Sun et al., 2014, Sun et al., 2017), I mapped the direct input connections specifically to the excitatory pyramidal cells of proximal, intermediate, and distal CA1, respectively. As the starter neurons can be unambiguously identified in the injection site, I was able to assess the intra- and para-hippocampal input connections from CA3, entorhinal cortex, and the subiculum complex to each of the specific CA1 subfields in a quantitative manner. These results provide a new understanding of topographic organization of canonical and non-canonical inputs to CA1 excitatory neurons, and allows for functional considerations of how different intra- and para-hipppocampal inputs modulate CA1-associated spatial navigation and memory behaviors.

In Chapter 3 and 4, I focus my research on characterizing the circuit organization and function of the non-canonical subiculum to CA1 back-projection pathway that I have reported in Chapters 1 and 2 (Sun et al., 2014, Xu et al., 2016). The earliest evidence for a backward projection from the subiculum to area CA1 came from conventional anatomical tracing studies in the 1980s. While supported by several electrophysiological studies, the subiculum-CA1 pathway was not determined with great certainty (Berger et al., 1980, Finch et al., 1983, Kohler, 1985, Witter et al., 1990, Harris and Stewart, 2001, Commins et al., 2002, Shao and Dudek, 2005). Using genetically targeted rabies tracing, we unambiguously found that there are significant direct inputs from the subiculum to hippocampal CA1. Both excitatory and inhibitory subicular neurons project to CA1, and both CA1 excitatory neurons and inhibitory interneurons are innervated by subicular inputs. Our quantitative analysis indicates that non-canonical back projections from the subiculum to CA1 have connectivity strengths similar to the well-studied medial septal projections to CA1. The subicular back-projection pathway is direct and local, thus

`

is potentially faster and more powerful than distant feedback loops via hippocampal-cortical connections. Therefore, I focus on CA1-projecting excitatory subicular neurons due to their apparent importance in long-range circuit projections.

In Chapter 3, I test the hypothesis that CA1-projeting subicular neurons are a distinct group of neurons in the subiculum with unique circuit connection properties compared to other subicular excitatory and inhibitory neurons. As subicular neurons are diverse in terms of their axonal projections (Kim and Spruston, 2012), it is likely that different types of subicular neurons also have distinct circuit inputs. To test this hypothesis, I mapped the circuit connections of subicular excitatory neurons, inhibitory neurons, as well as the CA1-projecting subicular neurons by using combinatorial viral genetic tracing (Gore et al., 2013, Schwarz et al., 2015). The mapping studies have determined brain-wide inputs and outputs of CA1-projecting and other subicular neuron types, and provide a strong circuit basis to interpret in vivo physiology and functional contributions of CA1-projecting subicular neurons.

In Chapter 4, I continue to study spatial memory behavioral relevance of the subiculum to CA1 back-projection. It has been shown that the subiculum work together with CA1 in a timely concerted while complementary manner to encode the memory (Hampson and Deadwyler, 2003, Deadwyler and Hampson, 2004). The subiculum contains several functional cell types including place cells (Sharp and Green, 1994), boundary vector cells (Lever et al., 2009), and axis-tuned cells (Olson et al., 2017), which are critical in spatial navigation and task related behaviors. Therefore, we hypothesize the CA1-projecting subicular neurons are actively involved in hippocampus-associated learning and memory behaviors. I investigated the functional role of the subiculum to CA back-projection in the location-dependent object recognition (LOR) (Haettig et al., 2013) as well as the novel object recognition (NOR) (Vogel-Ciernia et al., 2013, Wang et al.,

`

2015) combined with genetically targeted inactivation of CA1 projecting subicular neurons via the Designer Receptors Exclusively Activated by Designer Drugs (DREADDs) system (Sternson and Roth, 2014, Sun et al., 2016). The DREADDs-mediated inactivation effect of CA1-projecting subicular neurons is specific to object location memory, but does not affect object recognition hippocampus-independent memory. These results validate the functional significance of the subiculum to CA1 back-projection pathway.

In chapter 5, I provide concluding remarks regarding the circuit organization and function of hippocampal CA1 and the subiculum. I discuss future relevant studies and propose to further test our hypothesis that CA1-projecting subicular neurons are functionally implicated in spatial memory behaviors with emerging technologies. Together, this large body of dissertation work has helped to significantly advance our understanding of the neuronal circuit mechanisms and functions of hippocampal CA1 and the adjacent subiculum. Given previous findings implicate early-stage degeneration of the subiculum and CA1 in the progression of Alzheimer's disease in humans and animal models (George et al., 2014, Carlesimo et al., 2015), this research has additional implications in understanding the neural circuit mechanisms underlying Alzheimer's disease and other learning and memory disorders.

`

REFERENCES

Amaral DG (1993) Emerging principles of intrinsic hippocampal organization. Curr Opin Neurobiol 3:225-229.

Amaral DG, Scharfman HE, Lavenex P (2007) The dentate gyrus: fundamental neuroanatomical organization (dentate gyrus for dummies). Prog Brain Res 163:3-22.

Amaral DG, Witter MP (1989) The three-dimensional organization of the hippocampal formation: a review of anatomical data. Neuroscience 31:571-591.

Berger TW, Swanson GW, Milner TA, Lynch GS, Thompson RF (1980) Reciprocal anatomical connections between hippocampus and subiculum in the rabbit evidence for subicular innervation of regio superior. Brain Res 183:265-276.

Brun VH, Otnass MK, Molden S, Steffenach HA, Witter MP, Moser MB, Moser EI (2002) Place cells and place recognition maintained by direct entorhinal-hippocampal circuitry. Science 296:2243-2246.

Cappaert NL, Van Strien NM, Witter MP (2015) Hippocampal formation. In: The Rat Nervous System (Fourth Edition) (Paxinos, G., ed), pp 511-573 London: Elsevier.

Carlesimo GA, Piras F, Orfei MD, Iorio M, Caltagirone C, Spalletta G (2015) Atrophy of presubiculum and subiculum is the earliest hippocampal anatomical marker of Alzheimer's disease. Alzheimers Dement (Amst) 1:24-32.

Chevaleyre V, Siegelbaum SA (2010) Strong CA2 pyramidal neuron synapses define a powerful disynaptic cortico-hippocampal loop. Neuron 66:560-572.

Commins S, Aggleton JP, O'Mara SM (2002) Physiological evidence for a possible projection from dorsal subiculum to hippocampal area CA1. Exp Brain Res 146:155-160.

Craig MT, McBain CJ (2015a) Fast gamma oscillations are generated intrinsically in CA1 without the involvement of fast-spiking basket cells. J Neurosci 35:3616-3624.

Deadwyler SA, Hampson RE (2004) Differential but complementary mnemonic functions of the hippocampus and subiculum. Neuron 42:465-476.

Finch DM, Nowlin NL, Babb TL (1983) Demonstration of axonal projections of neurons in the rat hippocampus and subiculum by intracellular injection of HRP. Brain Res 271:201-216.

Freund TF, Buzsaki G (1996) Interneurons of the hippocampus. Hippocampus 6:347-470.

George S, Ronnback A, Gouras GK, Petit GH, Grueninger F, Winblad B, Graff C, Brundin P (2014) Lesion of the subiculum reduces the spread of amyloid beta pathology to interconnected brain regions in a mouse model of Alzheimer's disease. Acta Neuropathol Commun 2:17.

Gore BB, Soden ME, Zweifel LS (2013) Manipulating gene expression in projection-specific neuronal populations using combinatorial viral approaches. Curr Protoc Neurosci 4:4 35 31-34 35 20.

Haettig J, Sun Y, Wood MA, Xu X (2013) Cell-type specific inactivation of hippocampal CA1 disrupts location-dependent object recognition in the mouse. Learn Mem 20:139-146.

Hafting T, Fyhn M, Molden S, Moser MB, Moser EI (2005) Microstructure of a spatial map in the entorhinal cortex. Nature 436:801-806.

Hampson RE, Deadwyler SA (2003) Temporal firing characteristics and the strategic role of subicular neurons in short-term memory. Hippocampus 13:529-541.

Harris E, Stewart M (2001) Propagation of synchronous epileptiform events from subiculum backward into area CA1 of rat brain slices. Brain Res 895:41-49.

`

Hartzell AL, Burke SN, Hoang LT, Lister JP, Rodriguez CN, Barnes CA (2013) Transcription of the immediate-early gene Arc in CA1 of the hippocampus reveals activity differences along the proximodistal axis that are attenuated by advanced age. J Neurosci 33:3424-3433.

Henriksen EJ, Colgin LL, Barnes CA, Witter MP, Moser MB, Moser EI (2010) Spatial representation along the proximodistal axis of CA1. Neuron 68:127-137.

Ishizuka N, Weber J, Amaral DG (1990) Organization of intrahippocampal projections originating from CA3 pyramidal cells in the rat. J Comp Neurol 295:580-623.

Jackson J, Amilhon B, Goutagny R, Bott JB, Manseau F, Kortleven C, Bressler SL, Williams S (2014) Reversal of theta rhythm flow through intact hippocampal circuits. Nat Neurosci 17:1362-1370.

Kepecs A, Fishell G (2014) Interneuron cell types are fit to function. Nature 505:318-326.

Kim JJ, Fanselow MS (1992) Modality-specific retrograde amnesia of fear. Science 256:675-677.

Kim Y, Spruston N (2012) Target-specific output patterns are predicted by the distribution of regular-spiking and bursting pyramidal neurons in the subiculum. Hippocampus 22:693-706.

Kitamura T, Pignatelli M, Suh J, Kohara K, Yoshiki A, Abe K, Tonegawa S (2014) Island cells control temporal association memory. Science 343:896-901.

Klausberger T, Magill PJ, Marton LF, Roberts JD, Cobden PM, Buzsaki G, Somogyi P (2003) Brain-state- and cell-type-specific firing of hippocampal interneurons in vivo. Nature 421:844-848.

Knierim JJ, Neunuebel JP (2016) Tracking the flow of hippocampal computation: Pattern separation, pattern completion, and attractor dynamics. Neurobiol Learn Mem 129:38-49.

Kohler C (1985) Intrinsic projections of the retrohippocampal region in the rat brain. I. The subicular complex. The Journal of comparative neurology 236:504-522.

Lever C, Burton S, Jeewajee A, O'Keefe J, Burgess N (2009) Boundary vector cells in the subiculum of the hippocampal formation. J Neurosci 29:9771-9777.

Monory K, Massa F, Egertova M, Eder M, Blaudzun H, Westenbroek R, Kelsch W, Jacob W, Marsch R, Ekker M, Long J, Rubenstein JL, Goebbels S, Nave KA, During M, Klugmann M, Wolfel B, Dodt HU, Zieglgansberger W, Wotjak CT, Mackie K, Elphick MR, Marsicano G, Lutz B (2006) The endocannabinoid system controls key epileptogenic circuits in the hippocampus. Neuron 51:455-466.

Morris RG, Anderson E, Lynch GS, Baudry M (1986) Selective impairment of learning and blockade of long-term potentiation by an N-methyl-D-aspartate receptor antagonist, AP5. Nature 319:774-776.

Moser EI, Kropff E, Moser MB (2008) Place cells, grid cells, and the brain's spatial representation system. Annu Rev Neurosci 31:69-89.

Murray AJ, Sauer JF, Riedel G, McClure C, Ansel L, Cheyne L, Bartos M, Wisden W, Wulff P (2011) Parvalbumin-positive CA1 interneurons are required for spatial working but not for reference memory. Nat Neurosci 14:297-299.

Naber PA, Lopes da Silva FH, Witter MP (2001) Reciprocal connections between the entorhinal cortex and hippocampal fields CA1 and the subiculum are in register with the projections from CA1 to the subiculum. Hippocampus 11:99-104.

Nakazawa Y, Pevzner A, Tanaka KZ, Wiltgen BJ (2016) Memory retrieval along the proximodistal axis of CA1. Hippocampus 26:1140-1148.

O'Keefe J (1976) Place units in the hippocampus of the freely moving rat. Exp Neurol 51:78-109.

`

O'Keefe J, Dostrovsky J (1971) The hippocampus as a spatial map. Preliminary evidence from unit activity in the freely-moving rat. Brain Res 34:171-175.
Olson JM, Tongprasearth K, Nitz DA (2017) Subiculum neurons map the current axis of travel. Nat Neurosci 20:170-172.
Royer S, Zemelman BV, Losonczy A, Kim J, Chance F, Magee JC, Buzsaki G (2012) Control of timing, rate and bursts of hippocampal place cells by dendritic and somatic inhibition. Nat Neurosci 15:769-775.
Scharfman HE (2007) The CA3 "backprojection" to the dentate gyrus. Prog Brain Res 163:627-637.
Schwarz LA, Miyamichi K, Gao XJ, Beier KT, Weissbourd B, DeLoach KE, Ren J, Ibanes S, Malenka RC, Kremer EJ, Luo L (2015) Viral-genetic tracing of the input-output organization of a central noradrenaline circuit. Nature 524:88-92.
Scoville WB, Milner B (1957) Loss of recent memory after bilateral hippocampal lesions. J Neurol Neurosurg Psychiatry 20:11-21.
Shao LR, Dudek FE (2005) Electrophysiological evidence using focal flash photolysis of caged glutamate that CA1 pyramidal cells receive excitatory synaptic input from the subiculum. J Neurophysiol 93:3007-3011.
Sharp PE, Green C (1994) Spatial correlates of firing patterns of single cells in the subiculum of the freely moving rat. J Neurosci 14:2339-2356.
Squire LR, Wixted JT (2011) The cognitive neuroscience of human memory since H.M. Annu Rev Neurosci 34:259-288.
Sternson SM, Roth BL (2014) Chemogenetic tools to interrogate brain functions. Annu Rev Neurosci 37:387-407.
Steward O (1976) Topographic organization of the projections from the entorhinal area to the hippocampal formation of the rat. J Comp Neurol 167:285-314.
Sun Y, Grieco SF, Holmes TC, Xu X (2017) Local and Long-Range Circuit Connections to Hilar Mossy Cells in the Dentate Gyrus. eNeuro 4.
Sun Y, Ikrar T, Davis MF, Gong N, Zheng X, Luo ZD, Lai C, Mei L, Holmes TC, Gandhi SP, Xu X (2016) Neuregulin-1/ErbB4 Signaling Regulates Visual Cortical Plasticity. Neuron 92:160-173.
Sun Y, Nguyen AQ, Nguyen JP, Le L, Saur D, Choi J, Callaway EM, Xu X (2014) Cell-type-specific circuit connectivity of hippocampal CA1 revealed through Cre-dependent rabies tracing. Cell Rep 7:269-280.
Tamamaki N, Nojyo Y (1995) Preservation of topography in the connections between the subiculum, field CA1, and the entorhinal cortex in rats. J Comp Neurol 353:379-390.
Taniguchi H, He M, Wu P, Kim S, Paik R, Sugino K, Kvitsiani D, Fu Y, Lu J, Lin Y, Miyoshi G, Shima Y, Fishell G, Nelson SB, Huang ZJ (2011) A resource of Cre driver lines for genetic targeting of GABAergic neurons in cerebral cortex. Neuron 71:995-1013.
Tsien JZ, Chen DF, Gerber D, Tom C, Mercer EH, Anderson DJ, Mayford M, Kandel ER, Tonegawa S (1996) Subregion- and cell type-restricted gene knockout in mouse brain. Cell 87:1317-1326.
Vogel-Ciernia A, Matheos DP, Barrett RM, Kramar EA, Azzawi S, Chen Y, Magnan CN, Zeller M, Sylvain A, Haettig J, Jia Y, Tran A, Dang R, Post RJ, Chabrier M, Babayan AH, Wu JI, Crabtree GR, Baldi P, Baram TZ, Lynch G, Wood MA (2013) The neuron-specific chromatin regulatory subunit BAF53b is necessary for synaptic plasticity and memory. Nat Neurosci 16:552-561.

`

Wall NR, Wickersham IR, Cetin A, De La Parra M, Callaway EM (2010) Monosynaptic circuit tracing in vivo through Cre-dependent targeting and complementation of modified rabies virus. Proc Natl Acad Sci U S A 107:21848-21853.

Wang L, Alachkar A, Sanathara N, Belluzzi JD, Wang Z, Civelli O (2015) A Methionine-Induced Animal Model of Schizophrenia: Face and Predictive Validity. Int J Neuropsychopharmacol 18.

Wickersham IR, Lyon DC, Barnard RJ, Mori T, Finke S, Conzelmann KK, Young JA, Callaway EM (2007b) Monosynaptic restriction of transsynaptic tracing from single, genetically targeted neurons. Neuron 53:639-647.

Witter MP (2007) The perforant path: projections from the entorhinal cortex to the dentate gyrus. Prog Brain Res 163:43-61.

Witter MP, Ostendorf RH, Groenewegen HJ (1990) Heterogeneity in the Dorsal Subiculum of the Rat. Distinct Neuronal Zones Project to Different Cortical and Subcortical Targets. Eur J Neurosci 2:718-725.

Xu X, Sun Y, Holmes TC, Lopez AJ (2016) Noncanonical connections between the subiculum and hippocampal CA1. J Comp Neurol 524:3666-3673.

`

Chapter 1:

Cell-type specific circuit connectivity of hippocampal CA1 revealed through Cre-dependent rabies tracing

`

ABSTRACT

We applied a new Cre-dependent, genetically modified rabies-based tracing system to map direct synaptic connections to CA1 excitatory and inhibitory neuron types in mouse hippocampus. We found common inputs to excitatory and inhibitory CA1 neurons from CA3, CA2, entorhinal cortex and the medial septum (MS), and unexpectedly also from the subiculum. Excitatory CA1 neurons receive inputs from both cholinergic and GABAergic MS neurons while inhibitory CA1 neurons receive a great majority of input from GABAergic MS neurons; both cell types also receive weaker input from glutamatergic MS neurons. Comparisons of inputs to CA1 PV+ interneurons versus SOM+ interneurons showed similar strengths of input from the subiculum, but PV+ interneurons receive much stronger input than SOM+ neurons from CA3, entorhinal cortex and MS. Differential input from CA3 to specific CA1 cell types was also demonstrated functionally using laser scanning photostimulation and whole cell recordings.

`

INTRODUCTION

The general anatomy and circuit organization of the hippocampal CA1 area has been particularly well studied, due to its single principal cell layer coupled with a highly organized laminar distribution of its extrinsic inputs (Amaral and Witter, 1989). The CA1 area receives major input connections from several extrinsic sources (Takacs et al., 2012), including CA3 pyramidal cells via their ipsilateral Schaffer collaterals and contralateral commissural fibers (Amaral and Witter, 1989) and layer 3 excitatory cells of the entorhinal cortex through the temporo-ammonic pathway (Steward and Scoville, 1976), as well as the medial septum and diagonal band (MS-DB) area (Freund and Antal, 1988, Gulyas et al., 1990). Functionally, MS-DB inputs are important for hippocampal network oscillations (Buzsaki, 2002), and behavioral evidence indicates functionally separable roles of CA3 and entorhinal inputs to CA1 in hippocampus-dependent learning and memory (Brun et al., 2002, Remondes and Schuman, 2004, Nakashiba et al., 2008, Suh et al., 2011). Like many other cortical areas, CA1 contains diverse types of excitatory and inhibitory neurons that form intricate circuit connections for information processing (Klausberger and Somogyi, 2008). Differential inhibitory control of excitatory cell activity by inhibitory interneurons is largely determined by extrinsic and intrinsic CA1 excitation to different inhibitory cell types (Klausberger and Somogyi, 2008). However, due to technical limitations, there is a limited understanding of whether or how the different sources of input to CA1 are distributed in different strengths onto each of its constituent cell types, which is essential for a mechanistic understanding of hippocampal functional circuit operations.

Until recently, there has been no efficient means for performing cell-type specific circuit analyses in the intact brain over a large scale. New advances in virology and genetic technology are now beginning to complement more traditional approaches and offer powerful tools for

`

mapping cell-type specific circuit connectivity and function (Callaway, 2008). Among them, genetically modified and monosynaptically restricted rabies tracing has proved to be a useful mapping tool for identifying direct circuit inputs to specific cell populations that can be genetically targeted (Wickersham et al., 2007b, Marshel et al., 2010, Wall et al., 2010, Nakashiba et al., 2012).

In the present study, we applied a strategy based upon a Cre-dependent, genetically modified rabies-based tracing system to map local and long-range monosynaptic connections in the intact brain to targeted cell types defined by Cre expression in four different mouse lines including excitatory pyramidal cells (Camk2a-Cre), mixed inhibitory cell types (Dlx5/6-Cre), parvalbumin-expressing (PV-Cre) inhibitory cells and somatostatin-expressing (SOM-Cre) inhibitory cells in CA1 of the mouse hippocampus. Using the new approach, we were able to examine circuit connections of excitatory and inhibitory cell types in the intact brain, and demonstrate quantitative differences in presynaptic local and distant circuit connections to these cell types. These data provide insights into differential circuit mechanisms for hippocampal functional operations.

MATERIALS AND METHODS

Subjects

All experiments were conducted according to National Institutes of Health guidelines for animal care and use and were approved by the Institutional Animal Care and Use Committee of the University of California, Irvine. Although the genetically modified rabies viruses used for the proposed experiments are deletion-mutant rabies and are based on a vaccine strain (SAD-B19), they still pose a limited potential health risk with the helper virus. All personnel working with the rabies are therefore vaccinated and experiments are conducted under biosafety level

`

(BSL) 2 conditions with a protocol approved by the institutional biosafety committee.

To achieve Cre-directed, cell type specific expression of TVA receptors in hippocampal CA1, we used a LSL-R26$^{Tva\text{-}lacZ}$ mouse line conditionally expressing TVA receptor (avian retroviral receptor, tumor virus A) in a Cre-recombinase-dependent manner (Seidler et al., 2008); the LSL-R26$^{Tva\text{-}lacZ}$ mouse line was cross-bred with Camk2a-Cre (T29) mouse line (Tsien et al., 1996), Dlx5/6-Cre mouse line (Monory et al., 2006), respectively. We termed the double transgenic mice as Camk2a-Cre:TVA and Dlx5/6-Cre:TVA, respectively, in which Cre-expressing cells also express TVA to restrict initial infection of EnvA-SADΔG rabies virus. The mice of 8-12 weeks old (either sex) were used for experiments and had free access to food and water in their home-cages before and after surgeries.

Viral injections

To perform stereotaxic viral injections into the brain, mice were anesthetized under 1.5% isoflurane for 10 minutes with a 0.8 L/min oxygen flow rate using a isoflurane table top unit (HME109, Highland Medical Equipment). Mice were then placed in a rodent stereotax (Leica Angle Two™ for mouse) with continuous 1% isoflurane anesthesia with the head secured. A small incision was made in the head, the skin reflected, and the skull exposed to show the landmarks of bregma and lambda, and desired injection sites. A three-axis micromanipulator guided by a digital atlas was used to determine coordinates for the bregma and lambda. The injection site was calculated relative to these landmarks, using canonical coordinates. The following injection coordinates targeting dorsal hippocampal CA1 were used: anteroposterior −1.94 mm, lateromedial -1.40 mm; dorsoventral −1.35 mm (all values given relative to the bregma). A small drill hole was made in the skull over the injection site, exposing the pia surface. A pulled glass pipette (tip diameter, ≈30 μm) was loaded with virus and then lowered

`

into the brain with the appropriate coordinates. A Picospritzer (General Valve, Hollis, NH) was used to pulse virus into the brain. A total of 0.1 ul of the helper virus (AAV8-EF1a-FLEX-HB, $\sim 2 \times 10^{11}$ genome units per ml) (Addgene, Plasmid 37452) was injected into the brain at a rate of 20 - 30 nl/min, with 10 ms pulse duration. To prevent backflow of virus, the pipette remained in the brain for 5 min after completion of the injection. Once the injection pipette was withdrawn, the mouse was removed from the stereotax, and the incision was closed with either wound clips or tissue adhesive (3M Vetbond, St. Paul, MN). Mice were taken back and recovered in their home cages. After 3 weeks of the AAV injection which allowed for the infected neurons to express high contents of RGs and GFP, the pseudotyped, RG-deleted rabies virus (EnvA-SADΔG-mCherry rabies, 0.1 ul, $\sim 2 \times 10^{9}$ infectious units per ml) was injected into the same location of the previous injection. The rabies virus was allowed to replicate and retrogradely spread from targeted Cre+ cell types to directly connected presynaptic cells for 9-10 days before the animals were perfused for tissue processing. Since it has been estimated that rabies virus requires only 24 h to cross a synapse (Ugolini, 2008), the rabies infection time would be sufficient for crossing sparse and weak synaptic contacts, which is confirmed by our results.

Histology, immunohistochemistry and image data acquisition

The mice were transcardially perfused with 5 ml of phosphate buffered saline (PBS), followed by 25 ml PBS containing 4% paraformaldehyde. The brains were removed and left in 4% paraformaldehyde overnight, then transferred into 30% sucrose in PBS in the next day. The brain was sectioned coronally in 30 μm thickness on a freezing microtome (Leica SM2010R, Germany). Every one out of 3 sections was mounted for examination and quantification of starter cells and their presynaptic cells in different brain structures. For the cases of Dlx5/6-Cre:TVA , PV-Cre:TVA and SOM-Cre:TVA, these sections were stained with a GFP antibody

`

to amplify GFP signal resulting from the helper AAV expression for dependable identification of starter cells. As mCherry expression is strong in rabies labeled cell, we did not perform immunostaining against mCherry. Selected sections were also immunostained with various antibodies for neurochemical characterization of starter cells and rabies labeled cells in different regions. Conventional immunochemistry was performed as described previously (Xu et al., 2010). For GFP staining, a chicken anti-GFP primary antibody (Aves Labs, 1:500 dilution) followed with an Alexa Fluor (AF) 488-conjugated donkey anti-chicken secondary antibody (Jackson ImmunoResearch, 1:200 dilution) applied to the sections. To immunochemically identify GABAergic cells, GAD or GABA immunostaining was used with a rabbit anti-GAD65/67 primary antibody (Millipore, 1:500) or rabbit anti-GABA primary antibody (Sigma-Aldrich, 1:1000) followed with a AF488 or AF647-conjugated donkey anti-rabbit secondary antibody (Jackson ImmunoResearch). To identify cholinergic cells in the MS/DB area, choline acetyltransferase (ChAT) immunostaining was used, with a goat anti-ChAT primary antibody (Millipore, 1:250) followed with a AF488-conjugated donkey anti-goat secondary antibody (Jackson ImmunoResearch). To immunochemically examine whether rabies labeled cells are glutamatergic neurons, selected sections were double immunolabeled against excitatory amino acid transporter type1 (EAAC1) (goat anti-EAAC1, Millipore 1:500) and GABA (rabbit anti-GABA), followed with secondary antibodies of AF488-conjugated donkey anti-goat and AF647-conjugated donkey anti-rabbit (Jackson ImmunoResearch). For lacZ (beta galactosidase) staining, a rabbit anti-lacZ primary antibody (5prime->3'prime inc., 1:200) followed with a AF647-conjugated donkey anti-rabbit secondary antibody (Jackson ImmunoResearch) was used. Sections were counter-stained with 10 μM DAPI, then mounted and cover-slipped. Using Automated Slide Scanning and Analysis software (Metamorph, Inc) in a high-capacity computer

`

coupled with a fluorescent BX61 Olympus microscope and a high-sensitive Hamamatsu CCD camera, under a 10X objective we were able to obtain sufficient-resolution images suitable for all subsequent computer-based analyses. We also imaged labeled cells in selected sections with a confocal microscope (LSM 700, Carl Zeiss). Image stitching, overlaying, cell counting and further imaging analysis were completed by using Metamorph imaging and analysis tools. Quantitative examinations across the series of sections were conducted for complete and unbiased analyses of rabies-mediated, direct synaptic connections to targeted Cre-defined cell types.

Electrophysiology and laser scanning photostimulation

We used wild type and transgenic mice of 3-4 weeks old for physiological experiments. Horizontal hippocampal slices of 400 μm thick were cut at the angle optimized to conserve the intrahippocampal axonal projections in ice-cold sucrose-containing cutting solution (in mM: 85 NaCl, 75 sucrose, 2.5 KCl, 25 glucose, 1.25 NaH_2PO_4, 4 $MgCl_2$, 0.5 $CaCl_2$, and 24 $NaHCO_3$). Two morphologically intact slices intermediate between dorsal and ventral hippocampus from each animal was used for experiments. Slices were first incubated in sucrose-containing ACSF for 30 minutes–one hour at 32°C, and then transferred to recording ACSF (in mM: 126 NaCl, 2.5 KCl, 26 $NaHCO_3$, 2 $CaCl_2$, 2 $MgCl_2$, 1.25 NaH_2PO_4, and 10 glucose). Throughout the cutting, incubation and recording, the solutions were continuously supplied with 95% O_2–5% CO_2.

Our overall system of electrophysiological recording, photostimulation, and imaging was described previously (Xu et al., 2010; San Antonio et al., 2013). The solution was fed into the slice recording chamber through a pressure driven flow system with pressurized 95% O_2–5% CO_2 with a perfusion flow rate of about 2 ml/minute. To perform whole-cell recording, individual neurons were visualized at high magnification (60x objective), and were patched with

`

glass electrodes of 4–6 MΩ resistance that were filled with an internal solution containing (in mM) 126 K-gluconate, 4 KCl, 10 HEPES, 4 ATP-Mg, 0.3 GTP-Na, and 10 phosphocreatine (pH 7.2, 300–305 mOsm). The internal solution also contained 0.1% biocytin for cell labeling and morphological identification. Once stable whole-cell recordings were achieved with good access resistance (usually <20 MΩ), basic electrophysiological properties were examined through hyperpolarizing and depolarizing current injections. For laser scanning photostimulation (LSPS) experiments, the microscope objective was switched from 60x to 4x. Stock solution of MNI-caged-l-glutamate (Tocris Bioscience, Ellisville, MO) was added to 20 ml of ACSF for a concentration of 0.2 mM caged glutamate. The slice image was acquired by a high resolution digital CCD camera, which in turn was used for guiding and registering photostimulation sites.

During mapping experiments, photostimulation was usually applied to 16×16 patterned sites (with an inter-site space of 100 μm^2) covering the whole hippocampus in a nonraster, nonrandom sequence to avoid revisiting the vicinity of recently stimulated sites; whole-cell voltage-clamp recordings were made from the recorded neurons to measure photostimulation-evoked excitatory postsynaptic current (EPSC) responses at the holding potential around -70mV, which was based upon the empirically determined GABAergic reversal potentials at the recorded mouse ages.

Photostimulation data analysis has been described in detail (Shi et al., 2010). Photostimulation can induce two major forms of excitatory responses (Xu and Callaway, 2009, Shi et al., 2010): (1) direct glutamate uncaging responses (direct activation of the recorded neuron's glutamate receptors); and (2) synaptically mediated responses (EPSCs) resulting from the suprathreshold activation of presynaptic excitatory neurons. Responses within the 7 ms window from laser onset are considered direct. Synaptic currents with such short latencies are not possible because they occur before the generation of action potentials in photostimulated

`

neurons. To exclude direct responses, candidate EPSCs with their arrival times occurring within the direct response window (within 7 ms of the laser onset) are dismissed. As for individual map construction, input measurements from different stimulation sites were assigned to their corresponding anatomical locations in the hippocampus; color-coded maps of average input amplitude, the number of events per site were plotted to illustrate overall input pattern to the recorded cell. The input amplitude/strength of each stimulation site was measured by the sum of individual EPSCs or IPSCs from each photostimulation site with the baseline spontaneous response subtracted, and then normalized by the analysis window of 150 ms after photostimulation. This average integrated value was expressed in picoamperes (pA) for the analysis window. To quantitatively compare input strength and connections across cell groups, we measured the total ESPC inputs and the numbers of EPSCs across specific hippocampal subfields for individual cells. Note that as stratum lacunosum-moleculare (SLM) only has sparse inhibitory neurons but pyramidal neurons located in the pyramidal cell layer could fire action potentials when their distal apical dendrites were stimulated in the SLM layer (e.g., see Fig. 1.13), EPSCs detected after photostimulation in the SLM layer were not included for analysis to avoid repeated sampling.

After physiological assays had been completed, the brain slices were fixed in 4% paraformaldehyde in PBS overnight and transferred to 30% sucrose solution in PBS. The slices were stained against biocytin with 1:1,000 Alexa Fluor 488 or Cy3-conjugated streptavidin (Jackson ImmunoResearch) to show the morphology of the recorded cells. Neuron reconstructions were computer-assisted and based on stacks of optical sections acquired by a confocal microscope (LSM 700, Carl Zeiss).

Statistical Analysis

`

Data were presented as mean ± SE. For statistical comparisons between groups, the data were checked for normality distribution and equal variance. If the criteria where met, a t-test was performed to compare two groups; when the criteria were not met, a Mann–Whitney U-test was used. For statistical comparisons across more than two groups, we used the Kruskal–Wallis test (non-parametric One-Way ANOVA) and the Mann–Whitney U-test for group comparisons. In all experiments, the level of statistical significance was defined as $p < 0.05$.

RESULTS

Cre-dependent rabies tracing approach

Naturally occurring rabies virus has been known for its extremely high efficiency in trans-synaptic labeling, as it propagates exclusively between connected neurons by strictly unidirectional (retrograde) transneuronal transfer (Ugolini, 2008, 2011). We take advantage of the ability to target rabies infection to specific cell types using EnvA pseudotyping and limit trans-synaptic spread to direct inputs by using glycoprotein gene-deleted (ΔG) rabies virus and transcomplementation (Wickersham et al., 2007b, Wall et al., 2010). Specifically, ΔG rabies virus (deletion mutant, SAD-B19 strain) is pseudotyped with the avian sarcoma leucosis virus glycoprotein EnvA (EnvA-SADΔG rabies virus), which can only infect neurons that express avian tumor virus receptor A (TVA), an avian receptor protein that is absent in mammalian cells unless provided through exogenous gene delivery. The deletion-mutant rabies virus then can be transcomplemented with the expression of rabies glycoprotein (RG) in the same TVA-expressing cells to enable its retrograde spread restricted to direct presynaptic neurons.

Our current approach was developed based on a Cre-dependent rabies tracing system reported previously, in which a Cre-dependent helper virus (adeno-associated virus, AAV) targets gene expression of both RG and TVA to Cre-expressing cells to assist with subsequent

`

rabies infection and monosynaptic retrograde tracing (Wall et al., 2010). However, there were two issues with the previous system. With the helper virus used in the previous system, there was leaky TVA expression in non-Cre expressing cells. In addition, GFP that is encoded in the viral construct and intended to mark the starter cells failed to fluoresce. In the current system we have corrected both problems. Rather than using a helper AAV to express TVA, we use a Cre-dependent TVA expressing mouse line (Seidler et al., 2008); there is no leaky TVA expression using the mouse line (see below). A functional helper AAV expressing histone-tagged GFP that robustly labels starter cells as well as RG to complement the SADΔG rabies virus and allow trans-synaptic spread.

As illustrated in Fig. 1.1A, specific Cre mouse lines are first crossed with a Cre-dependent TVA expressing mouse line, LSL-R26$^{TVA\text{-}lacZ}$ (Seidler et al., 2008) so that Cre-expressing neurons express TVA (Fig. 1.8), thus restricting initial EnvA-ΔG rabies virus infection to Cre + cells. Then a Cre-dependent AAV virus (the helper virus, AAV8-EF1α-FLEX-HB) with a coding sequence of RG required for trans-synaptic rabies virus retrograde spread as well as nuclear localized histone-GFP, is injected into CA1 of the double transgenic mice (Cre:TVA mice). The AAV-targeted subset of Cre+ cells are identified by their nuclear GFP expression from the AAV genome (Fig. 1.1B, C). Following the AAV injection, a pseudotyped, deletion-mutant rabies virus encoding a red fluorescent protein mCherry (EnvA-SADΔG-mCherry rabies) (Fig. 1.1B) is injected into the same location of the previous AAV injection. EnvA pseudotyped, ΔG-mCherry rabies enters the Cre+ and TVA+ neurons, and replicates its genome with mCherry expression. Using RGs expressed by the helper vector in the Cre+ cells, ΔG-mCherry rabies undergoes transcomplementation (forming new infectious viral particles), and spreads to the presynaptic partners of the Cre+ starter neurons (Fig. 1.1C). Because their

`

presynaptic neurons do not express RGs and the ΔG rabies has no RG-coding sequence in its genome, these presynaptic cells cannot produce infectious rabies virus particles, restricting infection to the targeted cell type and its direct monosynaptic inputs. For control experiments, the Cre:TVA animals are only injected with EnvA-SADΔG-mCherry rabies. As expected, without the helper AAV delivering RGs in Cre+ cells, the ΔG-mCherry rabies cannot spread from Cre+ and TVA+ cells so that in control cases rabies labeling is restricted to Cre+, TVA-expressing cells at the rabies injection site (Fig. 1.9).

After histological processing, brain sections are imaged, and quantitative examinations across hundreds of sections (every one out of three 30-µm thick sections of the whole brain) are conducted for unbiased analyses of rabies-mediated, direct synaptic connections to targeted cell types in hippocampal CA1 (Fig. 1.10). In every case, the first analysis step is to visualize the injection site and assure that GFP and mCherry double-labeled starter cells are restricted to CA1 (Fig. 1.2A, C-D). The starter cells are marked and quantified across sections at and around the targeted injection site. As for the measurement of rabies-labeled presynaptic neurons, every image is examined to identify and mark the locations of mCherry-expressing cell bodies. These labeled cells are assigned to specific anatomical structures, such as different hippocampal subfields, entorhinal cortex and the medial septum for regional input quantification. Thus, through quantitative evaluations of the numbers of targeted postsynaptic (starter) cells and the numbers of their presynaptic cells labeled in various brain structures (Fig. 1.10), we are able to quantify cell type-specific connections in local and long-range circuits and perform cell-type specific circuit analyses over a large scale. Normalization to the numbers of starter cells also controls for variability between animals and mouse lines.

Comparison of monosynaptic inputs to excitatory versus inhibitory CA1 neurons

`

Canonical inputs

We first mapped circuit connections to CA1 pyramidal neurons using Camk2a-Cre (T29) mice (Tsien et al., 1996), in which Cre recombinase expression is largely restricted to CA1 pyramidal cells. In the double-transgenic mice (Camk2a-Cre:TVA), we virally traced circuit connections to a small population of starter CA1 pyramidal cells (N = 109.6 ± 16.7 per animal across 5 cases), which are unambiguously identified by their GFP and mCherry expression from the helper AAV and ΔG-mCherry rabies genomes, respectively (Fig. 1.2 A, C-D). Typically, for each representative case (as shown in Fig. 1.10), the total number of labeled CA3 cells following rabies infection of CA1 excitatory cells was measured between 3000 and 4500, while the overall number of labeled neurons across different regions was estimated to be ~ 9000, indicating that trans-synaptic rabies labeling is reasonably efficient. Strong labeling of individual neurons presynaptic to CA1 excitatory neurons is seen in ipsilateral and contralateral CA3 (Fig. 1.2A, B). Essentially all the labeled CA3 cells are located in stratum pyramidale (SP), and morphologically and neurochemically confirmed to be excitatory neurons (Fig. 1.11A, B). The input connection strength index (CSI) (defined as the ratio of the number of presynaptic neurons versus the number of starter neurons) between CA3 and CA1 excitatory cells is 7.10 ± 0.28 and 3.44 ± 0.22 (mean ± SE, averaged across 5 animals) for ipsilateral and contralateral CA3, respectively (Table 1.1A). There are putative inhibitory cells labeled outside the pyramidal cell layer of ipsilateral CA3 (Fig. 1.2A), accounting for a CSI of 0.13 ± 0.03. Almost none of the labeled contralateral CA3 cells are inhibitory.

Local inhibitory interneurons, identified based on their laminar locations and morphology, are also labeled in ipsilateral CA1 with a CSI of 3.26 ± 0.39 for putative inhibitory cells outside CA1 pyramidal cell layer. We did not quantify the labeled inhibitory cells in the

`

pyramidal cell layers due to masking by strong excitatory cell labeling. There are some putative pyramidal cells labeled in ipsilateral CA2 and fewer in contralateral CA2, with their CSIs being 0.47 ± 0.10, and 0.07 ± 0.01, respectively. While contralateral CA1 pyramidal cells provide input with a CSI of 0.54 ± 0.17, few putative inhibitory cells in contralateral CA1 are labeled (CSI = 0.01 ± 0.004). Thus CA1 excitatory cells receive much stronger local inhibition than long-rang inhibition. Robust labeling is also seen in very distant structures such as the medial septum and diagonal band (MS-DB) area (about 3mm anterior to the CA1 injection site) and entorhinal cortex (EC, about 3 mm posterior to the CA1 injection site) (Fig. 1.2H, I, J). The labeled entorhinal cells are excitatory neurons, mostly located in layer 3. The connection strength of ipsilateral EC is much stronger than contralateral EC, with their CSIs being 0.54 ± 0.08 and 0.01 ± 0.01 ($p < 0.01$), respectively.

Additionally, following viral tracing in Camk2a-Cre:TVA mice (as well as in other Cre:TVA mice), there is scarce retrograde labeling of neurons in areas known to weakly project to hippocampal CA1 using conventional tracing techniques (Somogyi and Klausberger, 2005). These areas include amygdala, reuniens thalamic nucleus and the raphe nucleus. Note that despite weak inputs, rabies labeling of these neurons is as equally clear as those providing strong synaptic inputs due to self-replication of rabies viral cores in presynaptic neurons and subsequent strong expression of mCherry (Wickersham et al., 2007a).

We then mapped circuit connections to a mixed population of CA1 inhibitory neuron types using Dlx5/6-Cre mice (Monory et al., 2006), in which selective Cre expression is targeted to forebrain GABAergic neurons. As expected, spatially restricted AAV and EnvA rabies viral injections infected a small population of different inhibitory cells located in different CA1 laminae (Fig. 1.3A, C, D; Fig. 1.9), with the average numbers of starter cells being 47.75 ± 9.48,

`

38.35 ± 2.59, 11.25 ± 4.40, and 9.75 ± 4.53 (N = 4 cases, Table 1.1B) for stratum oriens (SO), stratum pyramidale (SP), stratum radiatum (SR), and stratum lacunosum-moleculare (SLM), respectively. These mixed CA1 inhibitory cell types have strong input connections from putative excitatory cells located in SP of CA1 with a CSI of 9.72 ± 0.49. Overall CA1 inhibitory neurons have a similar connectivity pattern of extrinsic CA1 sources to that of excitatory pyramidal cells, but with differing connection strengths (Fig. 1.12A; Table 1.1A, B). The CSIs of inhibitory cell types for ipsilateral CA2, ipsilateral and contralateral CA3 are 0.17 ± 0.01, 1.63 ± 0.37 and 0.60 ± 0.18, respectively, which differ significantly from those of pyramidal cells ($p < 0.05$ for each comparison). Whereas excitatory connection strength of contralateral CA1 tends to be greater for these inhibitory cells compared with that of pyramidal cells, entorhinal cortex appears to have weaker connections to inhibitory cells (ipsilateral EC CSI: 0.21 ± 0.15).

Non-canonical subicular inputs to both CA1excitatory and inhibitory neurons

Although it is generally believed that there is no direct back-projection from the subiculum to CA1 (however, see (Berger et al., 1980, Kohler, 1985)), our tracing data show that a significant number of subicular cells are retrogradely labeled by rabies tracing from either CA1 pyramidal neurons or inhibitory neurons (Fig. 1.2E, 1.3E). We also determined that there are both excitatory and inhibitory subicular cells labeled as determined from their morphology and confirmed using immunochemical staining. Overall, the labeled subicular cells have a connection strength index of 0.81± 0.01 and 1.00 ± 0.20 for these CA1 cell types, respectively.

To further understand the nature of this under-described subiculum-CA1 pathway, we performed neurochemical characterization of rabies labeled subicular cells to examine the potential difference of subicular excitatory versus inhibitory cells projecting to different CA1 cell types. Double immunochemical staining against excitatory amino acid transporter

`

type1(EAAC1) and GABA allowed for identification of glutamatergic or GABAergic CA1-projecting subicular cells in Camk2a-Cre:TVA and Dlx5/6-Cre:TVA sections (Fig. 1.4A-D). Interestingly, glutamatergic and GABAergic percentages of labeled subicular cells are similar for Camk2a-Cre:TVA and Dlx5/6-Cre:TVA cases with about 58% of CA1-projectinig subicular neurons being glutamatergic neurons, and about 36% of them being GABAergic neurons (Fig. 1.4E). This indicates no preferential subicular innervation of CA1 excitatory or inhibitory neurons.

Neurochemical specific septohippocampal inputs to CA1

As the MS-DB region contains cholinergic, GABAergic and glutamatergic neurons, we are interested in examining whether all these neurochemical specific MS neurons have cell-type specific preferences in innervating CA1 excitatory versus inhibitory cell types. Septohippocampal connections of cholinergic and GABAergic MS cells have been examined in highly localized hippocampal microcircuits using conventional anatomical tracing combined with electron microscopy (Freund and Antal, 1988, Gulyas et al., 1990). As septohippocampal circuit connections of more recently described glutamatergic MS-DB neurons are much less understood than cholinergic and GABAergic MS cells (Colom et al., 2005, Manseau et al., 2005, Huh et al., 2010), we also would like to examine whether glutamatergic MS neurons have direct, monosynaptic connections to CA1 neurons using rabies tracing.

Consistent with the previous studies, our rabies tracing indicates that MS-DB neurons provide significant inputs to CA1 (Fig. 1.2 and 1.3). For Camk2a-Cre:TVA cases, the overall CSI for MS-DB neurons to CA1 excitatory starter cells is 0.95 ± 0.05, while for Dlx5/6-Cre:TVA cases, the overall CSI for MS-DB neurons to CA1 inhibitory starter cells is 1.17 ± 0.18. Our data show that cholinergic and GABAergic septohippocampal cells differentially

`

innervate CA1 excitatory and inhibitory cell types, and MS-DB glutamatergic neurons also directly innervate CA1 neurons (Fig. 1.5). In conjunction with immunochemical examinations, for Camk2a-Cre:TVA cases we found that 66% of rabies-labeled septohippocampal cells are cholinergic (Fig. 1.5A-D), and that 27% of the labeled septohippocampal cells are GABAergic (Fig. 1.5J). Therefore GABAergic neurons comprise a significant portion of the septal input to CA1 excitatory neurons. We also found that septohippocampal glutamatergic neurons only account for 7% of rabies labeled cells in MS-DB in Camk2a:TVA cases (Fig. 1.5J). In contrast, for Dlx5/6-Cre:TVA cases, a great majority of the labeled septohippocampal cells in the MS region innervating CA1 inhibitory neuron are GABAergic (67%), while cholinergic and glutamatergic MS neurons account for 12% and 21% of the total labeled cells, respectively (Fig. 1.5E-I, K).

Comparison of monosynaptic inputs to PV+ versus SOM+ inhibitory CA1 neurons

Given the diversity of inhibitory cells targeted using Dlx5/6-Cre mice, we further examined whether specific sub-groups of inhibitory cells in CA1, targeted by using PV-Cre and SOM-Cre mice, have differential circuit connections. The PV+ and SOM+ inhibitory cell types were examined because they are most numerous and functionally important in the cerebral cortex including the hippocampus (Freund and Buzsaki, 1996, Xu et al., 2010). Compared with Camk2a-Cre:TVA and Dlx5/6-Cre:TVA cases, the total starter cells are fewer in PV-Cre:TVA and SOM-TVA cases, as expected due to the restriction of Cre-dependent gene expression to targeted subpopulations (Fig. 1.8 and 1.9). The average numbers of PV+ starter cells found in SO, SP, SR and SLM are 11.4 ± 1.21, 17.8 ± 1.59, 1.2 ± 0.58 and 0 (N = 5 cases; Table 1.1C), respectively, while the average numbers of SOM+ starter cells found in SO, SP, SR and SLM are 52.6 ± 11.73, 3.2 ± 1.2, 1.4 ± 0.75 and 0.2 ± 0.2, respectively (N = 5 cases; Table 1.1D).

`

Immunostaining of PV and SOM validated chemical identities of starter cells in the PV-Cre:TVA and SOM-Cre:TVA mouse, respectively (Fig. 1.11C-F). Most of SOM+ cells labeled by rabies display O-LM cell morphology (Fig. 1.9E, K), as their cell bodies and horizontal dendrites are located in stratum oriens but their axons ascend through SP and SR to branch heavily in SLM, which contains distal dendrites and apical tufts of pyramidal neurons. The axons of O-LM cells with strong mCherry expression clearly form a prominent band in SLM.

Although the input connection pattern of PV+ inhibitory neurons mapped using the PV-Cre: TVA mouse generally resemble that of mixed types of inhibitory cells observed with Dlx5/6-Cre:TVA mice (Fig. 1.6A-B, E-H; Table 1.1C; Fig. 1.12B), SOM+ inhibitory neurons targeted using the SOM-Cre: TVA mouse have a different pattern of circuit connections (Fig. 1.6 C-D, I-L; Table 1.1D; Fig. 1.12B). SOM+ cells have predominant excitatory connections from within ipsilateral CA1 with few CA3 inputs and little entorhinal input. The CSIs of SOM+ cells for ipsilateral and contralateral CA3 are 0.41 ± 0.12 and 0.11 ± 0.05, respectively, which are much less than those of PV+ cells (2.97 ± 0.37 and 0.72 ± 0.10, respectively) ($p < 0.001$ for either comparison). On average, CA1 excitatory input connections to PV+ and SOM+ cells are comparable to those of Dlx5/6-Cre cells, with their CSIs being 9.46 ± 0.36, 9.13 ± 0.54, respectively. Both PV+ cells and SOM+ cells in CA1 have input connections from the subiculum, with their CSIs being 0.69 ± 0.16 versus 1.24 ± 0.31, respectively. In addition, PV+ cells have a greater input connection strength of MS-DB compared with SOM+ cells (CSIs: 2.12 ± 0.2 versus 1.07 ± 0.16, $p < 0.05$). PV+ cells also have a greater CSI of MS-DB than excitatory and mixed inhibitory cell types ($p < 0.05$ for either comparison).

Our results above demonstrate that the Cre-dependent rabies-based system can target selected cell groups in hippocampal CA1 and effectively label their monosynaptic connections in

`

the intact brain. The tracing data allow for determination of the relative weight of the distributed synaptic connections to these cell groups in the large circuit context of the entire brain, which helps to evaluate hypotheses about differential functions of these selected cell groups/types (see below).

LSPS local circuit mapping supports rabies tracing

As rabies tracing is a new method for anatomical examination of circuit connections to small Cre-defined neuronal populations in hippocampal CA1, we followed up with circuit mapping using LSPS which allows functional mapping of local synaptic inputs to identified cell types. The LSPS method has been previously used in the neocortex and hippocampus (Brivanlou et al., 2004, Xu and Callaway, 2009, San Antonio et al., 2014). Under our experimental conditions, this method has a sufficient spatial resolution to map synaptic inputs to CA1 cells from specific hippocampal subfields (Fig. 1.13A-B).

We conducted photostimulation mapping experiments to examine intrahippocampal excitatory circuit connections to excitatory pyramidal cells, PV+/FS basket cells and SOM+ O-LM inhibitory cells. LSPS mapping data confirmed cell-type specific differences of intra-hippocampal circuit connections as identified in rabies tracing-based circuit mapping. Targeted recordings of inhibitory neurons were facilitated by using transgenic mouse lines expressing GFP in inhibitory neurons (Oliva et al., 2000, Tamamaki et al., 2003, Xu and Callaway, 2009) (Fig. 1.14). As illustrated in Fig. 1.13C, the LSPS approach involves recording from single neurons, then stimulating at surrounding sites on the LSPS mapping grid in order to generate action potentials from neurons in those sites, thus providing an input map for the recorded neuron based on activation of presynaptic inputs. We found that CA1 pyramidal cells receive a great majority of excitatory input from extensive CA3 locations, while having weak inputs from CA2 and from

`

within CA1 (Fig. 1.7A, D). PV+/FS basket cells receive strong excitatory input from both CA3 and CA1, as well as some input from CA2 (Fig. 1.7B, D). In contrast, O-LM cells receive all of their excitatory inputs exclusively from within CA1 (Fig. 1.7C, D). Generally, the differences in pattern and amplitudes of excitatory inputs to these cell types revealed by LSPS mapping experiments verify cell-type specific intrahippocampal connections to Camk2a-Cre, PV-Cre and SOM-Cre cell groups observed with rabies tracing. However, as the LSPS method allows high resolution mapping of local functional input to identified cell types within the Cre-defined cell groups targeted by the rabies tracing, it is capable of detecting more detailed features in intrahippocampal excitatory inputs at the level of more precise cell types. For example, although strong excitatory connections within CA1 of PV+/FS cells fit well with rabies tracing results, PV+/FS basket cells receive equally strong CA3 excitatory input as pyramidal cells (Fig. 1.7D), which reflects stronger CA3 excitatory connections than the overall PV+ cell group targeted by rabies tracing in PV-Cre:TVA mice (Table 1.1). Similarly, as a subtype of SOM+ cells, O-LM cells show more localized excitatory connections than the overall SOM cell group targeted by rabies tracing in SOM-Cre:TVA mice (Table 1.1).

Furthermore, the LSPS mapping provided functional information such as the amplitudes and numbers of excitatory postsynaptic current (EPSC) events (Fig. 1.7D, E), which complements anatomical rabies tracing. Excitatory cells, PV+ basket cells and O-LM cells appear to have relatively similar amplitudes of individual EPSCs, but EPSCs of excitatory cells are less frequent with longer durations in response to presynaptic photostimulation compared to those of PV+ basket cells and O-LM cells (Fig. 1.7A-C, E). This indicates these cell types have differential synaptic contacts, kinetics and connection probabilities of presynaptic neurons.

DISCUSSION

`

Technical considerations

We have combined transgenic mouse technology and recently developed monosynaptic rabies virus-based tracing techniques (Wickersham et al., 2007b, Wall et al., 2010) for mapping cell type specific circuit connections to hippocampal CA1 in a quantitative manner in the intact brain. This method restricts initial infection and subsequent complementation of EnvA-ΔG rabies viruses to a small population of Cre-defined specific cell types and enables robust monosynaptic retrograde spread of ΔG rabies from these targeted cells to their direct presynaptic cells in local and distant brain structures. We believe that the complemented virus in the starter cell can cross all input synapses with equal efficiency, as previous studies have established that rabies virus receptors are ubiquitously distributed within the CNS and all neuronal populations of the same synaptic order are infected regardless of their neurotransmitters, synaptic strength, and distance (Ugolini, 2011). This is evidenced by consistent labeling of neurons in ipsilateral and contralateral CA3 and no trans-synaptic spread to dentate granule cells, which directly project to CA3 but not CA1. This new approach makes it possible to identify the sources and cell types providing direct monosynaptic input to any Cre-defined population in various mouse lines. However, as Cre mouse lines are crossed to the TVA mouse, all Cre+ cells expressing TVA can be directly infected by local injection of EnvA-ΔG rabies, thus making it difficult to examine local connections between Cre+ starter cells and other Cre+ cells at the injection site. Nevertheless, local circuit connections to specific cell types can be examined more precisely with other methods such as LSPS.

Our data indicate that the current system of rabies labeling works in a non-biased fashion. The new method of rabies labeling is reliable as labeled cells are seen in very distant structures such as the MS-DB area (about 3mm anterior to the CA1 injection site) and other areas (e.g.,

`

amygdala, reuniens thalamic nucleus and the raphe nucleus) known to weakly project to hippocampal CA1. However, we do not expect that the method that we use label every input to each neuron. But this limitation does not mean that our method is not useful or not effective. As rabies labels inputs to different cell types in a similar manner, we assess the relative numbers of inputs from each source onto each target cell type, and quantify the numbers of cells that are labeled at various input locations following rabies virus infection of different types of postsynaptic cells in CA1. Different from single cell targeting, this approach benefits from targeting a small population of Cre+ postsynaptic cells and can provide weighted connection strengths for defined cell types. Because the number of postsynaptic starter cells and the numbers of direct presynaptic labeled cells in specified structures across the entire brain can be quantitatively determined, this approach allows for assessment of relative abundance of connected populations. Specifically, we measure the connection strength index (CSI) which is defined as the ratio of the number of presynaptic neurons versus the number of starter neurons and reflects a comparative number of presynaptic cells labeled by rabies in each region. Thus, this approach enables us to address the proposed questions of whether or how the different sources of input to CA1 are distributed in different strengths onto each of its constituent cell types.

Major extrinsic inputs to different CA1 cell types.

Our results both confirm previous findings, validating the new methods that we use, and also go on to extend those findings to reveal new details about the sources of input to various CA1 cell types. Our rabies tracing of circuit connections to excitatory and inhibitory cell types show that major extrinsic inputs to CA1 innervate both principal cells and interneurons in differential weights according to the pathways and cell types. Based on our quantification of

`

input connection strengths, we confirm the strongest excitatory input to the CA1 area is from CA3 via the Schaffer collaterals/commissural input (Amaral and Witter, 1989, Wittner et al., 2006, Takacs et al., 2012). We also show its differential innervations of excitatory cells and interneurons, with excitatory cells having about 4-5 fold greater input connection strength over mixed inhibitory cell types. Compared to CA3 Schaffer / commissural inputs, the temporoammonic pathway (the monosynaptic pathway originating from EC layer 3 to CA1), is weak to both excitatory and inhibitory cell types. However, entorhinal innervation of excitatory cells is still significantly greater than inhibitory cell types. Overall, the comparative input strengths of CA3 - CA1 and entorhinal - CA1 monosynaptic pathways to excitatory neurons appear to be related to differential operations of these functionally distinct circuits. The entorhinal - CA circuit is required for long-term spatial memory consolidation and maintenance (Brun et al., 2002, Remondes and Schuman, 2004, Brun et al., 2008) (however see (Suh et al., 2011)) and nonspatial temporal association (Suh et al., 2011) , while the trisynaptic pathway including intact CA3 - CA1 connectivity is required for rapid new learning, pattern completion-based memory recall (Nakashiba et al., 2008, Nakashiba et al., 2009).

Interestingly, the rabies tracing shows non-canonical inputs from the subiculum to CA1 excitatory and inhibitory cell types, in contrast to the general belief of unidirectional information flow from CA1 to the subiculum. The data establish the existence of a subicular-CA1 back projection pathway in the mouse as previously indicated in other mammalian species (Berger et al., 1980, Kohler, 1985, Shao and Dudek, 2005). Furthermore, we have found that both subicular excitatory and inhibitory cells project back to CA1, and that the proportions of subicular excitatory versus inhibitory cells projecting to either CA1 excitatory or inhibitory neurons are

`

similar. These findings may have functional implications about how subicular neurons modulate their CA1 input resources.

Our rabies tracing has further provided information on neurochemical specific septo-hippocampal inputs. Consistent with previous reports with more traditional approaches, we find that CA1 excitatory cells receive a great majority (~66%) of MS-DB innervation from cholinergic cells. But CA1 excitatory cells also receive significant GABAergic septohippocampal innervation (~27%) which has not been explicitly examined (Freund and Antal, 1988, Gulyas et al., 1990). In comparison, CA1 inhibitory cell types receive much less cholinergic MS-DB innervation (~12% of the total labeled MS-DB cells) and much stronger GABAergic septohippocampal innervation (~67%). Although glutamatergic MS-DB cells are known to exist (Colom et al., 2005, Manseau et al., 2005, Huh et al., 2010), rabies tracing firmly establishes direct glutamatergic septohippocampal connections to CA1. Compared to CA1 excitatory neurons, CA1 inhibitory neurons receive much stronger glutamatergic septohippocampal projections (~21% vs. 7%). These new findings can have functional implications in understanding septo-hippocampal circuit operations which are likely to be dictated by differential neurochemical interactions between medial septum and CA1 excitatory and inhibitory cell types (Huh et al., 2010).

Functional implications of inhibitory cell type specific connectivity

Different types or groups of inhibitory neurons coordinate or interact with excitatory neurons in space and time; they are believed to differentially contribute to regulation of circuit dynamics and network oscillations (Glickfeld and Scanziani, 2006, Freund and Katona, 2007, Klausberger and Somogyi, 2008). Although functional differences have been measured (Klausberger and Somogyi, 2008), the mechanisms that underlie different activation patterns of

`

distinct inhibitory cell types have not been understood. In the present study, mapping local and more distant circuit connections to specific inhibitory cell types should help us to further understand the contribution of circuit connection differences of specific inhibitory neurons to their functional differences. In particular, we have examined all the potential input sources to specific CA1 neuron types and presented new information on circuit connections to excitatory neurons, mixed inhibitory cells and PV+ and SOM+ cells in CA1, which could not be examined to this scale in the past.

Within the context of previous literature, our new data provide insights into differential circuit mechanisms of inhibitory neuronal control of hippocampal excitatory neurons in terms of their local and long-range input sources. It has been known that inhibitory cells can regulate excitatory cell activity via feedforward and feedback inhibitory mechanisms (Freund and Buzsaki, 1996, Freund and Katona, 2007). Although past studies performed degeneration or stimulation of the known afferents to examine synaptic inputs to identified CA1 inhibitory neuron types (Blasco-Ibanez and Freund, 1995, Ali and Thomson, 1998, Glickfeld and Scanziani, 2006), specific input sources to inhibitory interneurons remain to be further investigated. Now we are able to identify global input sources to mixed inhibitory cell types, PV+ inhibitory cells and SOM+ inhibitory cells with the rabies method, which are confirmed by the LSPS method for intrahippocampal connections. CA1 PV+ and SOM+ interneurons show similar strengths of input from the subiculum, but PV+ cells have a greater strength of MS input than SOM+ cells. PV+ cells have strong excitatory connections from other input source such as CA3 and entorhinal cortex, while having strong CA1 excitatory connections as well. In contrast, the tracing data indicate that SOM+ cells receive predominant excitatory connections within CA1, and do not receive much input from CA3 or entorhinal cortex. Thus, compared to SOM+

`

cells, PV+ inhibitory cells are apparently a primary mediator of feedforward inhibition from the longer distance input sources. In fact, the differential circuit connections of PV+ and SOM+ inhibitory cells in CA1 are analogous to those cell types in layer 4 of primary sensory cortex, in which PV+/FS cells, but not SOM+ cells receive strong thalamocortical inputs (Gibson et al., 1999, Cruikshank et al., 2007). Similarly PV+/FS cells in cortical layer 2/3 receive strong feedforward and recurrent excitation from layers 4 and 2/3 respectively, while SOM cells receive stronger input from layer 2/3 than layer 4 (Xu and Callaway, 2009). These observations suggest that the differential roles of PV+ versus SOM+ cells in mediating feedforward versus feedback inhibition are conserved between hippocampal cortex and neocortex. Taken together with previous studies, these salient features of specific inhibitory circuit connections are important for inhibitory neuronal functions.

`

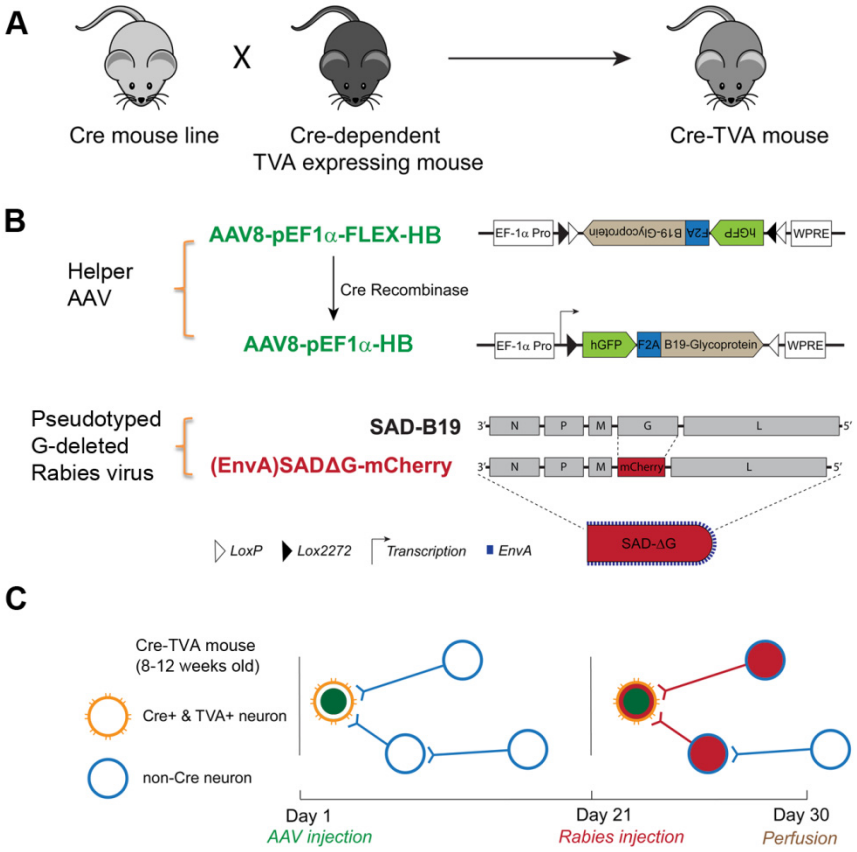

Figure 1.1. Cre-dependent rabies tracing approach. (A) A mouse transgenic line that expresses Cre in specific type/group of hippocampal neurons is first crossed with the Cre-dependent TVA expressing mouse line, LSL-R26$^{TVA\text{-}lacZ}$ (Seidler et al., 2008) to target gene expression and control initial rabies virus infection. (B) The AAV helper virus and EnvA pseudotyped G-deleted rabies virus are used for circuit tracing. Using the AAV8-pEF1α-FLEX-HB (H: nuclear localized histone GFP; B: B19 rabies glycoprotein, RG), the initial AAV injection (0.1 µL, spatially restricted in CA1) allows for expression of RG and GFP transgenes after Cre-recombinase mediated activity in Cre-expressing neurons. The second injection delivers 0.1 µL EnvA-SADΔG-mCherry (ΔG: RG deleted, mCherry: a red fluorescent protein) into the same location of the previous AAV injection. (C) Timeline of viral injections and schematic illustration of rabies-mediated monosynaptic retrograde labeling. Green indicates GFP expression from the helper AAV genome, labeling the rabies receptive target cells while red indicates mCherry expression from SADΔG-mCherry rabies genome in the target cells (starter cells) and their first-order presynaptic neurons. The starter cells are identified as GFP and mCherry double-labeled. At 9 days after the rabies injection, the animal is perfused with 4% paraformaldehyde and the brain extracted for histological processing.

`

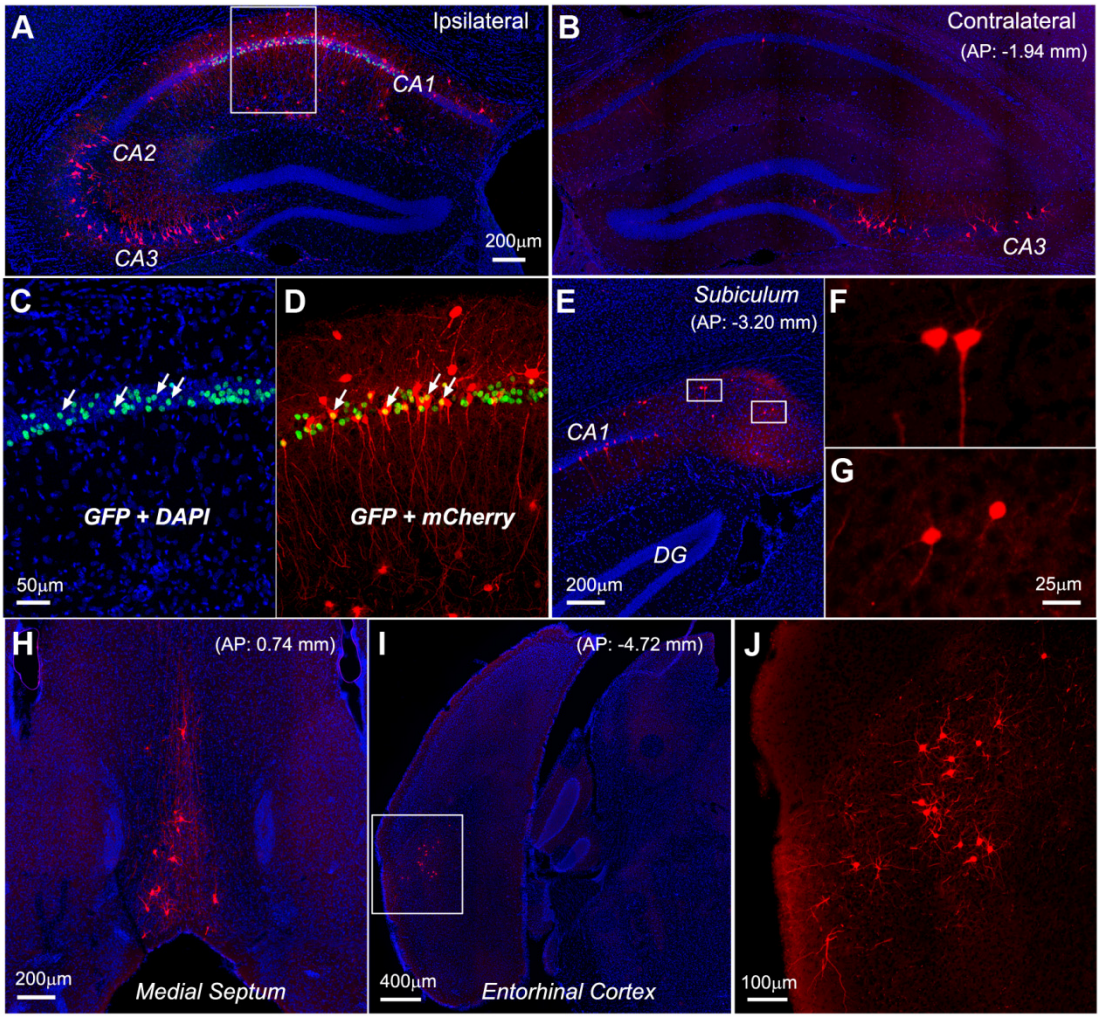

Figure 1.2. Rabies labeling of presynaptic neurons shows direct local and more distant circuit connections to CA1 excitatory pyramidal cells in Camk2a-Cre: TVA mouse hippocampus. (A-B) Ipsilateral and contralateral hippocampal images of the viral injection site. Strong rabies-mediated labeling of putative excitatory neurons is seen in both ipsilateral and contralateral CA3. Local CA1 inhibitory neurons outside stratum pyramidale are also labeled. (C-D) An enlarged view of the white box in A, with GFP and DAPI overlay in C showing restricted AAV-mediated infection and gene expression in stratum pyramidale, and with GFP and mCherry overlay in D showing the GFP-mCherry double labeled starter cells (indicated by the arrows in C and D). (E-J). Rabies-labeled (mCherry-expressing) presynaptic neurons (distant from the injection site) are seen in the subiculum, the medial septum and diagonal band (MS-DB) area, and entorhinal cortex, respectively. F and G show the enlarged view of the two white-boxed regions in E, while J shows the enlarged view of the white-boxed region in I. AP numbers indicate the positions of the coronal sections relative to the bregma landmark.

`

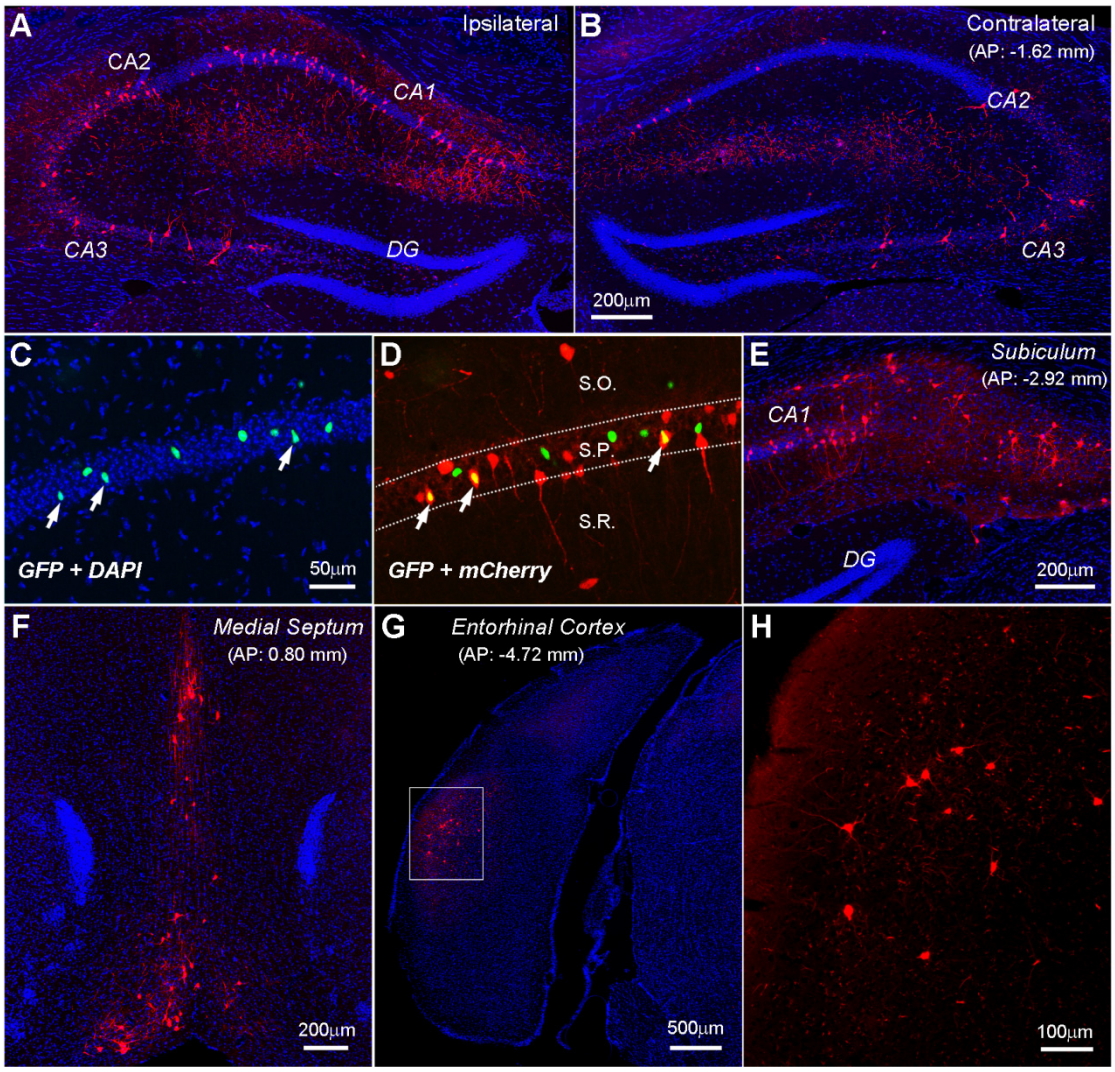

Figure 1.3. CA1 inhibitory neurons targeted using the Dlx5/6-Cre: TVA mouse and CA1 excitatory pyramidal cells have similar patterns of input circuit connections. (A-B) Ipsilateral and contralateral hippocampal images close to the viral injection site. Rabies-mediated labeling of putative excitatory neurons is seen in both ipsilateral and contralateral CA3, as well as in CA2 in these sections. (C-D) An enlarged view of a section at the injection site (AP: -1.94 mm), showing DAPI staining and GFP expression from the helper AAV both in and outside stratum pyramidale in C, and with the GFP and mCherry overlay in D showing the GFP-mCherry double labeled starter cells (indicated by the arrows in C and D). (E-G). Rabies-labeled presynaptic neurons in the subiculum, the medial septum and diagonal band area, and entorhinal cortex, respectively. H shows the enlarged view of the white-boxed region in G.

`

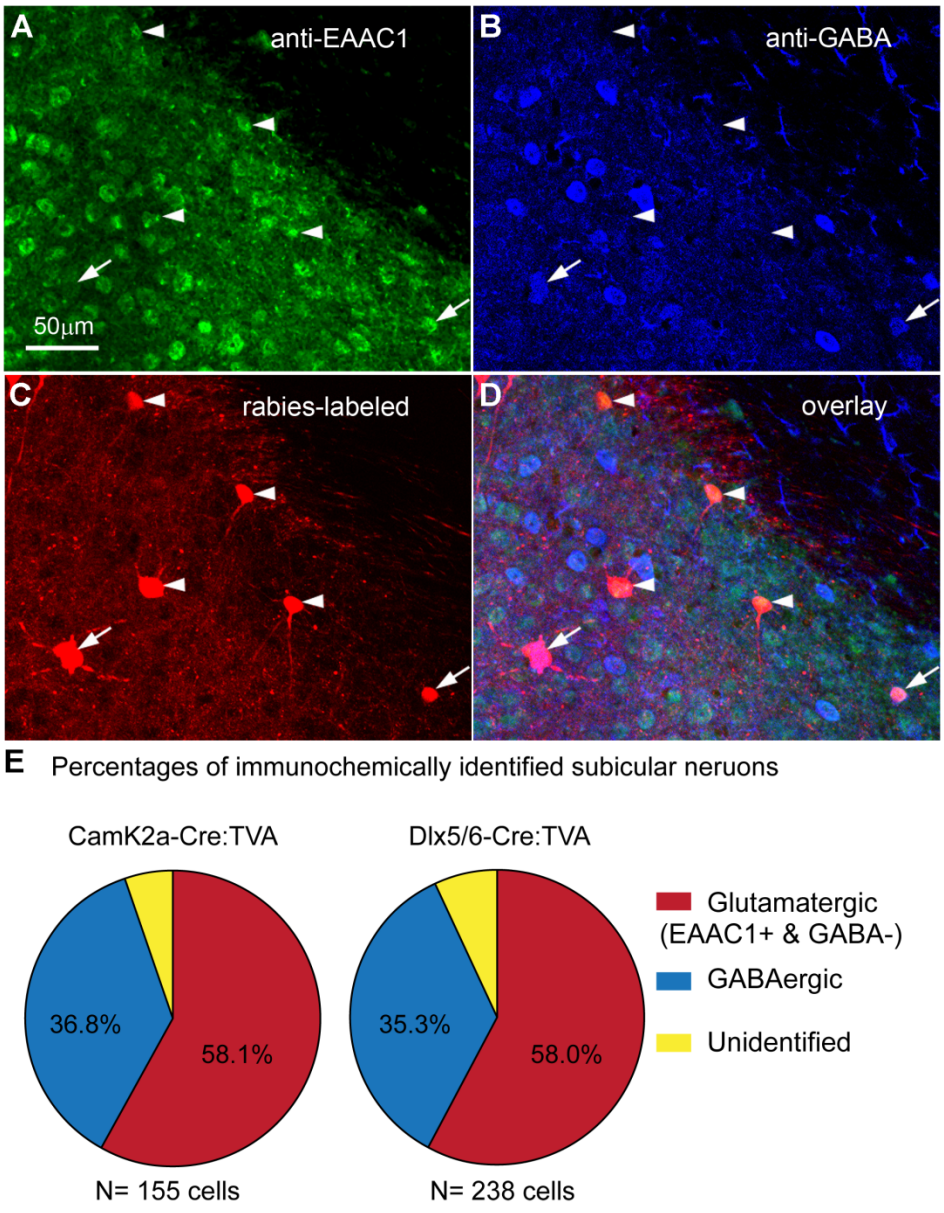

Figure 1.4. Immunochemical characterization and quantification of rabies-labeled CA1-projecting subicular neurons. (A-D) Immunostaining of excitatory amino acid transporter type1 (EAAC1) and GABA in brain slices with rabies-labeled subicular neurons from a Camk2-Cre: TVA case, in which the immunoreactivity of EAAC1, GABA and rabies mCherry expression is shown in green, blue (pseudocolor from AF647-conjugated secondary antibody), red, respectively. For the rabies-labeled neurons, the arrows point at subicular GABAergic neurons (GABA+) while glutamatergic neurons (EAAC1+ and GABA-) are pointed at by the arrowheads. Note that many GABAergic neurons also show strong EAAC1 staining (Conti et al., 1998). (E) Quantification of rabies-labeled, immunochemically identified subicular glutamatergic (excitatory) neurons and GABAergic inhibitory neurons. There are a small

`

percentage of rabies labeled cells that were neurochemically unidentified, as they did not show robust staining against EAAC1 or GABA.

`

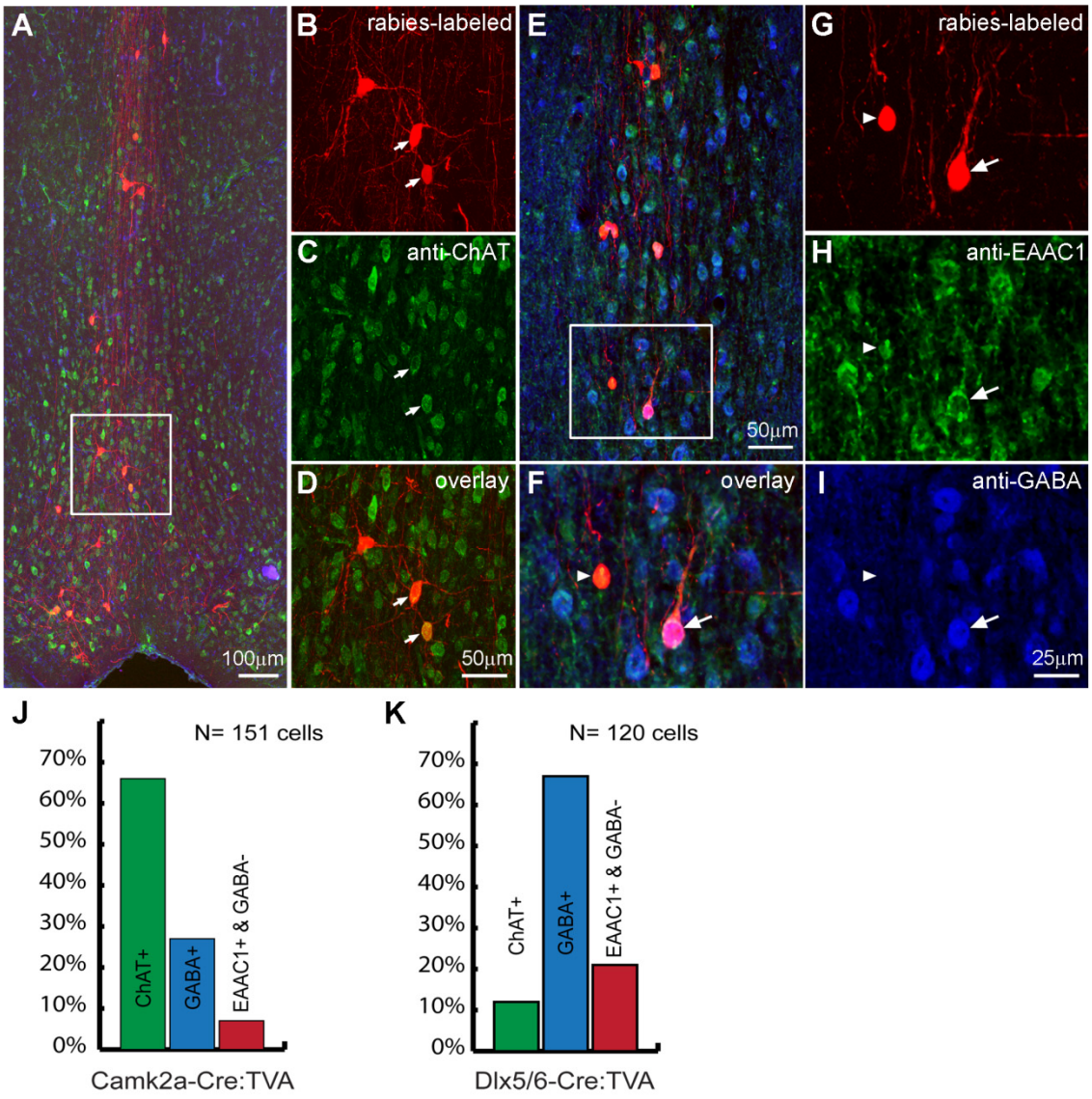

Figure 1.5. Neurochemical characterization and quantification of rabies-labeled neurons in medial septum and diagonal band of broca complex (MS-DB) presynaptic to CA1 excitatory and inhibitory neurons. (A) Immunostaining of choline acetyltransferase (ChAT) in brain slices with rabies-labeled medial septum neurons from Camk2a-Cre: TVA case to identify septal cholinergic neurons. (B-D) Enlarged view of the region indicated by the white box in A which immunoreactivity of ChAT shows in green, and rabies mCherry shows in red. Arrows point at medial septum cholinergic neurons labeled by rabies virus. (E) Immunostaining of EAAC1 and GABA in brain slices with rabies-labeled medial septum neurons from Dlx5/6-Cre: TVA case to identify septal GABAergic and glutamatergic neurons. (F-I) Enlarged view of the region indicated by the white box in E. The immunoreactivity of EAAC1, GABA and rabies mCherry expression is shown in green, blue (pseudocolor from AF647-conjugated secondary antibody), red, respectively. For rabies-labeled neurons, the arrows point at medial septum

`

GABAergic neurons (GABA+), while glutamatergic neurons (EAAC1+ and GABA-) are pointed at by the arrowheads. (J-K) Quantification of rabies-labeled, immunochemically identified MS-DB cholinergic, GABAergic, and glutamatergic neurons in both Camk2-Cre: TVA and Dlx5/6-Cre: TVA cases.

`

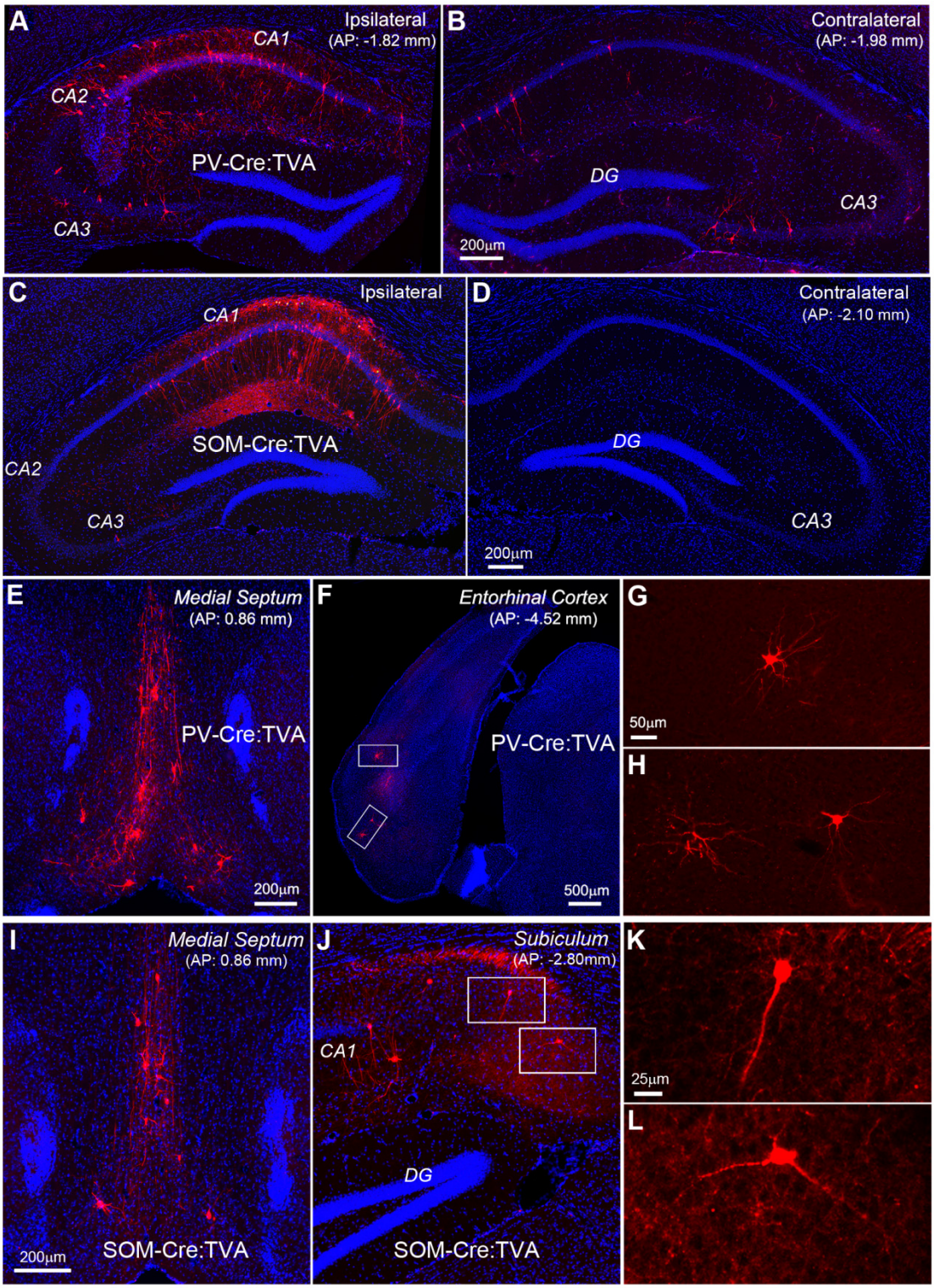

Figure 1.6. Comparison of circuit input connections between parvalbumin-expressing (PV+) inhibitory neurons and somatostatin-expressing (SOM+) inhibitory neurons. PV+ cells are targeted using the PV-Cre: TVA mouse, while SOM+ cells are targeted using the SOM-Cre: TVA mouse. (A-B) A PV-Cre: TVA case. Ipsilateral and contralateral hippocampal images

`

close to the viral injection site. Rabies-mediated labeling of putative excitatory neurons is seen in both ipsilateral and contralateral CA3, as well as in contralateral CA1 in the section. (C-D) A SOM-Cre:TVA case. Ipsilateral and contralateral hippocampal images around the viral injection site. Rabies labeling is predominately found throughout ipsilateral CA1, while no or little labeling is found in contralateral hippocampus**.** Rabies-mediated labeling of putative excitatory neurons is seen in stratum pyramidale of ipsilateral CA1. (E-F) Examples from the PV-Cre: TVA case. Rabies-labeled presynaptic neurons in the medial septum and diagonal band area, and entorhinal cortex, respectively. (G-H) The enlarged view of the two white-boxed regions in F. (I-J). Examples from the SOM-Cre:TVA case. Rabies-labeled presynaptic neurons in the medial septum and diagonal band area, and the subiculum, respectively. (K-L) The enlarged view of the two white-boxed regions in G. Note that there is no or little labeling in entorhinal cortex.

`

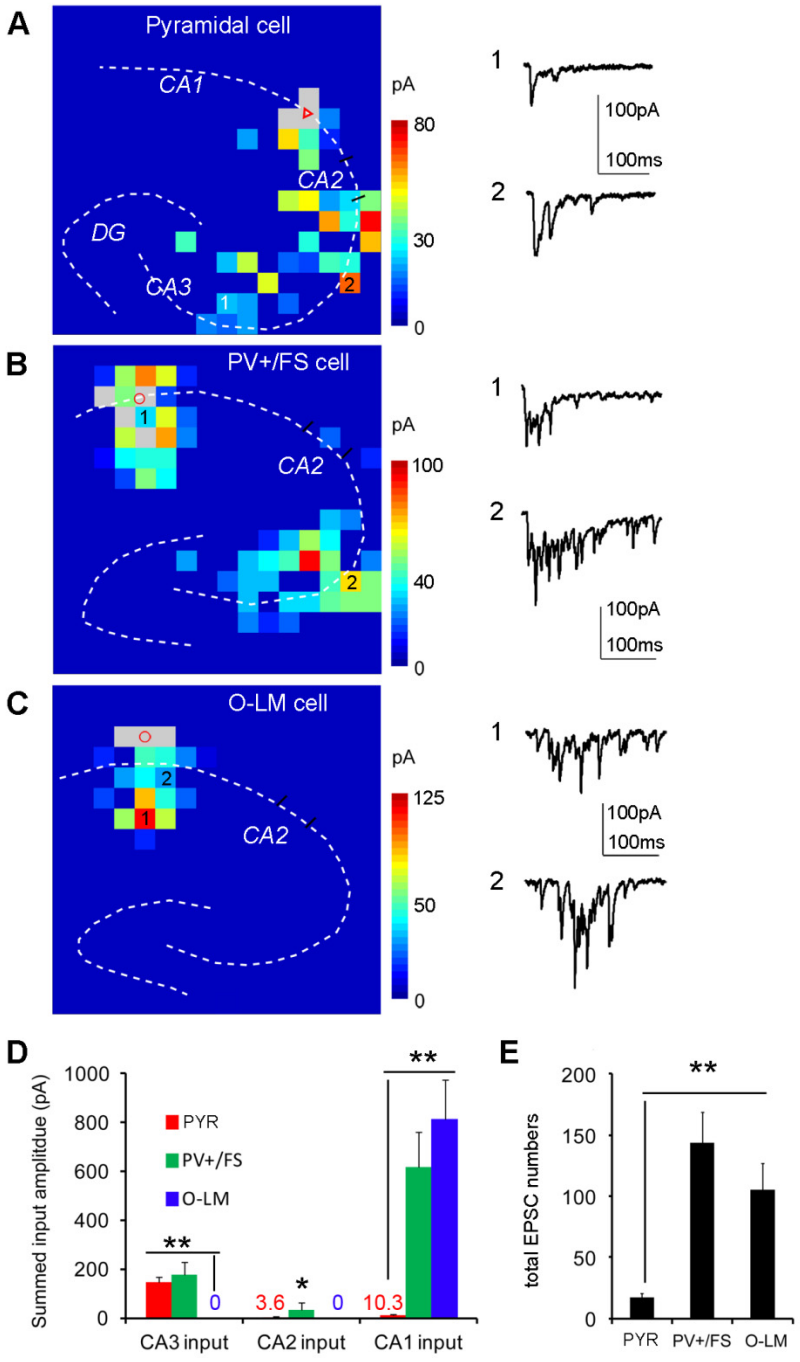

Figure 1.7. Laser scanning photostimulation (LSPS) mapping functionally verifies rabies tracing in identifying cell-type specific differences of intra-hippocampal circuit connections. (A) A color-coded, averaged input map (with each square corresponding to one stimulation site) superimposed with the hippocampal contour, illustrating the pattern and strength of synaptic inputs to a recorded excitatory pyramidal neuron in CA1. Its somatic location is indicated by the red triangle. The grey squares indicate the removal of direct responses from these sites. For the scale of input amplitudes, the warmer color indicates stronger amplitude. The grey squares indicate the removal of direct responses from these sites. The numbered sites

`

correspond to the illustrated photostimulation response traces plotting from the onset of photostimulation. (B) A color-coded, averaged input map, illustrating the pattern and strength of synaptic inputs to an example PV+/FS inhibitory cell in CA1. (C) A color-coded, averaged input map, illustrating the pattern and strength of synaptic inputs to an example SOM+ O-LM inhibitory cell in CA1. (D) Summary data showing input strength differences across CA3, CA2 and CA1 to targeted pyramidal cells (PYR) (N = 7), PV+/FS inhibitory cells (N = 8) and O-LM inhibitory cells (N = 7). As for CA3 excitatory inputs, the average total input amplitudes of pyramidal cells and PV+/FS inhibitory cells did not differ from each other, but these cell types differed significantly from O-LM cells. PV+/FS inhibitory cells had stronger CA2 inputs than either pyramidal cells or O-LM cells. As for CA1 excitatory inputs, PV+/FS and O-LM inhibitory cells did not differ from each other, but these cell types differed significantly from pyramidal cells. * and ** indicate the statistical significance levels of $p < 0.05$ and 0.01, respectively, for statistical comparisons. (E) Summary data showing average total EPSC events per cell measured from the records cells. PV+/FS and O-LM inhibitory cells did not differ from each other, but these cell types differed significantly from pyramidal cells.

`

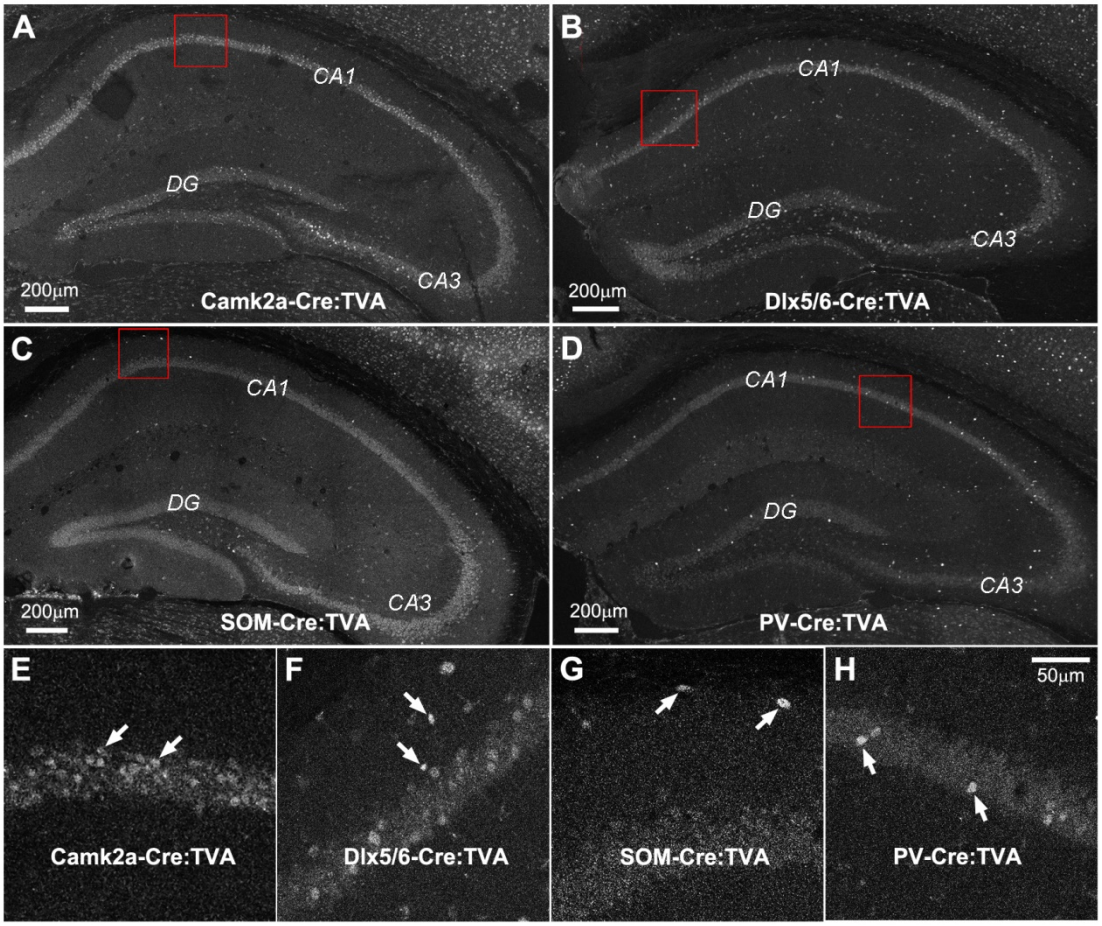

Figure 1.8. LacZ staining indicates effective TVA expression in different Cre mouse lines. As the Cre-dependent TVA expressing mouse line, LSL-R26TVA-lacZ, express both TVA and nuclear lacZ following Cre-mediated recombination in Cre+ cells, lacZ staining is used as a surrogate to examine TVA expression. (A) In the CamK2a-Cre:TVA mouse section, lacZ staining is dense in putative excitatory pyramidal cells in CA1 stratum pyramidale, with sparse labeling in proximal CA3 and DG, which is identical to restricted Cre expression shown in the Camk2a-Cre (T29 line) mouse. (B) In the Dlx5/6-Cre:TVA mouse section, strong lacZ staining is seen in putative inhibitory neurons distributed across hippocampal laminae. (C) In the SOM-Cre:TVA mouse section, strong lacZ staining is seen in putative O-LM cells in stratum oriens. (D) In the PV-Cre:TVA mouse section, robust lacZ staining is seen in putative PV+ basket cells located in stratum pyramidale. (E, F, G and H) Enlarged views of the regions indicated in the red boxes in A, B, C and D, respectively. Arrows indicate example cells with clear lacZ immunoreactivity.

`

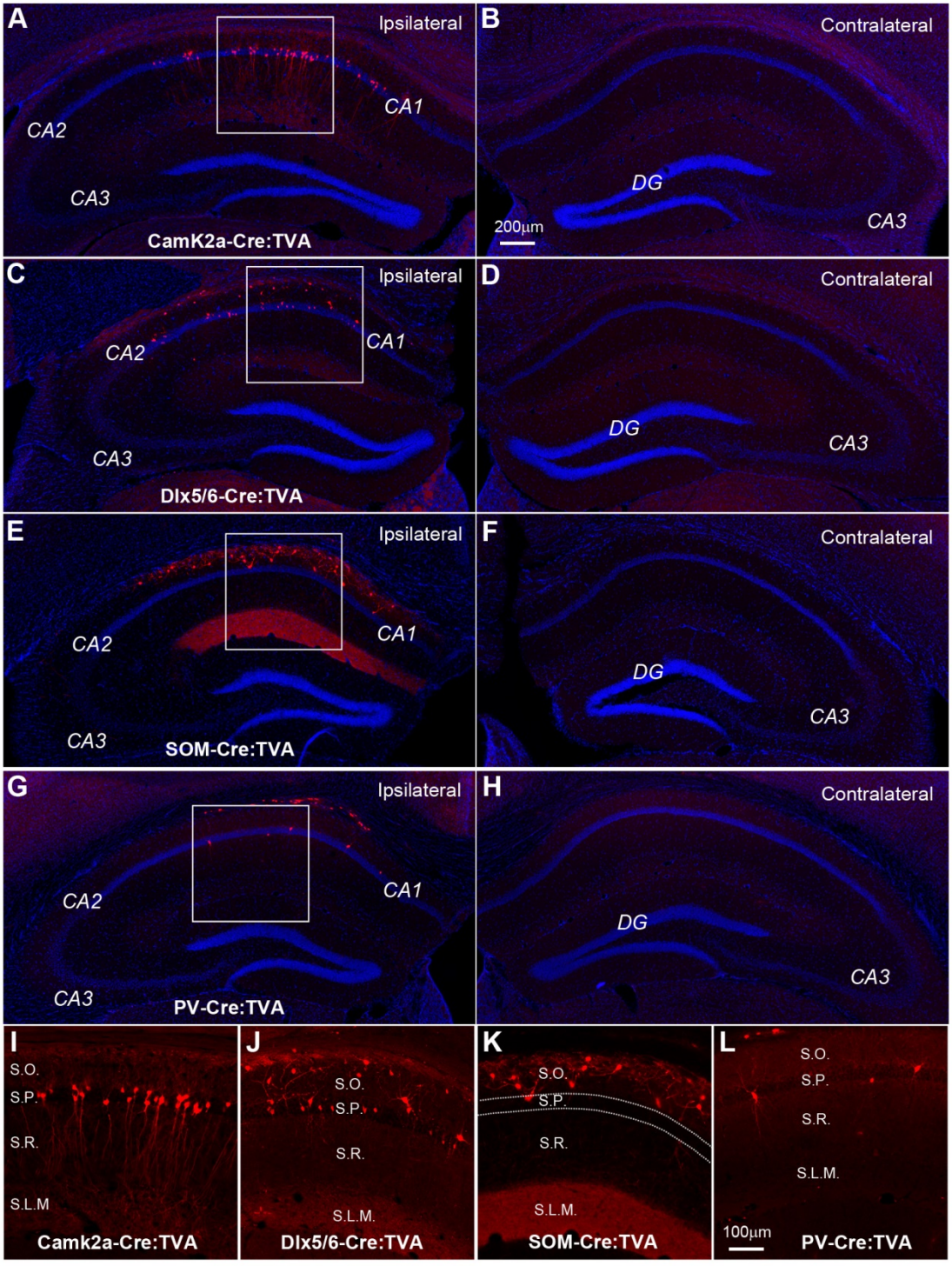

Figure 1.9. Control cases only show restricted rabies labeling of Cre+, TVA-expressing cells at the injection site. The control experiments were performed without the AAV helper virus injection but with the injection of EnVA-SADΔG-mCherry rabies virus only. (A-B, C-D, E-F, G-H) Rabies labeling (mCherry expression) is evident only at the CA1 injection site in the CamK2a-Cre:TVA, Dlx5/6-Cre:TVA, SOM-Cre:TVA, PV-Cre:TVA mouse, respectively. There

`

is no ipsilateral CA3 or long-range transynaptic labeling as shown in the contralateral side of the hippocampus. (I, J, K and L) Enlarged views of the regions indicated in the white boxes in A, C, E and G, respectively.

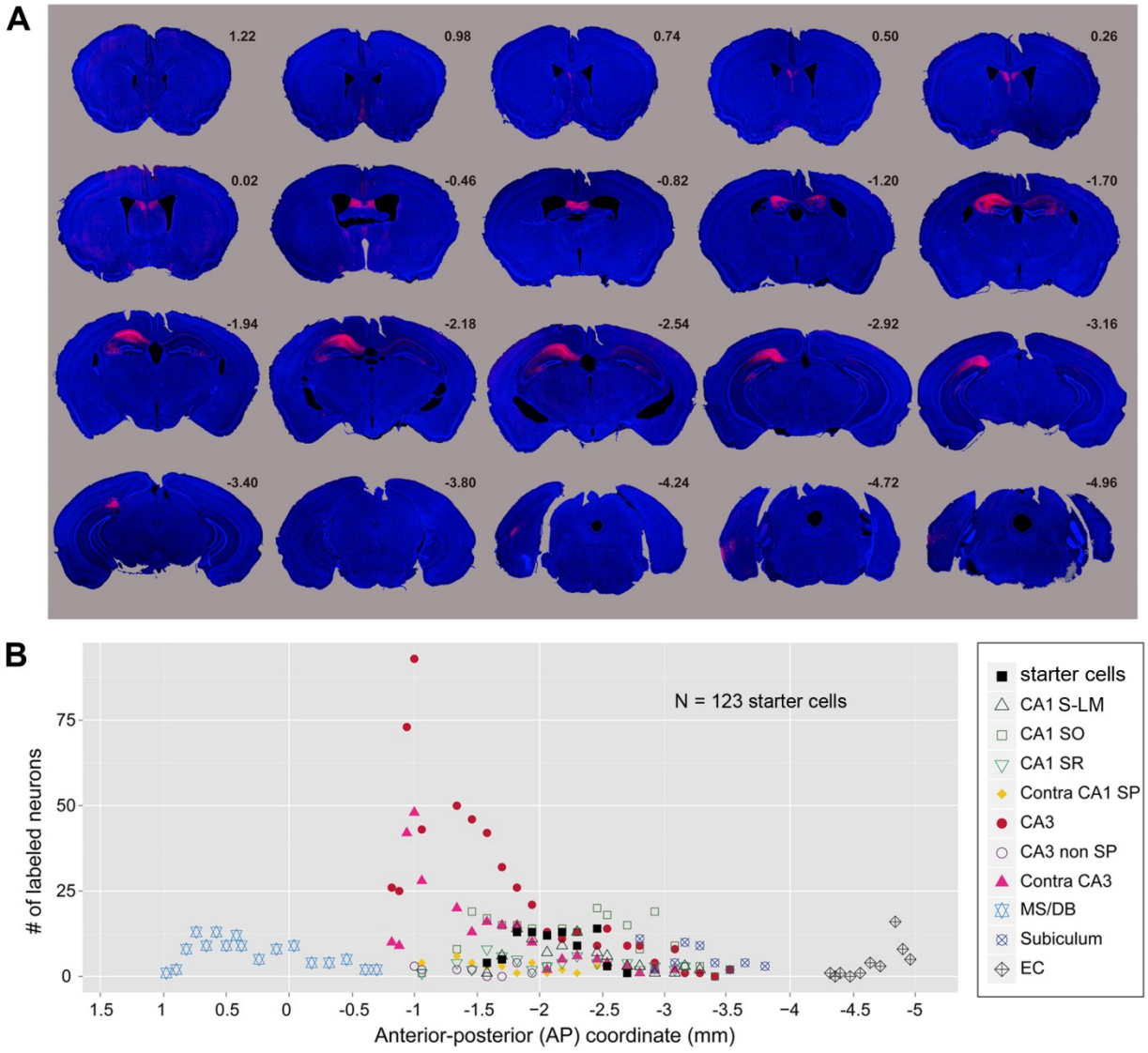

Figure 1.10. Analysis of rabies-mediated tracing of monosynaptic inputs to a Cre-expression defined neuronal population. The example data set shown in (A-B) is from a Camk2a-Cre (T29):TVA mouse case. The brain was sectioned coronally in 30 µm thickness, sections counterstained with DAPI for better visualization of cortical and subcortical structures, then mounted and cover-slipped. Every one in three sections across the whole brain were used for complete and unbiased analyses of rabies-mediated, direct synaptic connections to a small population of targeted cell types/groups. The first analysis step was to visualize the injection site and assure that GFP-expressing starter cells are restricted to CA1. Each GFP and mCherry double-labeled starter cell at the injection site was marked and quantified. Each computerized image of all brain sections was then manually examined to identify and mark the locations of mCherry-expressing cell bodies. Labeled cells were assigned to anatomical structures for region specific quantification. These measurements allow for quantitative evaluations of the numbers

`

of postsynaptic (starter) cells and how those relate to the numbers of presynaptic cells labeled in various brain structures. (A) Selected sections from a representative Camk2a-Cre (T29): TVA case, arranged from anterior to posterior (AP), with AP numbers corresponding to the coronal section positions relative to the bregma landmark. Rabies-mediated tracing signals are shown in red against the DAPI staining background (blue). The coordinates for CA1 injections were −1.94 mm (AP), -1.40 mm (lateromedial) and −1.35 mm (dorsoventral). Note the range of direct input sources to CA1 excitatory pyramidal neurons, including the medial septum and diagonal band area (MS/DB), ipsilateral and contralateral hippocampus, the subiculum and entorhinal cortex (EC). (B) The quantitative distribution of rabies-labeled neurons across different structures in the intact brain for the example case shown in A. In this case, a total of 123 starter cells were counted. Putative inhibitory neurons were measured from CA1 stratum lacunosum-moleculare (SLM), stratum oriens (SO) and stratum radiatum (SR), and CA3 non-stratum pyramidale (non SP). Putative excitatory pyramidal cells were measured from contralateral CA1 stratum pyramidale (SP), both ipsilateral and contralateral CA3 SP. EC labeling was seen predominantly in the ipsilateral hemisphere (mostly layer 3 putative excitatory cells with pyramidal forms) and very sparsely in the contralateral hemisphere. Although immunostaining has been done for neurochemical characterization of the labeled cells, we do not distinguish neurochemical cell types of the labeled cells in the subiculum and MS/DB for quantification. As we conducted quantitative examinations across every one out of three 3 sections, the total number of labeled neurons across different regions would reach ~9000 in this case.

`

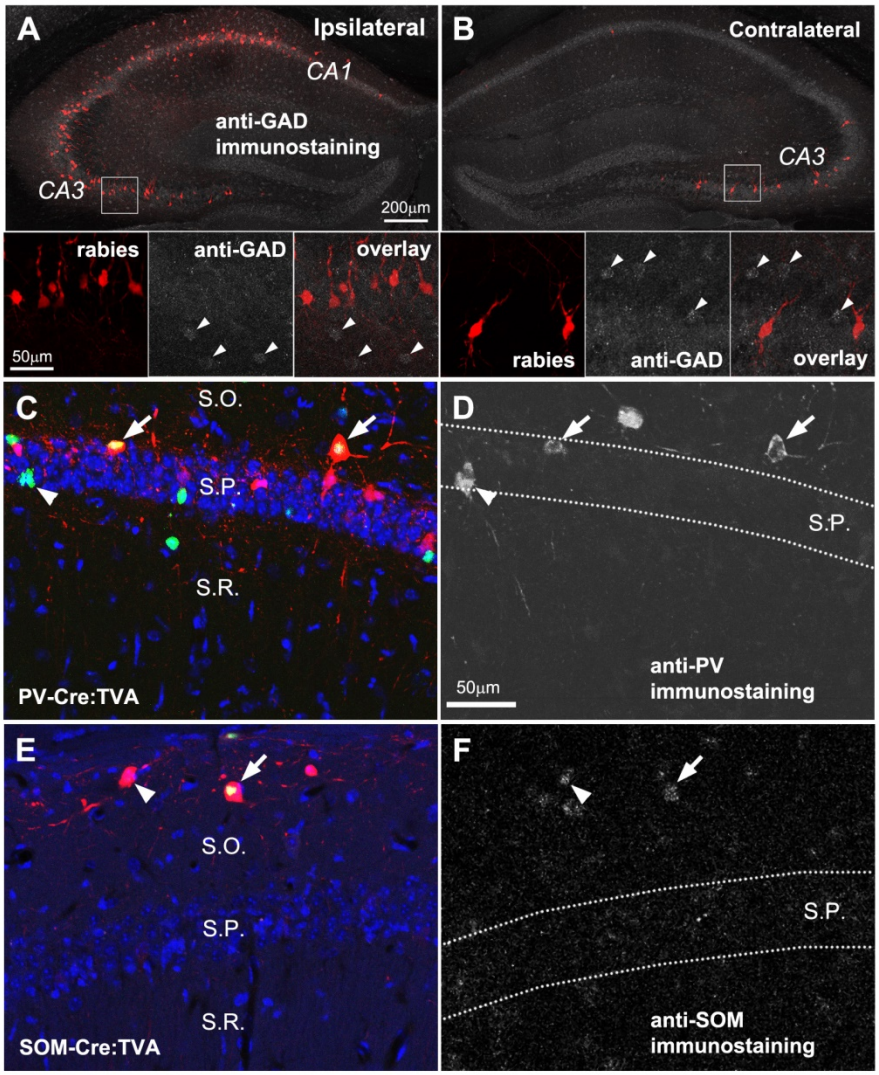

Figure 1.11. Morphological and neurochemical characterization of rabies-labeled CA3 neurons presynaptic to CA1 excitatory cells in the Camk2a-Cre:TVA mouse, and immunostaining of inhibitory neuronal markers, PV and SOM, validating identities of starter cells in the PV-Cre:TVA and SOM-Cre:TVA mouse, respectively. (A-B) The rabies-labeled cells in ipsilateral and contralateral CA3 are essentially all excitatory cells determined based on their pyramidal cell morphology and GAD immuno-negativity. The panels under A show an enlarged view of the region indicated by the white box in A, while the panels under B show an enlarged view of the region indicated by the white box in B. GAD immunoreactivity is visualized with an AF647-conjugated secondary antibody. The strong GAD immunopositive cells are indicated by the white arrowheads. (C-D) PV immunostaining of an example section of PV-Cre:TVA. Two starter cells (both GFP and mCherry labeled, indicated by the arrows) in C are PV+ as confirmed in D. The arrowhead in C-D points to one GFP+, Cre-expressing cell positive for PV staining. (E-F) SOM immunostaining of an example section of SOM-Cre:TVA.

`

One starter cell indicated by the arrow and another cell infected with rabies (mCherry expression, indicated by the arrowhead) are immuo-positive for somatostatin. PV and SOM immunoreactivity was visualized with an AF647-conjugated secondary antibody as well.

`

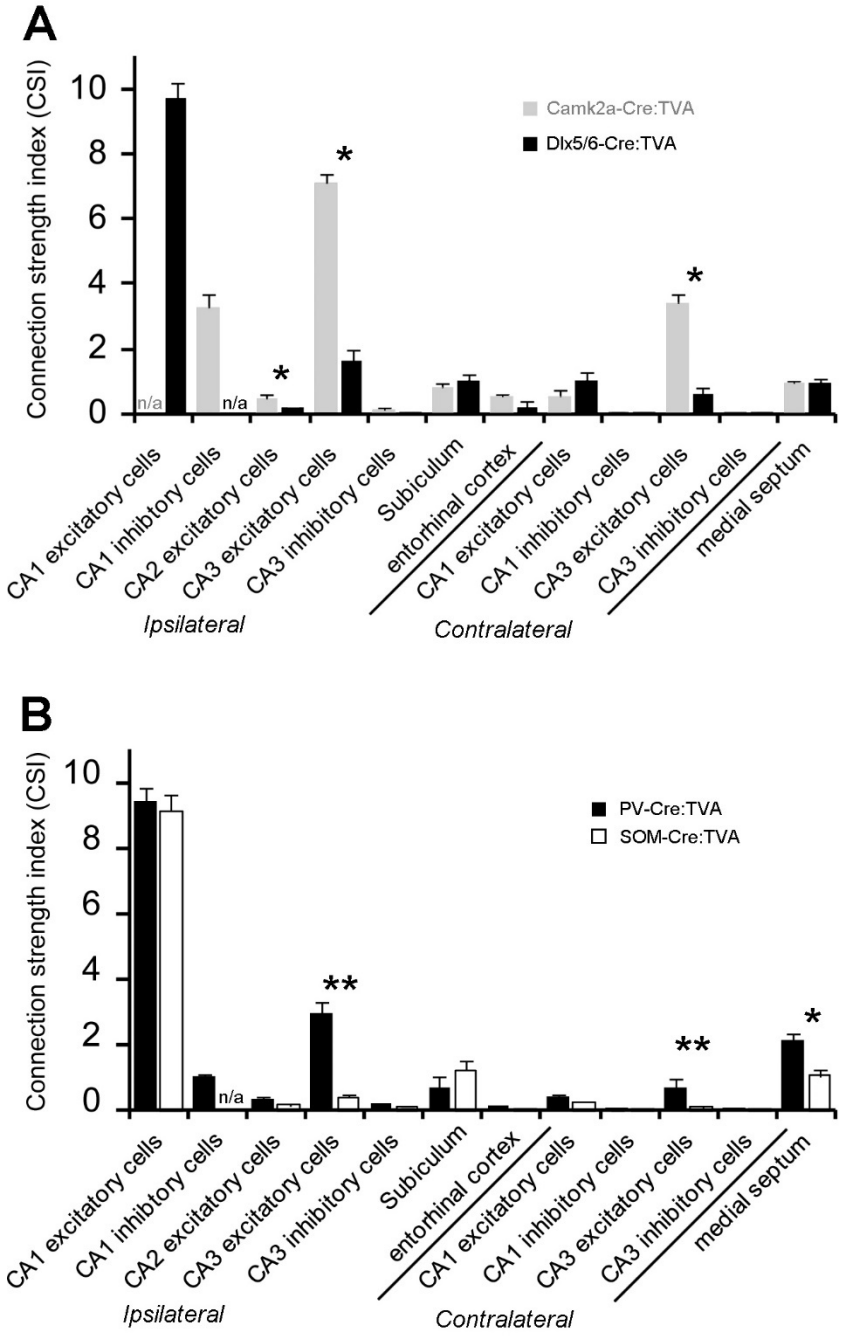

Figure 1.12. Quantitative comparison of circuit connection strengths between excitatory pyramidal cells and mixed types of inhibitory cells, and between PV+ and SOM+ inhibitory cells in hippocampal CA1. In these plots, the Y axis indicates the input connection strength index (CSI) measured by the average ratio of the total number of presynaptic neurons in a specific brain region versus the number of starter neurons in CA1 for a given mouse line, while the X axis denotes input sources of different brain regions. (A) The data from Camk2a-Cre:TVA and Dlx5/6-Cre:TVA cases are shown in grey and black bars, respectively, presented as mean ±

`

SE. As labeled CA1 excitatory cells (presumably expressing both Cre and TVA) could not be distinguished primarily vs. secondarily infected by rabies (see Fig. 1.9), we did not quantify local excitatory connections in CA1 to targeted excitatory pyramidal cells (i.e., not analyzed, n/a) for the Camk2a-Cre:TVA cases. Similarly, as labeled CA1 inhibitory cells (presumably expressing both Cre and TVA) could not be distinguished primarily vs. secondarily infected by rabies, we did not quantify local inhibitory connections in CA1 to targeted mixed inhibitory cell types for the Dlx5/6-Cre:TVA cases. Furthermore, the CSI of local CA1 inhibitory cells for Camk2a-Cre:TVA cases only refers to the inhibitory cells outside the SP layer, which therefore is an under-estimate of the total labeled local CA1 inhibitory cells. (B) The data from PV-Cre:TVA and SOM-Cre:TVA cases are shown in solid and open bars, respectively. The quantification of local CA1 inhibitory connections to PV+ cells in the PV-Cre:TA cases only applies to the inhibitory cells located in the SLM layer (which has no PV+ cells). As SOM+ inhibitory cells are distributed across labeled CA1 laminae, the inhibitory cells (expressing both Cre and TVA) could not be distinguished primarily vs. secondarily infected by rabies, we did not quantify local inhibitory connections in CA1 (i.e., n/a) to SOM+ cells in the SOM-Cre:TVA cases. * and ** indicate the significance levels of $p < 0.05$ and 0.01, respectively, for statistical comparisons for the corresponding input sources.

`

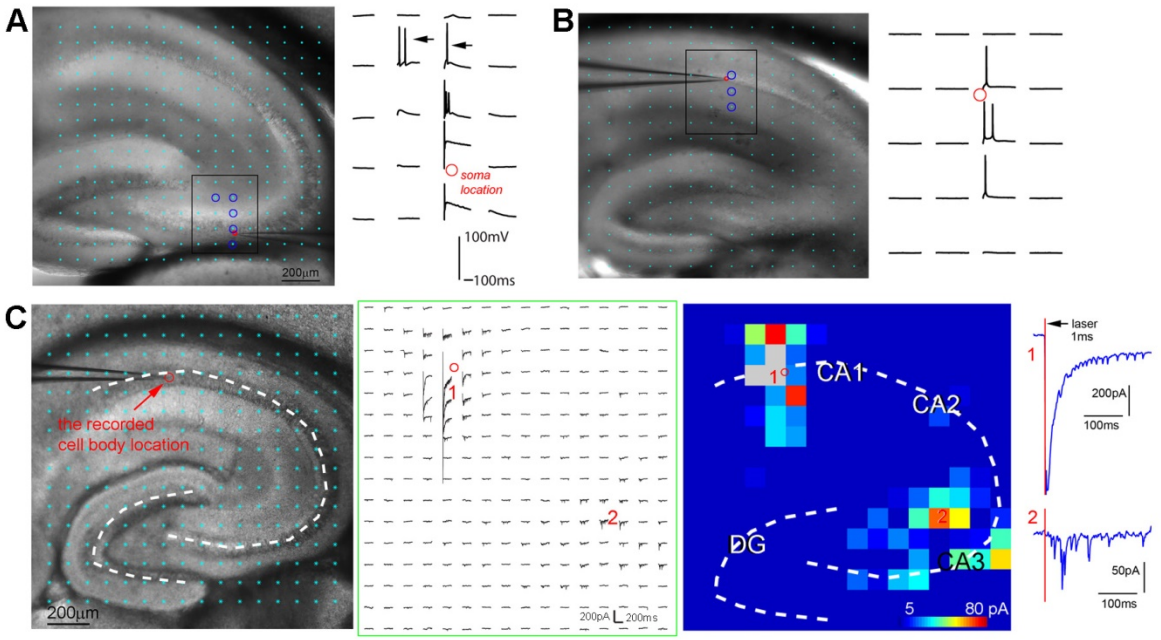

Figure 1.13. LSPS and whole-cell recordings to mapping intrahippocampal synaptic connections to CA1 neurons in living slice preparations. (A-B) Validation of spatial resolution of laser scanning photostimulation (LSPS) by examining the excitability profiles of excitatory neurons in CA3, CA1. In A, the excitability profile (i.e., spatial distribution of uncaging sites (cyan dots) that produce action potentials) of a CA3 excitatory cell recorded in current clamp mode. Photostimulation-evoked action potentials (spikes) are restricted to a small region (blue circles, at the left), and the response traces are separately shown at the right. In B, the excitability profile of a CA1 cell is shown. The arrows in A indicate the evoked spikes in response to photostimulation of the cell's apical dendrites, which decreases the LSPS resolution along the vertical dimension. However, as we are concerned about excitatory input from different hippocampal subfields (CA3-1), the most relevant spatial resolution is defined as the lateral distance in the main axonal projection axis of CA3->CA1, relative to the photostimulation site. By this definition, the average spatial resolution of the method is 108 ± 10.2 μm (mean ± SE, N =17 cells). Considering the total distance from CA3 to CA1 is more than 1500 μm, this approach enables accurate measures of differences of input to different cell types in CA1 from specific hippocampal subfields (CA3-1). (C) LSPS allows for extensive and quantitative mapping of intrahippocampal circuit inputs. At the left panel is shown a hippocampal slice image with the superimposed photostimulation sites (16 x 16 cyan dots). The red circle indicates the somatic location of the recorded cell (PV+ basket cell). Stimulation sites are spaced at 90 μm x 90 μm. This distance has been empirically determined (1) to capture the smallest predicted distance in which photostimulation differentially activates adjacent neurons and (2) to avoid overlap of the laser illuminated area. During the experiment, the slice is bathed the solution containing MNI-caged glutamate, which only turns active through focal UV photolysis to activate a small number of neurons (i.e., glutamate uncaging). The whole hippocampal region is

`

stimulated sequentially with an interval of 1 second in a non-raster and non-random sequence that avoids visiting the vicinity recently stimulated. The middle panel shows photostimulation-evoked response traces from most sites shown at the left panel, with the recorded cell held at -70 mV in voltage clamp mode to detect inward excitatory postsynaptic currents (EPSCs). The small red circle indicates the recorded cell body location. Only the 200 ms of the response traces after laser photostimulation (20 mW, 1 ms) are shown. Different forms of photostimulation-evoked responses are illustrated by the traces of 1 and 2, expanded and separately shown by the right panel. Trace 1 is an example of the direct response to glutamate uncaging on the cell body (excluded for further analysis), which can be distinguished by its large amplitude and short latency. Trace 2 is a typical example of synaptic input responses. The right panel shows the quantitative, color-coded map measuring the EPSC input strength per stimulation site based on the photostimulation-evoked responses as shown in the middle panel. The grey squares indicate the removal of direct responses from these sites. For input data analysis, all the EPSC input values are summed and averaged within each hippocampal sub-regions and subfields for the cell examined; regional distributions and input strength are quantified and compared across cell types.

`

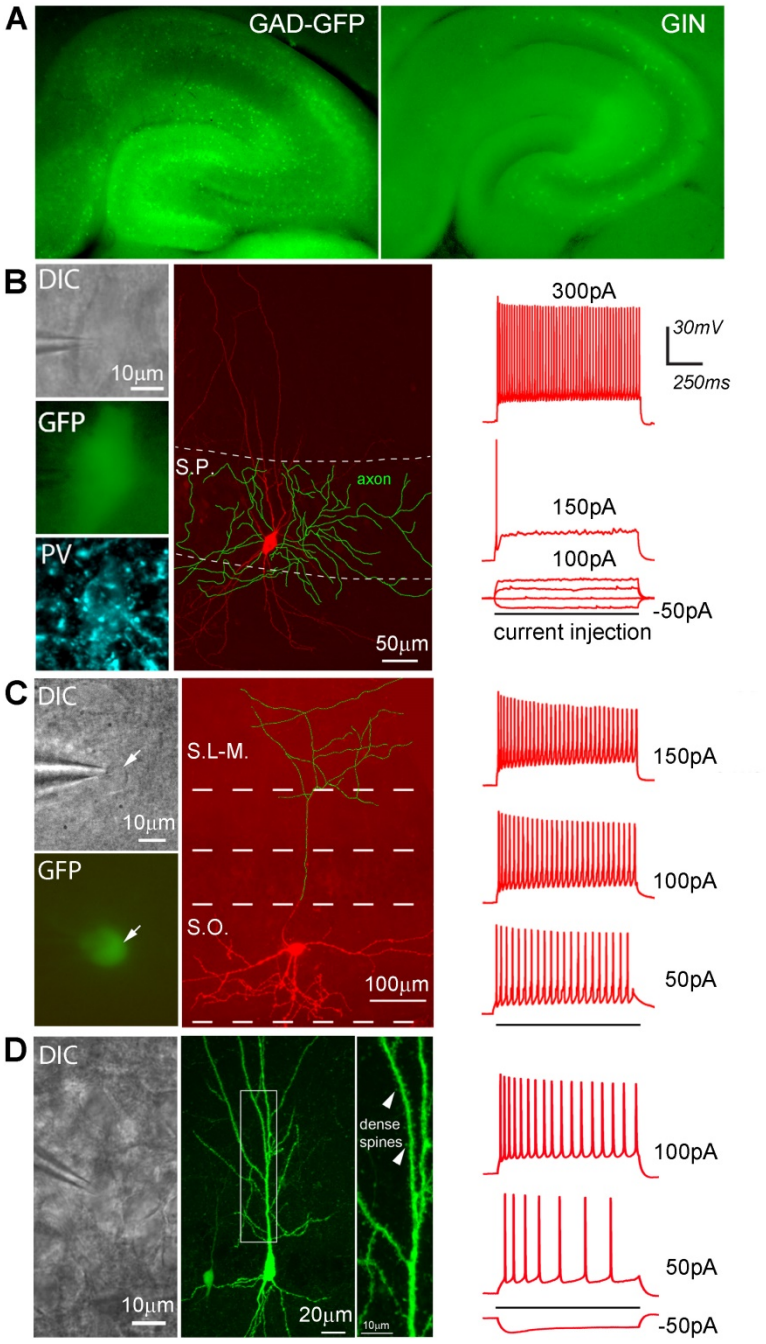

Figure 1.14. Targeted recordings of inhibitory neurons facilitated by using transgenic mouse lines expressing GFP in inhibitory neurons, and cell-type identification and characterization. (A) GFP expression in hippocampal sections of the GAD-GFP mouse (Tamamaki et al., 2003) and the GIN mouse (Oliva et al., 2000). We consistently sample GFP-expressing, PV+ basket cells located in the pyramidal layer using the GAD-GFP mouse in which GFP is expressed in almost all GABAergic cells, and SOM+ O-LM cells located in stratum oriens using the GIN mouse in which a subset of SOM+ cells express GFP. (B) Example

`

recording and characterization of PV+/fast-spiking basket cells with the cell type determined based upon the combined characterization of morphology, immunochemical and intrinsic electrophysiological property. (C) Example recording and characterization of O-LM cells. The example cell has its soma located in the oriens layer with horizontally oriented dendrites, but its axon (traced in green) ascends and branches in the stratum lacunosum moleculare (S.L.M.) layer. The cell exhibits low threshold spiking to intrasomatic current injections. (D) Excitatory pyramidal cells are targeted based upon their pyramidal appearance of the cell somata and thick apical dendrites under DIC microscopy, confirmed by their regular spiking patterns and post hoc morphological analysis. The example excitatory pyramidal cell recorded has typical pyramidal morphology with dense dendritic spines.

`

A. Camk2a-Cre:TVA, input connection strength index (# of labeled presynaptic neurons / # of starter neurons)

MS-DB	Ipsilateral									Contralateral					
	CA1				CA2	CA3		EC	Sub	CA1		CA2 SP	CA3		EC
	SO	SP	SR	SLM	SP	SP	Non SP			SO	SP		SP	non-SP	
0.95 ± 0.05	2.26±0.27	n/a	0.45 ± 0.10	0.54 ± 0.15	0.47 ± 0.10	7.10 ± 0.28	0.13 ± 0.03	0.54 ± 0.08	0.81±0.01	0.01 ± 0.00	0.54 ± 0.17	0.07 ± 0.01	3.44 ± 0.22	0.00 ± 0.00	0.01 ± 0.01
# of starter cells		109.6±16.7			N = 5 cases										

B. Dlx5/6-Cre:TVA, input connection strength index (# of labeled presynaptic neurons / # of starter neurons)

MS-DB	Ipsilateral									Contralateral					
	CA1				CA2	CA3		EC	Sub	CA1		CA2 SP	CA3		EC
	SO	SP	SR	SLM	SP	SP	Non SP			SO	SP		SP	Non-SP	
1.17 ± 0.18	n/a	9.72 ± 0.49	n/a	n/a	0.17 ± 0.01	1.63 ± 0.37	0.06 ± 0.01	0.21 ± 0.15	1.00± 0.20	0.02 ± 0.00	0.99 ± 0.27	0.02 ±0.01	0.60± 0.18	0.02 ± 0.01	0.01 ± 0.01
# of starter cells	47.8±9.5	38.3 ±2.6	11.3 ±4.4	9.8± 4.5	N = 4 cases										

C. PV-Cre:TVA, input connection strength index (# of labeled presynaptic neurons / # of starter neurons)

MS-DB	Ipsilateral									Contralateral					
	CA1				CA2	CA3		EC	Sub	CA1		CA2	CA3		EC
	SO	SP	SR	SLM	SP	SP	Non SP			SO	SP		SP	non-SP	
2.11 ±0.20	n/a	9.46 ± 0.36	n/a	1.02 ± 0.11	0.33 ± 0.09	2.97 ± 0.37	0.19 ± 0.05	0.12 ± 0.05	0.69± 0.16	0.01 ± 0.01	0.42 ±0.10	0.00 ± 0.00	0.72± 0.10	0.04 ± 0.02	0.02 ± 0.01
# of starter cells	11.4 ±1.2	17.8 ± 1.6	1.2± 0.6	0.00 ± 0.00	N = 5 cases										

D. SOM-Cre:TVA, input connection strength index (# of labeled presynaptic neurons / # of starter neurons)

MS-DB	Ipsilateral									Contralateral					
	CA1				CA2	CA3		EC	Sub	CA1		CA2	CA3		EC
	SO	SP	SR	SLM	SP	SP	Non SP			SO	SP		SP	Non-SP	
1.06 ± 0.16	n/a	9.13 ± 0.54	n/a	n/a	0.16 ± 0.05	0.41 ± 0.12	0.09 ± 0.01	0.01 ± 0.00	1.24± 0.31	0.03 ± 0.01	0.26 ± 0.05	0.00 ±0.00	0.11± 0.05	0.01 ± 0.00	0.00 ±0.00
# of starter cells	52.6 ± 11.73	3.2± 1.2	1.4± 0.75	0.2± 0.2	N = 5 cases										

Table 1.1. Quantitative strengths of specific circuit connections to Cre-defined hippocampal CA1 neurons. The input connection strength index (CSI) is defined as the ratio of the number of labeled presynaptic neurons in a specified structure versus the number of starter neurons. The medial septum and diagonal band area, MS-DB. Hippocampal subfields, CA1, CA2 and CA3. Stratum Oriens, SO; stratum pyramidale, SP; stratum radiatum, SR; stratum lacunosum-moleculare, SLM. In CA3, we only distinguish stratum pyramidale from non-stratum pyramidale (non SP). Entorhinal cortex, EC; subiculum, Sub. In (A), as labeled CA1

`

excitatory cells (presumably expressing both Cre and TVA) could not be distinguished primarily versus secondarily infected by rabies, we did not quantify local excitatory connections in CA1 to targeted excitatory cells (i.e., not analyzed, n/a) in the Camk2a-Cre:TVA cases. Also note that in (A), the quantification for CA1 inhibitory cells only refers to the inhibitory cells outside the SP layer, which therefore is an under-estimate of the total labeled CA1 inhibitory cells. Similarly, in (B), (C) and (D), as labeled CA1 inhibitory cells (presumably expressing both Cre and TVA) could not be distinguished primarily versus secondarily infected by rabies, we did not quantify local inhibitory connections (i.e., n/a) in CA1 to these inhibitory cells when deemed necessary. In C, the quantification for inhibitory connections to PV+ inhibitory cells only applies to the inhibitory cells located in the SLM layer which has no PV+ cells.

`

REFERENCES

Ali AB, Thomson AM (1998) Facilitating pyramid to horizontal oriens-alveus interneurone inputs: dual intracellular recordings in slices of rat hippocampus. J Physiol 507 (Pt 1):185-199.

Amaral DG, Witter MP (1989) The three-dimensional organization of the hippocampal formation: a review of anatomical data. Neuroscience 31:571-591.

Berger TW, Swanson GW, Milner TA, Lynch GS, Thompson RF (1980) Reciprocal anatomical connections between hippocampus and subiculum in the rabbit evidence for subicular innervation of regio superior. Brain Res 183:265-276.

Blasco-Ibanez JM, Freund TF (1995) Synaptic input of horizontal interneurons in stratum oriens of the hippocampal CA1 subfield: structural basis of feed-back activation. Eur J Neurosci 7:2170-2180.

Brivanlou IH, Dantzker JL, Stevens CF, Callaway EM (2004) Topographic specificity of functional connections from hippocampal CA3 to CA1. Proc Natl Acad Sci U S A 101:2560-2565.

Brun VH, Leutgeb S, Wu HQ, Schwarcz R, Witter MP, Moser EI, Moser MB (2008) Impaired spatial representation in CA1 after lesion of direct input from entorhinal cortex. Neuron 57:290-302.

Brun VH, Otnass MK, Molden S, Steffenach HA, Witter MP, Moser MB, Moser EI (2002) Place cells and place recognition maintained by direct entorhinal-hippocampal circuitry. Science 296:2243-2246.

Buzsaki G (2002) Theta oscillations in the hippocampus. Neuron 33:325-340.

Callaway EM (2008) Transneuronal circuit tracing with neurotropic viruses. Curr Opin Neurobiol 18:617-623.

Colom LV, Castaneda MT, Reyna T, Hernandez S, Garrido-Sanabria E (2005) Characterization of medial septal glutamatergic neurons and their projection to the hippocampus. Synapse 58:151-164.

Conti F, DeBiasi S, Minelli A, Rothstein JD, Melone M (1998) EAAC1, a high-affinity glutamate tranporter, is localized to astrocytes and gabaergic neurons besides pyramidal cells in the rat cerebral cortex. Cereb Cortex 8:108-116.

Cruikshank SJ, Lewis TJ, Connors BW (2007) Synaptic basis for intense thalamocortical activation of feedforward inhibitory cells in neocortex. Nat Neurosci 10:462-468.

Freund TF, Antal M (1988) GABA-containing neurons in the septum control inhibitory interneurons in the hippocampus. Nature 336:170-173.

Freund TF, Buzsaki G (1996) Interneurons of the hippocampus. Hippocampus 6:347-470.

Freund TF, Katona I (2007) Perisomatic inhibition. Neuron 56:33-42.

Gibson JR, Beierlein M, Connors BW (1999) Two networks of electrically coupled inhibitory neurons in neocortex. Nature 402:75-79.

Glickfeld LL, Scanziani M (2006) Distinct timing in the activity of cannabinoid-sensitive and cannabinoid-insensitive basket cells. Nat Neurosci 9:807-815.

Gulyas AI, Gorcs TJ, Freund TF (1990) Innervation of different peptide-containing neurons in the hippocampus by GABAergic septal afferents. Neuroscience 37:31-44.

Huh CY, Goutagny R, Williams S (2010) Glutamatergic neurons of the mouse medial septum and diagonal band of Broca synaptically drive hippocampal pyramidal cells: relevance for hippocampal theta rhythm. J Neurosci 30:15951-15961.

`

Klausberger T, Somogyi P (2008) Neuronal diversity and temporal dynamics: the unity of hippocampal circuit operations. Science 321:53-57.
Kohler C (1985) Intrinsic projections of the retrohippocampal region in the rat brain. I. The subicular complex. The Journal of comparative neurology 236:504-522.
Manseau F, Danik M, Williams S (2005) A functional glutamatergic neurone network in the medial septum and diagonal band area. J Physiol 566:865-884.
Marshel JH, Mori T, Nielsen KJ, Callaway EM (2010) Targeting single neuronal networks for gene expression and cell labeling in vivo. Neuron 67:562-574.
Monory K, Massa F, Egertova M, Eder M, Blaudzun H, Westenbroek R, Kelsch W, Jacob W, Marsch R, Ekker M, Long J, Rubenstein JL, Goebbels S, Nave KA, During M, Klugmann M, Wolfel B, Dodt HU, Zieglgansberger W, Wotjak CT, Mackie K, Elphick MR, Marsicano G, Lutz B (2006) The endocannabinoid system controls key epileptogenic circuits in the hippocampus. Neuron 51:455-466.
Nakashiba T, Buhl DL, McHugh TJ, Tonegawa S (2009) Hippocampal CA3 output is crucial for ripple-associated reactivation and consolidation of memory. Neuron 62:781-787.
Nakashiba T, Cushman JD, Pelkey KA, Renaudineau S, Buhl DL, McHugh TJ, Rodriguez Barrera V, Chittajallu R, Iwamoto KS, McBain CJ, Fanselow MS, Tonegawa S (2012) Young dentate granule cells mediate pattern separation, whereas old granule cells facilitate pattern completion. Cell 149:188-201.
Nakashiba T, Young JZ, McHugh TJ, Buhl DL, Tonegawa S (2008) Transgenic inhibition of synaptic transmission reveals role of CA3 output in hippocampal learning. Science 319:1260-1264.
Oliva AA, Jr., Jiang M, Lam T, Smith KL, Swann JW (2000) Novel hippocampal interneuronal subtypes identified using transgenic mice that express green fluorescent protein in GABAergic interneurons. J Neurosci 20:3354-3368.
Remondes M, Schuman EM (2004) Role for a cortical input to hippocampal area CA1 in the consolidation of a long-term memory. Nature 431:699-703.
San Antonio A, Liban K, Ikrar T, Tsyganovskiy E, Xu X (2014) Distinct physiological and developmental properties of hippocampal CA2 subfield revealed by using anti-Purkinje cell protein 4 (PCP4) immunostaining. J Comp Neurol 522:1333-1354.
Seidler B, Schmidt A, Mayr U, Nakhai H, Schmid RM, Schneider G, Saur D (2008) A Cre-loxP-based mouse model for conditional somatic gene expression and knockdown in vivo by using avian retroviral vectors. Proc Natl Acad Sci U S A 105:10137-10142.
Shao LR, Dudek FE (2005) Electrophysiological evidence using focal flash photolysis of caged glutamate that CA1 pyramidal cells receive excitatory synaptic input from the subiculum. J Neurophysiol 93:3007-3011.
Shi Y, Nenadic Z, Xu X (2010) Novel use of matched filtering for synaptic event detection and extraction. PLoS One 5:e15517.
Somogyi P, Klausberger T (2005) Defined types of cortical interneurone structure space and spike timing in the hippocampus. J Physiol 562:9-26.
Steward O, Scoville SA (1976) Cells of origin of entorhinal cortical afferents to the hippocampus and fascia dentata of the rat. J Comp Neurol 169:347-370.
Suh J, Rivest AJ, Nakashiba T, Tominaga T, Tonegawa S (2011) Entorhinal cortex layer III input to the hippocampus is crucial for temporal association memory. Science 334:1415-1420.

`

Takacs VT, Klausberger T, Somogyi P, Freund TF, Gulyas AI (2012) Extrinsic and local glutamatergic inputs of the rat hippocampal CA1 area differentially innervate pyramidal cells and interneurons. Hippocampus 22:1379-1391.

Tamamaki N, Yanagawa Y, Tomioka R, Miyazaki J, Obata K, Kaneko T (2003) Green fluorescent protein expression and colocalization with calretinin, parvalbumin, and somatostatin in the GAD67-GFP knock-in mouse. J Comp Neurol 467:60-79.

Tsien JZ, Chen DF, Gerber D, Tom C, Mercer EH, Anderson DJ, Mayford M, Kandel ER, Tonegawa S (1996) Subregion- and cell type-restricted gene knockout in mouse brain. Cell 87:1317-1326.

Ugolini G (2008) Use of rabies virus as a transneuronal tracer of neuronal connections: implications for the understanding of rabies pathogenesis. Dev Biol (Basel) 131:493-506.

Ugolini G (2011) Rabies virus as a transneuronal tracer of neuronal connections. Adv Virus Res 79:165-202.

Wall NR, Wickersham IR, Cetin A, De La Parra M, Callaway EM (2010) Monosynaptic circuit tracing in vivo through Cre-dependent targeting and complementation of modified rabies virus. Proc Natl Acad Sci U S A 107:21848-21853.

Wickersham IR, Finke S, Conzelmann KK, Callaway EM (2007a) Retrograde neuronal tracing with a deletion-mutant rabies virus. Nat Methods 4:47-49.

Wickersham IR, Lyon DC, Barnard RJ, Mori T, Finke S, Conzelmann KK, Young JA, Callaway EM (2007b) Monosynaptic restriction of transsynaptic tracing from single, genetically targeted neurons. Neuron 53:639-647.

Wittner L, Henze DA, Zaborszky L, Buzsaki G (2006) Hippocampal CA3 pyramidal cells selectively innervate aspiny interneurons. Eur J Neurosci 24:1286-1298.

Xu X, Callaway EM (2009) Laminar specificity of functional input to distinct types of inhibitory cortical neurons. J Neurosci 29:70-85.

Xu X, Roby KD, Callaway EM (2010) Immunochemical characterization of inhibitory mouse cortical neurons: three chemically distinct classes of inhibitory cells. J Comp Neurol 518:389-404.

`

Chapter 2:

Topographic organization of canonical and non-canonical circuit inputs to hippocampal CA1 revealed by monosynaptic rabies tracing

`

ABSTRACT

Most of our knowledge of hippocampal topographic connections comes from conventional anatomical tracing studies which lack cell-type specificity and do not have quantitative measurements of connectional strengths. Further, non-canonical circuit inputs to the hippocampus have been uncovered with new viral and genetic circuit mapping. Thus in the present study, we re-evaluate and quantify intra- and para- hipppocampal input connections to different CA1 subfields (proximal, intermediate, and distal CA1) by using a novel monosynaptic rabies tracing. In our experiments, excitatory pyramidal neurons in different subfields of dorsal CA1 are targeted, and direct retrogradely labeled presynaptic neurons are mapped in the intact brain. Our quantitative analysis reveals that pCA1 receives 4 fold stronger inputs from CA3 than that of dCA1. CA3a provide the most input connections to pCA1, while dCA1 receives its most CA3 inputs from CA3b instead. Consistent with the previous descriptions, pCA1 receives entorhinal cortex (EC) inputs mainly from medial EC; intermediate CA1 receives more inputs from medial EC than lateral EC; dCA1 receives more inputs from lateral EC than medial EC. This shows changes of EC input strengths to CA1 subfields in a topographic manner. In addition to the labeled neurons in EC layer III, we found ~15% of the mapped EC input neurons are putative layer II stellate cells. Furthermore, we confirm and extend our previous finding of non-canonical subiculum inputs to CA1, and the data show that dCA1 receives stronger inputs than intermediate CA1 and pCA1. Pre- and para- subiculum also project to CA1 directly with pCA1 receiving stronger inputs than intermediate CA1 and dCA1. Together, these results provide a new understanding of topographic organization of canonical and non-canonical inputs to CA1 excitatory neurons, and allows for functional considerations of how different intra- and para-hipppocampal inputs modulate CA1-associated spatial navigation and memory behaviors.

`

INTRODUCTION

In sensory system, adjacent cortical areas represent stimuli received from adjacent sensory receptor surfaces in order to continuously and completely mirror their relevant sensory or motor dimensions. This representation is known as topographic organization (Patel et al., 2014). This is a very prominent feature in sensory systems including vision (Hubel and Wiesel, 1962, 1969), somatosensation (Woolsey and Van der Loos, 1970), and motion (Penfield and Boldrey, 1937).

Topographic maps have also been found in higher order non-sensory brain areas. For example, hippocampus along with the parahippocampal regions show anatomical and functional topography along its dorsal-ventral axis (long axis) as well as the proximodistal axis (transverse axis) (Steward, 1976, Amaral and Witter, 1989, Tamamaki and Nojyo, 1995, Henriksen et al., 2010, Stensola et al., 2012, Giocomo et al., 2014, Igarashi et al., 2014a, Strange et al., 2014, Lee et al., 2015, Lu et al., 2015). Specifically, hippocampal CA1 receives inputs from CA3 Schaffer collaterals and contralateral commissural fibers in a topographic manner. Proximal CA3 mainly projects to distal CA1 by preferentially targeting the superficial part of the stratum radiatum, while distal CA3 projects to proximal CA1 via deeper part of the stratum radiatum and the stratum oriens (Ishizuka et al., 1990, Li et al., 1994, Cappaert et al., 2015). CA1 neurons, in turn, project to subiculum with a similar topography. Thus projections from proximal CA1 terminate in the distal third of the subiculum, while projections from distal CA1 terminate in the proximal subiculum close to the subiculum/CA1 border (Amaral et al., 1991). These topographies suggest that different hippocampal subfields have different operations to segregate the information flow, for example, pattern separation vs pattern completion (Lee et al., 2015), and direct the signals to selected downstream brain regions for further processing. Therefore, the cognitive functions of

`

the hippocampus are closely related to its topographic maps. For example, as a result of strong direct innervations by medial entorhinal cortex (MEC), neurons from proximal CA1 are much more spatially tuned by showing sharp place fields (Steward, 1976, Brun et al., 2002, Brun et al., 2008, Henriksen et al., 2010). On the contrary, neurons from distal CA1, which receives more direct inputs from lateral entorhinal cortex (LEC), show more dispersed spatial tuning but strongly respond to non-spatial stimuli, such as objects, items, and odor signals (Henriksen et al., 2010, Burke et al., 2011, Deshmukh and Knierim, 2011, Nakamura et al., 2013, Igarashi et al., 2014a, Igarashi et al., 2014b).

As the hippocampal topographic maps give rise to the functional cognitive maps, it is very important to have a complete and precise understanding of the anatomical topography of the hippocampal formation. Efforts have been made for decades by using traditional neuronal tracers or dyes (Steward, 1976, Ishizuka et al., 1990, Amaral et al., 1991, Li et al., 1994, Tamamaki and Nojyo, 1995, Naber et al., 2001). However, cell-type specific and quantitative analysis of hippocampal topographic organization are still lagging behind. Herein by using a Cre-dependent monosynaptic rabies tracing system (Wickersham et al., 2007b, Wall et al., 2010, Sun et al., 2014), we are able to map the topographic organization of input connections to dorsal hippocampal CA1 along its proximodistal axis in a whole brain quantitative manner. More importantly, this technique allow us to map the input connections restrict to CA1 pyramidal neurons, which are likely the functional cell types in CA1, such as place cells (Moser et al., 2008). We mapped the topography of the canonical projections from CA3 and EC to different CA1 subfields with quantitative details. In addition, the topographic organization of the subiculum to CA1 back-projections, a newly re-discovered pathway (Sun et al., 2014), has also been mapped out by showing distal CA1 receives strong back-projections from the subiculum,

`

while proximal CA1 receives weak projections from the subiculum. Unexpectedly, we found a novel projection arising from pre/parasubiculum to the CA1 which follows a reverse topography compared to the subiculum. Our data will provide in-depth mechanistic understanding of hippocampal circuit organization and function.

MATERIALS AND METHODS

Animals

All experiments were conducted according to National Institutes of Health guidelines for animal care and use and were approved by the Institutional Animal Care and Use Committee of the University of California, Irvine. Although the genetically modified rabies viruses used for the proposed experiments are deletion-mutant rabies and are based on a vaccine strain (SAD-B19), they still pose a limited potential health risk with the helper virus. All personnel working with the rabies are therefore vaccinated and experiments are conducted under biosafety level (BSL) 2 conditions with a protocol approved by the institutional biosafety committee.

To achieve Cre-directed, cell type specific expression of TVA receptors in hippocampal CA1, we used a LSL-R26$^{Tva\text{-}lacZ}$ mouse line conditionally expressing TVA receptor (avian retroviral receptor, tumor virus A) in a Cre-recombinase-dependent manner (Seidler et al., 2008); the LSL-R26$^{Tva\text{-}lacZ}$ mouse line was cross-bred with Camk2a-Cre (T29) mouse line (Tsien et al., 1996) to target cortical excitatory neurons. We termed the double transgenic mice as Camk2a-Cre;TVA, in which Cre-expressing cells also express TVA to restrict initial infection of EnvA-SADΔG rabies virus. The mice of 8-12 weeks old (either sex) were used for experiments and had free access to food and water in their home-cages before and after surgeries.

Viral injections for neural circuit tracing

`

To perform stereotaxic viral injections into the brain, mice were anesthesitized under 1.5% isoflurane for 10 minutes with a 0.8 L/min oxygen flow rate using an isoflurane table top unit (HME109, Highland Medical Equipment). Mice were then placed in a rodent stereotax (Leica Angle Two™ for mouse) with continuous 1% isoflurane anesthesia with the head secured. A small incision was made in the head, the skin reflected, and the skull exposed to show the landmarks of bregma and lambda, and desired injection sites. A three-axis micromanipulator guided by a digital atlas was used to determine coordinates for the bregma and lambda. The injection site was calculated relative to these landmarks, using canonical coordinates. The following injection coordinates targeting different brain regions were used (all values given relative to the bregma), intermediate CA1: anteroposterior (AP) −1.94 mm, lateromedial (ML) -1.40 mm; dorsoventral (DV) −1.35 mm; Proximal CA1: AP -2.06 mm, ML -1.94 mm, DV -1.51 mm; Distal CA1: AP -2.06 mm, ML -0.85 mm, DV -1.38 mm. A small drill hole was made in the skull over the injection site, exposing the pia surface. A pulled glass pipette (tip diameter, ≈30 μm) was loaded with virus and then lowered into the brain with the appropriate coordinates. A Picospritzer (General Valve, Hollis, NH) was used to pulse virus into the brain. A total of 0.1 ul of the helper virus (AAV8-EF1a-FLEX-hG, ∼2 × 10^{11} genome units per ml) (Addgene, Plasmid 37452) was injected into the brain of Camk2a-Cre;TVA mouse at a rate of 20 - 30 nl/min, with 10 ms pulse duration. For some of the cases, the AAV helper virus was delivered into the brain through iontophoresis with a positive 3 μA current at 7 s ‘on’ and 7 s ‘off’ cycles for 5-8 min. To prevent backflow of virus, the pipette remained in the brain for 5 min after completion of the injection. Once the injection pipette was withdrawn, the mouse was removed from the stereotax, and the incision was closed with either wound clips or tissue adhesive (3M Vetbond, St. Paul, MN). Mice were taken back and recovered in their home cages. After 3

`

weeks of the AAV injection which allowed for the infected neurons to express high contents of RGs and GFP, a pseudotyped, RG-deleted rabies virus (EnVA-SADΔG-dsRed rabies, 0.4 ul, ~3 × 10^8 infectious units per ml; or EnVA-SADΔG-mCherry rabies, 0.1 ul, ~2 × 10^9 infectious units per ml) was injected into the same location as the AAV injections via the Picospritzer. The rabies virus was allowed to replicate and retrogradely spread from targeted Cre+ cell types to directly connected presynaptic cells for 9-10 days before the animals were perfused for tissue processing. Since it has been estimated that rabies virus requires only 24 h to cross a synapse (Ugolini, 2008), the rabies infection time would be sufficient for crossing sparse and weak synaptic contacts, which is confirmed by our results.

Histology and immunohistochemistry

The mice were transcardially perfused with 5 ml of phosphate buffered saline (PBS), followed by 25 ml PBS containing 4% paraformaldehyde. The brains were removed and left in 4% paraformaldehyde overnight, then transferred into 30% sucrose in PBS in the next day. The brains were sectioned coronally in 30 μm thickness on a freezing microtome (Leica SM2010R, Germany). To better examine both the laminar structure of the entorhinal cortex as well as the CA1 injection site, for some of the cases, we used a combined coronal/ horizontal sectioning technique described in (Steward, 1976). Basically, the brains were divided with a coronal section at approximately the posterior border of the dorsal psalterium, and the rostral portion of the brain was sectioned in the coronal plane, while the caudal region was sectioned in the horizontal plane. Every one out of 3 sections was mounted for examination and quantification of starter cells and their presynaptic cells in different brain structures. As the GFP expression of AAV and dsRed expression of rabies are strong in labeled cell, we did not perform immunostaining against either GFP or dsRed. Selected presubiculum sections were immunostained with parvalbumin (PV) and

`

calbindin-D28K (CB) antibodies for distinguishing the entorhinal cortex from pre/parasubiculum (Fujise et al., 1995, Fujimaru and Kosaka, 1996). Conventional immunochemistry was performed as described previously (Xu et al., 2010). Calbindin D-28K (CB) immunostaining was performed with a rabbit anti-CB primary antibody (Swant, 1:1000) followed with an AF647-conjugated donkey anti-rabbit secondary antibody (Jackson ImmunoResearch, 1:200 dilution). For PV staining, a goat anti-PV primary antibody (Swant, 1:1000) followed with an AF488-conjugated donkey anti-goat secondary antibody (Jackson ImmunoResearch, 1:200). Sections were counter-stained with 10 μM DAPI, then mounted and cover-slipped with a Vectashield antifade mounting medium (Vecter Laboratories, Burlingame, CA).

Image data acquisition and analysis

Brain slice images were acquired by using an automated slide scanning and analysis software (Metamorph, Inc) in a high-capacity computer coupled with a fluorescent BX61 Olympus microscope and a high-sensitive Hamamatsu CCD camera, under a 10X objective we were able to obtain sufficient-resolution images suitable for all subsequent computer-based analyses. Image stitching, overlaying, cell counting and further imaging analysis were completed by using Metamorph imaging and analysis tools. In addition, we also imaged labeled cells in selected sections with a confocal microscope (LSM 700/780, Carl Zeiss Microscopy, Nussloch, Germany) coupled with z-stack and tile scanning features under a 20X objective lens.. Image stitching, overlaying, maximum projections and export were performed by using the ZEN software analysis tools.

Quantitative examinations across the series of sections were conducted for complete and unbiased analyses of rabies-mediated, direct synaptic connections to targeted Cre-defined cell

`

types by using either Metamorph or Adobe Photoshop software (CS4 extended version, Adobe Systems, San Jose, CA).

Statistical Analysis

Data were presented as mean ± SE. For statistical comparisons between groups, the data were checked for normality distribution and equal variance. If the criteria where met, a t-test was performed to compare two groups; when the criteria were not met, a Mann–Whitney U-test was used. For statistical comparisons across more than two groups, One-Way ANOVA with a tukey post hoc test was used for group comparisons. In all experiments, the level of statistical significance was defined as $p < 0.05$.

RESULTS

Mapping the topographic organization of CA3 projections along the proximodistal axis of CA1 by using the Cre-denpendent rabies tracing approach.

The Cre-dependent rabies tracing system has been thoroughly described by our published study (Sun et al., 2014). The system contains a Cre-dependent AAV helper virus and an EnvA-pseudotyped, glycoprotein mutated rabies virus to map the circuit connections to the Cre defined cell types in the intact brain (Fig. 2.1 A-C). In order to map direct synaptic connections to CA1 pyramidal neurons, we cross the Camk2a-Cre mouse line with a Cre-dependent TVA expressing LSL-R26$^{Tva\text{-}lacZ}$ mouse line, termed as Camk2a-Cre; TVA line. Therefore, after the helper AAV (AAV8-EF1a-FLEX-hG; h: histone GFP; G or RG: rabies B19 glycoprotein) was injected into the CA1, a starter population expresses both the EnvA receptor (TVA) via the transgenic mouse and rabies glycoprotein (RG) via the helper AAV. This population is then selectively infected with an EnvA-pseudotyped, RG-deleted rabies virus (EnvA-SADΔG-dsRed). Together, this conditional intersection results in transcomplementation and monosynaptic retrograde spread of

`

the rabies virus to presynaptic neurons of the starter population. Starter neurons, pyramidal cells in this case, in brain sections can be unambiguously identified by their nuclear GFP and dsRed expression from the helper AAV and ΔG-dsRed rabies genomes, respectively (Fig. 2.1). Because rabies replicates its core within starter neurons and their presynaptic neurons, this produces intense fluorescence with strong dsRed expression and thus reveals detailed cellular structures (Fig. 2.4).

We follow the basic nomenclature of Lorente de Nó (1934) (Lorente De Nó, 1934) and Ishizuka et al. (1990) (Ishizuka et al., 1990) to describe hippocampal sub-regions. The terms of proximal (nearer the dentate gyrus) and distal (farther from the dentate gyrus) are used to designate positions along the transverse axis of CA1 (Ishizuka et al., 1990) (Fig. 2.1). Subfields of CA3 are described as CA3a, CA3b, and CA3c, with CA3c as the nearest to the dentate gyrus. The midline of the fimbria separates CA3b and CA3a (Fig. 2.2). Excitatory neurons (CA1, CA3, and EC pyramidal cells) and inhibitory interneurons are identified based on their laminar locations and morphology. Quantitative strengths of specific circuit connections to CA1 pyramidal cells are assessed, and the input connection strength index (CSI) is defined as the ratio of the number of labeled presynaptic neurons in a specified brain structure versus the number of starter neurons in the CA1 (Fig. 2.7; Table 2.1).

We injected the helper AAV and rabies with a 3-week interval into the same brain region targeting a small population of pyramidal neurons in proximal CA1 (pCA1), intermediate CA1 (imCA1), and distal CA1 (dCA1) of the dorsal hippocampus, respectively (Fig. 2.1). The helper AAV virus was delivered into different CA1 subfields via pressure pulse injections (Fig 2.2). To achieve even more restricted injection site, we also deliver the AAV virus by using iontophretic current injections (Fig. 2.1). Pressure injections give rise to more starter neurons than

`

iontophretic injections (Table 2.1). However, both of the methods exhibit similar input connection patterns.

Hippocampal CA1 receives its predominant inputs from CA3 via the Schaffer collaterals. Consistent with the previous described "flipped" topographic map of CA3 projections to CA1 along the transvers axis (Ishizuka et al., 1990, Li et al., 1994, Brivanlou et al., 2004), we found that pCA1 receives its strongest CA3 projections from CA3a (CSI: 4.00 ± 0.55) both ipsilaterally and contralaterally (Fig 2.2 C; Fig 2.7 A). In comparison, imCA1 receives about equal amount of inputs from CA3a and CA3b (CSI: 2.61 ± 0.50 and 2.32 ± 0.41, respectively) (Fig. 2.2 B; Fig 2.7 A). On the contrary, dCA1 receives the most CA3 connections from CA3b (CSI: 1.23 ± 0.13) instead of CA3a (CSI: 0.61 ± 0.10; Fig. 2.2 A; Fig 2.7 A). Compared to other CA3 subfields, CA3c provide the least amount of inputs to CA1 across all different cases (Table 2.1). On the other hand, pCA1 receives the most overall CA3 projections, while dCA1 receives the least. imCA1 is in between (Fig 2.7 A). The overall number of rabies labeled CA3 neurons by targeting pCA1 are 3.7 fold greater than the dCA1 cases (Table. 2.1). Together, these data demonstrate that our rabies tracing system is capable of mapping the topographic organizations in the hippocampus. In addition to the "flipped" topography of CA3 projections to CA1, pCA1 receives greater amount of overall CA3 inputs than dCA1 which indicate the Schaffer collateral pathway may have much stronger influence to pCA1 than dCA1 in dorsal hippocampus.

Topographic organization of entorhinal projections along the proximodistal axis of CA1

We then characterized the topographic organization of the "direct pathway" from the entorhinal cortex (EC) to CA1. Consistent with the previous findings (Steward, 1976, Tamamaki and Nojyo, 1995) that MEC primarily projects to pCA1, while LEC projects more to dCA1, our results show pCA1 receives the direct MEC inputs with a CSI of 1.51 ± 0.24, which is about 3

`

fold greater than its LEC inputs (CSI: 0.49 ± 0.08; Fig. 2.3 A; Fig. 2.7 B). In addition, MEC also projects a little bit more to imCA1 than the LEC (CSI: 0.87 ± 0.10 vs 0.62 ± 0.04; Fig. 2.3 B; Fig. 2.7 B). Conversely, dCA1 receives the entorhinal inputs shifted to more lateral part of the EC with a CSI of 0.98 ± 0.11 from the LEC compared to the CSI of 0.45 ± 0.07 from the MEC (Fig. 2.3 C; Fig. 2.7 B). In contrast to CA3, different CA1 subfields receive about similar level of input connections from the entorhinal cortex as a whole (Table 2.1). These inputs mostly arise from dorsal part of the EC, as the injections in CA1 were made in the dorsal (Igarashi, 2016). Most of the MEC inputs arise from the septal part of the sections where MEC represents the most part of the EC. In contrast, when it shifts to more temporal sections, LEC inputs become the predominant (Fig. 2.3 A-C). There is an incremental gradient of LEC projections as well as a decremental gradient of MEC projections shifting from pCA1 to dCA1 (Fig. 2.7 B). There are also a small number of labeled cells seen in the contralateral EC, but we could not come up with a clear topographic map based on so few labeled neurons.

Meanwhile, the CA1 neurons also provide direct feedback projections to EC deep layers (Tamamaki and Nojyo, 1995). Pointing by the white arrows in Figure 2.3, prominent axons coming from the rabies labeled CA1 neurons around the injections site terminate in the layer V and layer VI of EC. Similar to the topography of the EC projections to CA1, the axons move from the medial to the lateral of EC along with the injection sites shifting from pCA1 to dCA1 (Fig. 2.3 A-C). Interestingly, the region of the rabies labeled entorhinal neurons located in EC matches the region of the CA1 incoming EC-projecting axons. This is consistent with previous reports that the origin and termination of the CA1 to EC projections are in register with the incoming entorhinal projections (Tamamaki and Nojyo, 1995, Naber et al., 2001). In addition,

`

the intensity of the axons terminating in MEC tends to be much stronger than the LEC, which may indicate pCA1 is projecting to the EC more extensively than the dCA1.

The general notion of the "direct pathway" and the "indirect pathway" are that CA1 neurons receive direct input from EC layer III, while EC layer II project to CA1 indirectly via the dentate gyrus or CA3. This is consistent with our result that most of the EC inputs arise from the layer III putative pyramidal cells (Fig. 2.4 A-B) However, we also found about 15% (N = 11; total cell counts: 483 neurons) of the rabies labeled EC neurons arise from layer II of the entorhinal cortex. They are presumably stellate cells based on their morphology (Fig. 2.4, arrow points). Considering these layer II neurons directly synapse onto the CA1 pyramidal cells, the CA1-projecting EC layer II neurons are likely one of the functional cell types in the EC, such as grid cells (Zhang et al., 2013). Together, our data showed there is a complementary transvers gradient between the MEC and LEC projections to different CA1 subfields. CA1 neurons, in turn, project to the deep layers of the incoming entorhinal projections. In addition, we also find a small population of EC layer II neurons that directly innervate the CA1 pyramidal cells.

Topographic organization of non-canonical subicular projections along the proximodistal axis of CA1

The circuit connections of the hippocampal formation are strongly feedforward in terms of the directionality of its information flow. However, along with previous findings in other species (Berger et al., 1980, Finch et al., 1983, Kohler, 1985, Harris and Stewart, 2001, Shao and Dudek, 2005), we recently discovered a non-canonical back-projection from the subiculum to CA1 in mouse, which contains both excitatory and inhibitory components (Sun et al., 2014, Xu et al., 2016). This previously unappreciated back-projection could potentially serve to modulate the hippocampal information processing (Jackson et al., 2014, Craig and McBain, 2015a). As the

`

CA1 projection to the subiculum has a mirrored topography so that distal CA1 projects to proximal subiculum, and proximal CA1 projects to distal subiculum (Amaral et al., 1991, Amaral, 1993), it is important to know whether the subiculum to CA1 back-projection shows any specific topographic relationship. In accordance with the previous physiological examination (Shao and Dudek, 2005), across cases with injections made in different CA1 subfields, there are consistently more CA1-projecting subicular neurons from the proximal subiculum than the distal (Fig. 2.5). All of the labeled neurons arise from the dorsal subiculum ipsilaterally, and there are no rabies labeled cells seen in the ventral subiculum (Fig. 2.5 H, P, X), likely due to the injections were made in the dorsal CA1 only. However, Distal CA1 (CSI: 1.33 ± 0.27) receives 2.5 fold and 4 fold more subicular back-projections than the imCA1 (CSI: 0.55 ± 0.05) and pCA1 (CSI: 0.31 ± 0.04), respectively (Fig. 2.5 C-F, K-N, S-V; Fig. 2.7 C; Table 2.1). The connection strength of the subicular back-projections to dCA1 is unexpectedly strong, even is comparable to the EC or CA3 inputs (Table 2.1). This suggests that in addition to the EC and CA3, the subiculum could also provide a considerable amount of influences to the CA1 in a topographic manner.

Interestingly, we also observed a group of neurons originating from the presubiculum as well as the parasubiculum that directly project to the CA1 (Fig. 2.3; Fig. 2.5 G, O, W; Fig. 2.6 A-C). Characterized by the staining pattern of layer II enriched calbindin D-28K (CB) and deep layer enriched parvalbumin (PV) in pre/parasubiculum versus the patchy-like CB staining in EC (Fujise et al., 1995, Fujimaru and Kosaka, 1996), we confirmed that the labeled neurons are indeed from the pre/parasubiculum, mostly layer III (Fig. 2.6 D-F). Furthermore, based on their morphology and devoid of CB and PV staining, the labeled neurons are likely pyramidal cells. Although there was a vague evidence showing the possible existence of this projection (Kohler,

`

1985), it is the first time here to firmly demonstrate that the CA1 neurons are innervated directly by the pre/parasubiculum. In addition, this pre/parasubiclum to CA1 projection also follows a topographic organization with pCA1 (CSI: 0.53 ± 0.11) receives more inputs from the pre/parasubiculum than the imCA1 (CSI: 0.28 ± 0.04) and the dCA1 (CSI: 0.24 ± 0.06; Fig. 2.7 C; Table 2.1). As it has been shown that pre/parasubiculum contains abundant functional cell types including grid cells, head-direction cells, and border cells (Boccara et al., 2010), our finding provides the first evidence that these functional cell types from pre/parasubiculum may directly influence the pCA1 place cells, which exhibit strong place modulations. Together, these data demonstrate the topographic map of the subiculum to CA1 projections with dCA1 receives more subicular inputs. Instead, we found a novel connection from pre/parasubiculum to the CA1 with pCA1 receives more innervations. This may suggest that the subiculum and the pre/parasubiculum involve in a segregated information flow to the CA1 and contribute to different cognitive functions.

DISCUSSION

By employing a novel Cre-dependent, monosynaptic rabies tracing system, we mapped the topographic organizations of the input connections from the CA3, EC, and subiculum specifically to the hippocampal CA1 pyramidal neurons along the proximodistal axis. The rabies technique allows us to perform a large-scale circuit mapping in a cell type specific and quantitative manner in the intact brain (Sun et al., 2014). In contrast to the previous circuit mapping studies by using the traditional tracers (i.e. PHA-L or BDA) or single-cell filling, our method benefits from targeting a small population of Cre+ postsynaptic cells and can provide weighted connection strengths for defined cell types. Because the number of postsynaptic starter cells and the number of direct presynaptic labeled cells in specified structures across the entire

`

brain can be quantitatively determined, this approach allows for assessment of the relative abundance of connected populations. The effectiveness of the rabies-based tracing is reflected by the extent of retrograde labeling in both local and distant structures in an unbiased fashion. Although we don't expect rabies to label every single presynaptic input to each neuron, the amount of labeled neurons with unambiguously identified cell soma are sufficient to provide a clear view of the three-dimensional organization of the projection sources. By providing the unprecedented quantitative analysis across the whole brain, our results confirmed and extended the understanding of the hippocampal topographic maps.

In the present study, we show that pCA1 receives a great amount of inputs from all regions of CA3 (CSI: CA3a > CA3b > CA3c). However, CA3 inputs to the dCA1 are unexpectedly low compared to the pCA1 (CSI: CA3b > CA3a > CA3c; Table 2.1). In contrast to the general notion that CA3c should provide more inputs to dCA1 than pCA1, our data show the projections from CA3c to pCA1 are much greater than it to dCA1. This discrepancy is likely due to all the injections were made in the septal level of the hippocampus, but CA3c tend to project to ventral dCA1 at more temporal levels (Ishizuka et al., 1990, Nakamura et al., 2013). CA3 is classically viewed as a homogenous module of the pattern completion. However, recent studies reveal the heterogeneity between CA3c and CA3a/b by showing CA3c has sharper place fields with constant remapping activities. In contrast, CA3a/b maintains coherent representations over time. These findings suggest a functional segregation for different CA3 subfields, which CA3c is responsible for pattern separation, while CA3a/b is responsible for pattern completion (Marrone et al., 2014, Lee et al., 2015, Lu et al., 2015). Our data provide further anatomical support for the functional segregation of the CA3. The extensive projections from dorsal CA3c to pCA1 provide a potential basis of the correlation between the sharp place fields for both areas and the

`

remapping activities in CA1 (Henriksen et al., 2010, Lu et al., 2015). Furthermore, projections from CA3a/b to pCA1 are required for spatial memory retrieval (Brun et al., 2002). In addition to the spatial and contextual memory, it has been shown that the CA3c projections to dCA1 preferentially contribute to the processing of non-spatial information as demonstrated by the expression of the immediately early gene *Arc* (Nakamura et al., 2013).

Several studies have shown that in a novel environment, CA1 can form a new stable spatial map ahead of CA3, which suggest the CA1 representation is not always under the control of CA3 projections (Lee et al., 2004, Leutgeb et al., 2004, Vazdarjanova and Guzowski, 2004, Leutgeb and Leutgeb, 2007). The faster appearance of the CA1 representation likely can be ascribed to the direct projections from the entorhinal cortex (Brun et al., 2002, Brun et al., 2008). Here we confirm the topographic map from the EC to CA1 projections with pCA1 receives more inputs from MEC, while dCA1 receives more inputs from LEC. In addition, imCA1 is similar to pCA1 in terms of the EC projections. The sharp spatial tuning of the pCA1 place cells could potentially attribute to the strong direct MEC inputs, rather than the CA3 inputs (Brun et al., 2002, Brun et al., 2008, Henriksen et al., 2010). On the other hand, consistent with our mapping data, by showing more non-spatial cognition to discrete objects, items, and odors, the representation of dCA1 is more resemble to the LEC rather than the MEC (Burke et al., 2011, Deshmukh and Knierim, 2011, Nakamura et al., 2013, Igarashi et al., 2014a, Igarashi et al., 2014b).

Typically, the direct pathway from EC to CA1 arises from layer III pyramidal cells and contributes to the temporal association of the episodic memory (Suh et al., 2011). However, it has been shown the EC layer II pyramidal cells (island cells) project directly to the CA1 interneurons to control the temporal association memory by mediating a feedforward inhibition,

`

while EC layer II stellate cells (ocean cells) projecting to DG and CA3 drive the context-specific memory (Kitamura et al., 2014, Kitamura et al., 2015). Interestingly, here we found a group a neurons (15% of total EC labeled cells), putative stellate cells, from layer II of both MEC and LEC that project directly to the CA1 pyramidal cells. As most of the layer II stellate cells of MEC are grid cells, this novel feedforward excitatory pathway could potentially convey spatial information to the CA1. Although LEC mainly represent non-spatial information, there are place cells in the superficial layers of the LEC (Hargreaves et al., 2005). Thus, it is unclear whether the LEC layer II to CA1 projections contribute to spatial or non-spatial information processing. Further experiments are needed to interrogate the specific function of this pathway.

In contrast to the view of the unidirectional circuit connections in the hippocampus, we found neurons from subiculum and pre/parasubiculum that directly project back onto the CA1 cells (Amaral and Witter, 1989, Sun et al., 2014, Xu et al., 2016). Interestingly, these two distinct back-projection pathways follow a complementary topography with subiculum projections terminate more in dCA1, while pre/parasubiculum projects more to pCA1. As neurons in the subiculum are much less spatially selective compared to neurons in the CA1 (Sharp and Green, 1994, Kim et al., 2012), subiculum to CA1 back-projections are likely contribute to the non-spatial information processing, which fit well with the function of dCA1 (Igarashi et al., 2014a). On the other hand, most of the CA1-projecting subicular neurons arise from the proximal subiculum, where there are numbers of subicular boundary vector cells (Lever et al., 2009). The subiculum to CA1 back-projections could also convey barrier information of the environment to the CA1 place cells (Barry et al., 2006). However, it remains to be seen whether the CA1-projecting subicular neurons contain any of the spatially-tuned functional cell types. In addition, neurons from pre/parasubiculum projecting to CA1 pyramidal cells are reported first time here.

`

The exact function of this novel connection is not clear. However, the existence of grid cells, head-direction cells, and border cells in the pre/parasubiculum and the preferred projections to pCA1 suggest this pathway may responsible for processing the spatial information (Boccara et al., 2010).

As CA1 receives inputs from both direct and indirect pathway, it has been hypothesized that direct pathway is responsible for generate the map of the current position, while the indirect pathway is important for the storage and retrieval of such information. However, by what mechanism that can control the information selection of direct and indirect pathway from CA1 with minimal interference is still illusive. It has been shown that the fast and slow gamma oscillations differentially route separate streams of information, which coupled to MEC and CA3, respectively. Importantly, both fast and slow gamma are modulated by theta oscillations and occurs at different theta phases and cycles. Interestingly, it has been demonstrated that hippocampal theta network activity can flow 'in reverse' from the subiculum to CA1 and CA3 to actively modulate spike timing and local network rhythms in these sub-regions (Jackson et al., 2014). In addition, a more recent slice physiology study demonstrated that disconnecting the subiculum from CA1 increased the pharmacologically induced gamma frequencies in rat CA1 (Craig and McBain, 2015a). This is perhaps due to removal of an inhibitory feedback mechanism from the subiculum to CA1. The subiculum to CA1 back-projections shown in our study likely contribute to the subiculum signaling that actively modulate the neural network activities in CA1. The back-projecting signals could potentially coordinate the information from the direct and indirect pathway for a final output. As the back-projection pathway is direct and local, it provides a potentially faster and more powerful feedback loop than the distant hippocampal-cortical connections. The concept of bidirectional connections between the subiculum and CA1

`

prompts an update of the idea that the subiculum is commonly regarded as an output structure of the hippocampal formation and not as an input structure. Feedback connections provide the means for modulating activity by immediately preceding events in contrast to strictly feedforward circuitry.

`

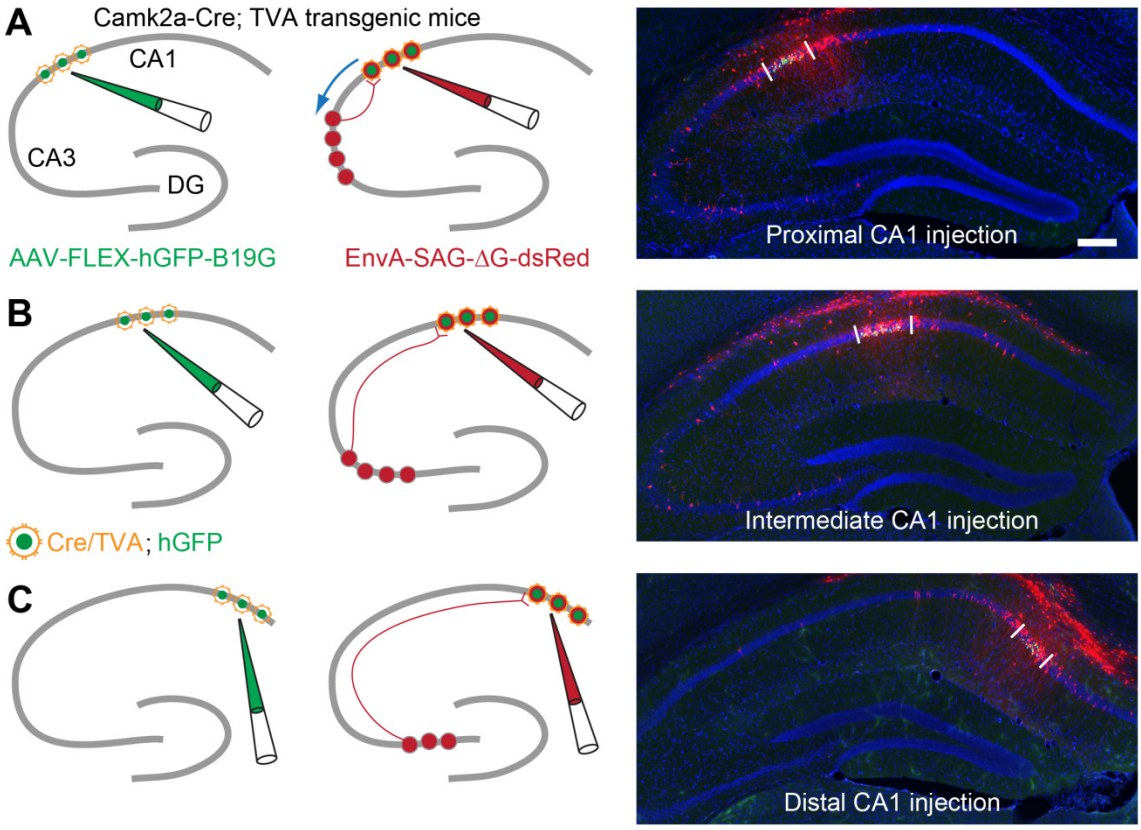

Figure 2.1. Rabies-based viral genetic targeting of CA1 pyramidal cells along the proximodistal axis for mapping the topographic organization of input connections to CA1 *in vivo*. (A-C) The schematic illustrates targeting proximal CA1 (A), intermediate CA1 (B), and distal CA1 (C) through a Cre-dependent rabies tracing technique. By using a Camk2a-Cre; TVA mouse line, a Cre-dependent AAV helper virus (AAV8-EF1a-FLEX-hG) carrying a histone GFP (hGFP) and a rabies B19 glycoprotein (B19G) is injected into different CA1 subfields. Thus, the AAV helper virus only expresses in CA1 excitatory pyramidal neurons. Three weeks later, an EnvA pseudotyped, glycoprotein deleted rabies virus encoding a dsRed fluorescent protein (EnvA-SAD-ΔG-deRed) is delivered into the same brain region of the AAV injection. Once rabies virus infected the same group of neurons via the TVA receptor, it undergoes transcomplementation and spreads to the presynaptic partners of the targeted neurons and labels the presynaptic neurons with dsRed. The right side of the figure shows examples of the injection sites in proximal CA1 (A), intermediate CA1 (B), and distal CA1 (C), respectively. Brain slices were sectioned coronally. DAPI staining is shown in blue, GFP expression of AAV helper virus is shown in green, and dsRed expression of rabies virus is shown in red. Neurons are infected by both AAV and rabies, termed as starter neurons, appear in yellow. Regions between two white

`

bars indicate the areas of the injections sites. AAV was delivered via an iontophoretic injection, while rabies was delivered via a pressure pulse injection. Scale bar in A = 200 μm also applies to B and C.

`

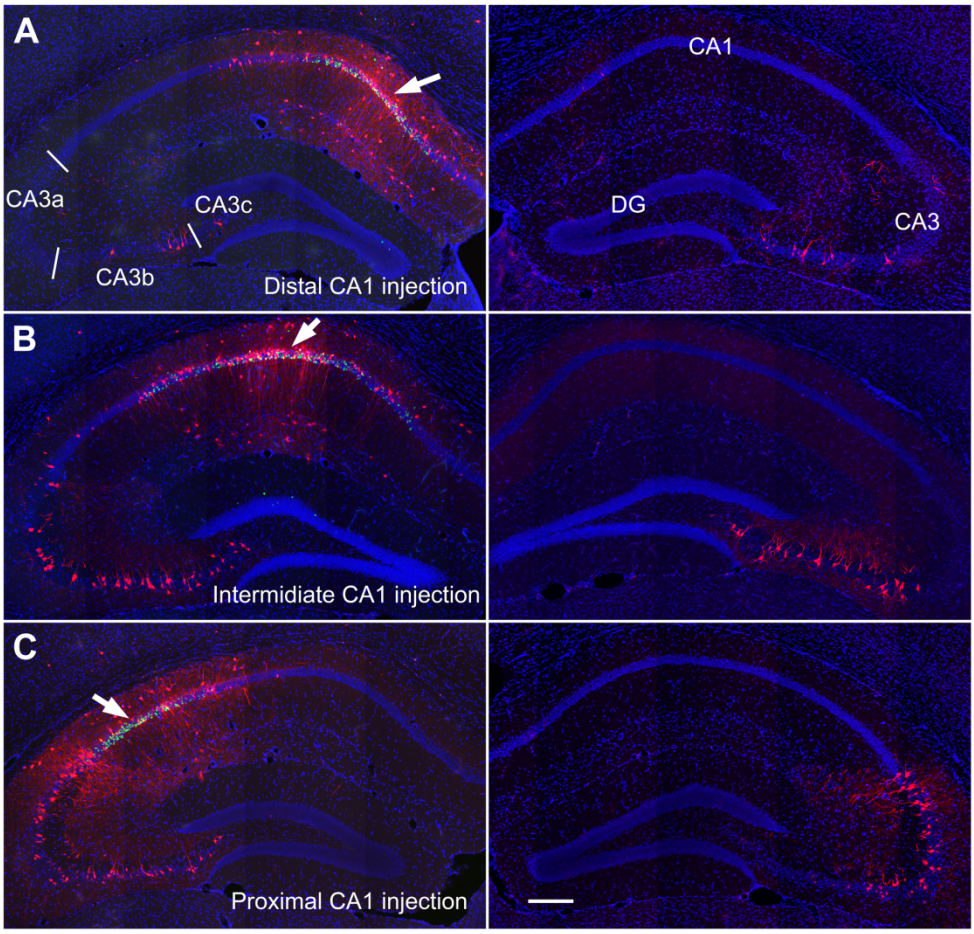

Figure 2.2. Topographic organization of CA3 projections to different CA1 subfields. (A) Ipsilateral (left) and contralateral (right) hippocampal images of coronal brain sections showing the pattern of CA3 projections to distal CA1. The white arrow points to the injection site of the AAV helper virus and rabies virus in distal CA1. CA3 neurons that are presynaptic to the starter neurons in the injections site are labeled with dsRed. GFP expression of AAV helper virus is shown in green; dsRed expression of rabies virus is shown in red; and DAPI staining is shown in blue. Both AAV and rabies were delivered into the brain via pressure pulse injections. Three white bars in CA3 indicate the criterion of defining CA3a, CA3b, and CA3c (subfields of CA3). (B) Organized similar to A, showing the pattern of CA3 projections to intermediate CA1. (C) Organized similar to A and B, showing the pattern of CA3 projections to proximal CA1.Scale bar = 200 μm applies to all the panels.

`

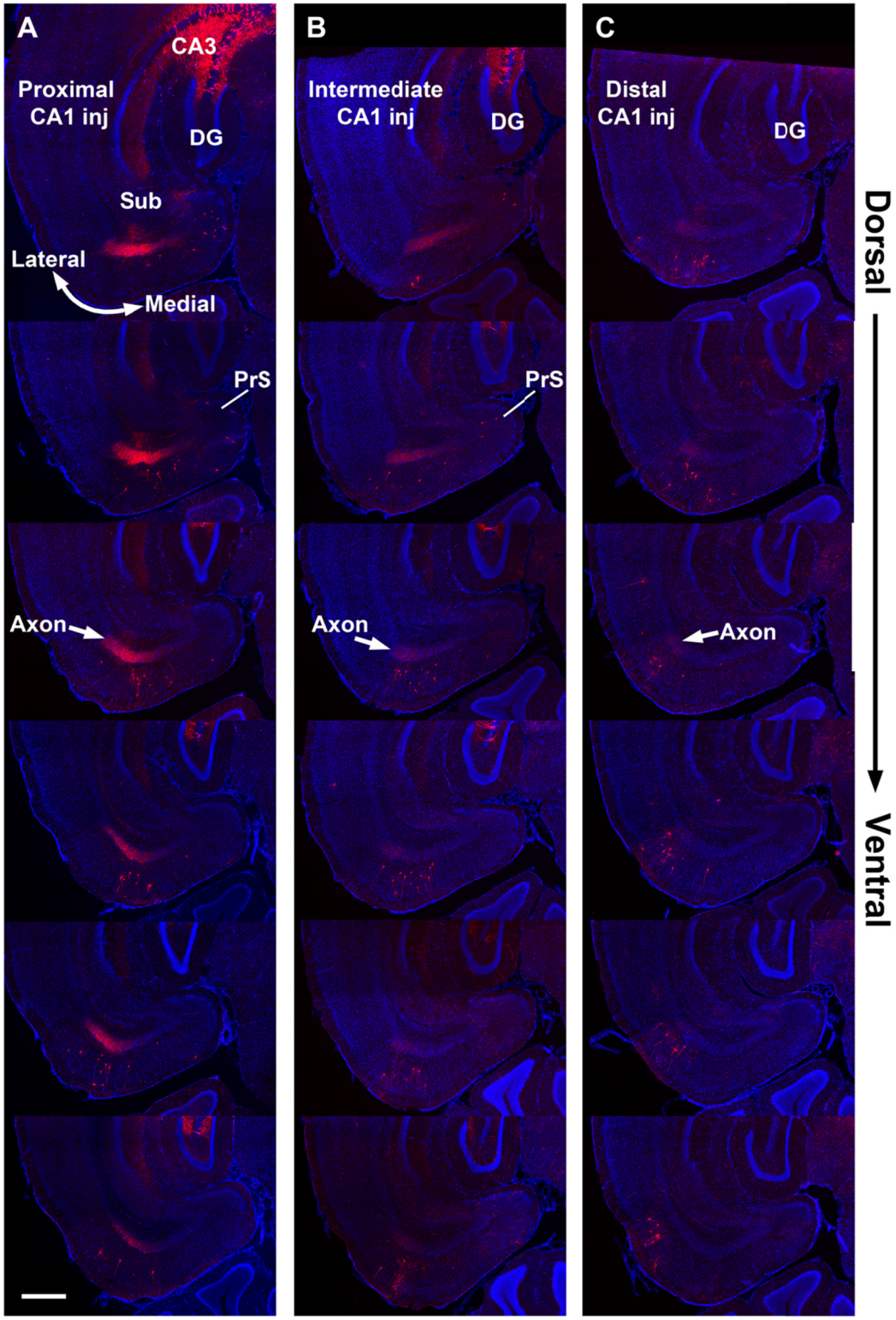

Figure 2.3. Topographic organization of EC projections to different CA1 subfields. (A) In horizontal brain sections, rabies labeled neurons show the input connection pattern from the entorhinal cortex to the proximal CA1 ipsilaterally. Images from the top to the bottom are

`

organized as the dorsal to ventral axis; the left to the right are organized from the lateral to medial axis. Rabies labeled neurons are shown in red. DAPI staining is shown in blue. The arrow points to the prominent axons terminating in the deeper layers of the entorhinal cortex. These axons come from rabies infected cells around the injection site in CA1. Scale bar = 500 μm applies to all the other panels. Note there is no injection site image showing in this figure. Please refer to figure 1 for the injection site information. (B) Organized similar to A. In horizontal brain sections, rabies labeled neurons show the input connection pattern from the entorhinal cortex to the intermediate CA1 ipsilaterally. (C) Organized similar to A and B. In horizontal brain sections, rabies labeled neurons show the input connection pattern from the entorhinal cortex to the distal CA1 ipsilaterally.

`

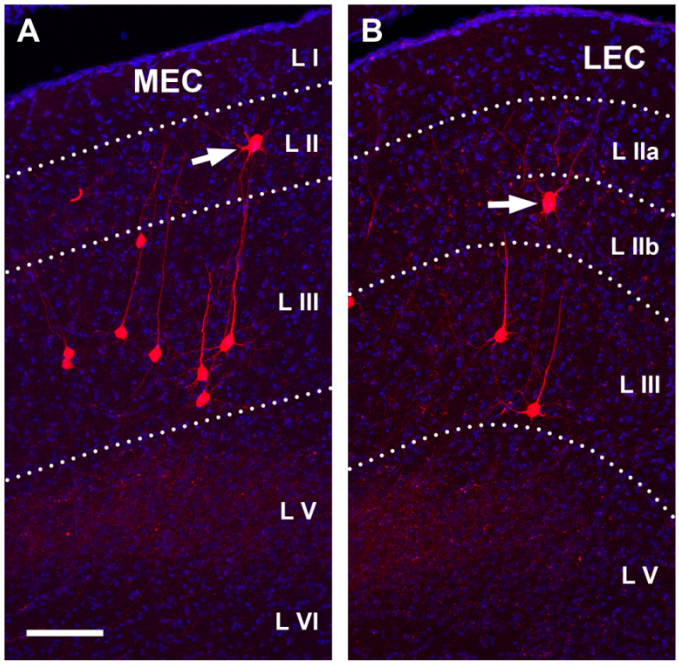

Figure 2.4. CA1-projecting entorhinal neurons contain both layer II and layer III cells from entorhinal cortex. (A) In a horizontal brain section, rabies labeled neurons in the medial entorhinal cortex (MEC) suggest the input connections from MEC to CA1 pyramidal cells are not only from MEC layer III pyramidal cells, but also putative stellate cells from MEC layer II. The white arrow points to a putative layer II stellate cell. Scale bar = 100 μm applies to both A and B. (B) Similar to A, rabies labeled neurons in the lateral entorhinal cortex (LEC) suggest the input connections from LEC to CA1 pyramidal cells are not only from LEC layer III pyramidal cells, but also putative stellate cells from LEC layer II.

`

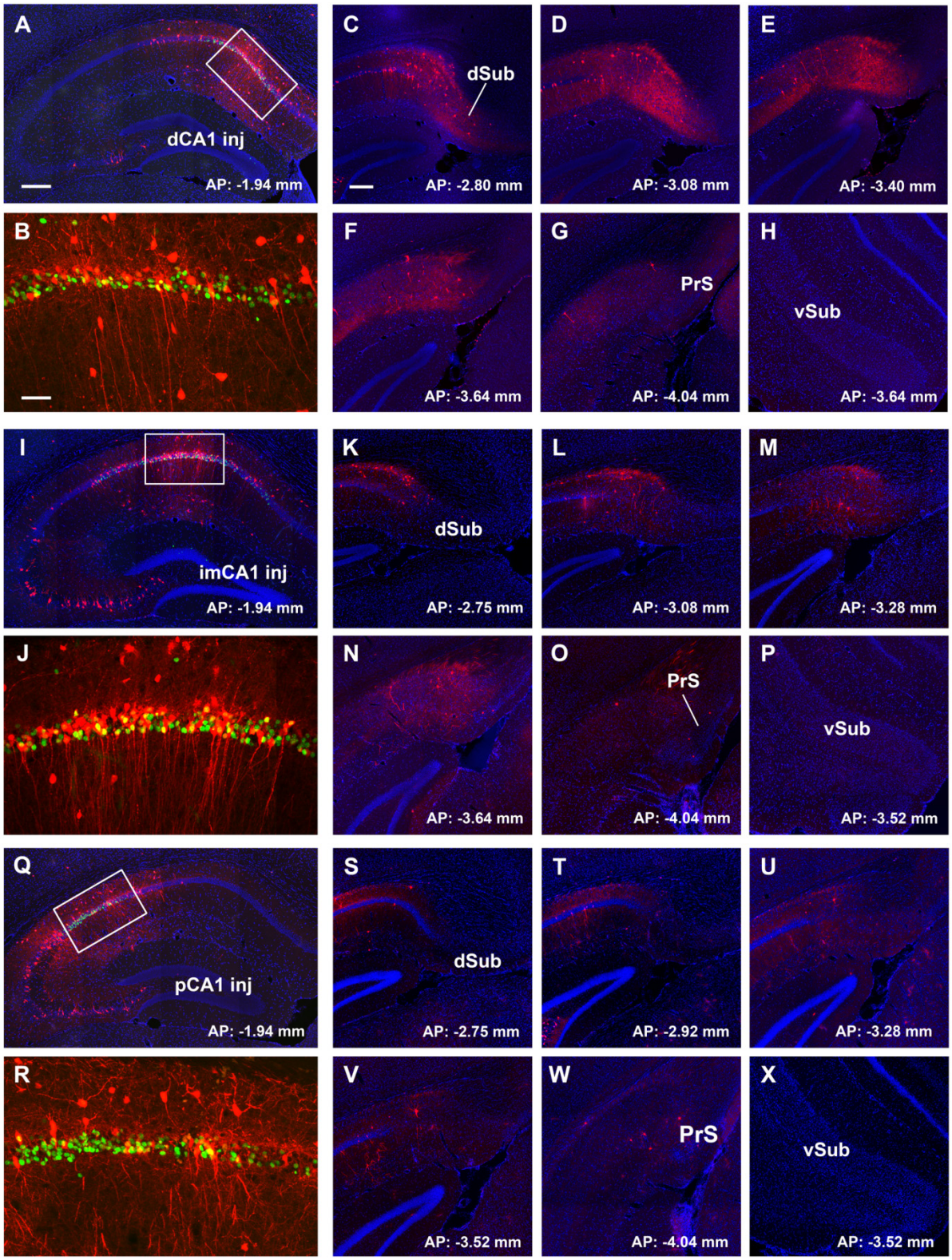

Figure 2.5. Topographic organization of subiculum projections to different CA1 subfields. (A) An image shows the injection site of a distal CA1 injection. Scale bar = 200 μm applies to A, I, and Q. (B) An enlarged view of the white box in A. The histone GFP expression of AAV

`

helper virus is shown in green, dsRed expression of rabies virus is shown in red. Double labeled starter neurons appear in yellow. Scale bar = 50 μm applies to B, J, and R. (C-F) labeling of distal CA1-projecting subicular neurons by rabies virus from dorsal subiculum (dSub) in a rostral-caudal axis. Scale bar in C = 200 μm applies to C-H, K-P, and S-X. (G) There are rabies labeled neurons from presubiculum (PrS) suggesting these neurons directly project to distal CA1. (H) There is no labeled neuron from ventral subiculum (vSub) suggesting ventral subiculum does not send direct input to distal CA1. (I) An image shows the injection site of an intermediate CA1 injection. (J) An enlarged view of the white box in J. (K-N) labeling of intermediate CA1-projecting subicular neurons by rabies virus from dorsal subiculum (dSub) in a rostral-caudal axis. (O) There are rabies labeled neurons from presubiculum (PrS) suggesting these neurons directly project to intermediate CA1. (P) There is no labeled neuron from ventral subiculum (vSub) suggesting ventral subiculum does not send direct input to intermediate CA1. (Q) An image shows the injection site of a proximal CA1 injection. (R) An enlarged view of the white box in Q. (S-V) labeling of proximal CA1-projecting subicular neurons by rabies virus from dorsal subiculum (dSub) in a rostral-caudal axis. (W) There are rabies labeled neurons from presubiculum (PrS) suggesting these neurons directly project to proximal CA1. (X) There is no labeled neuron from ventral subiculum (vSub) suggesting ventral subiculum does not send direct input to proximal CA1.

`

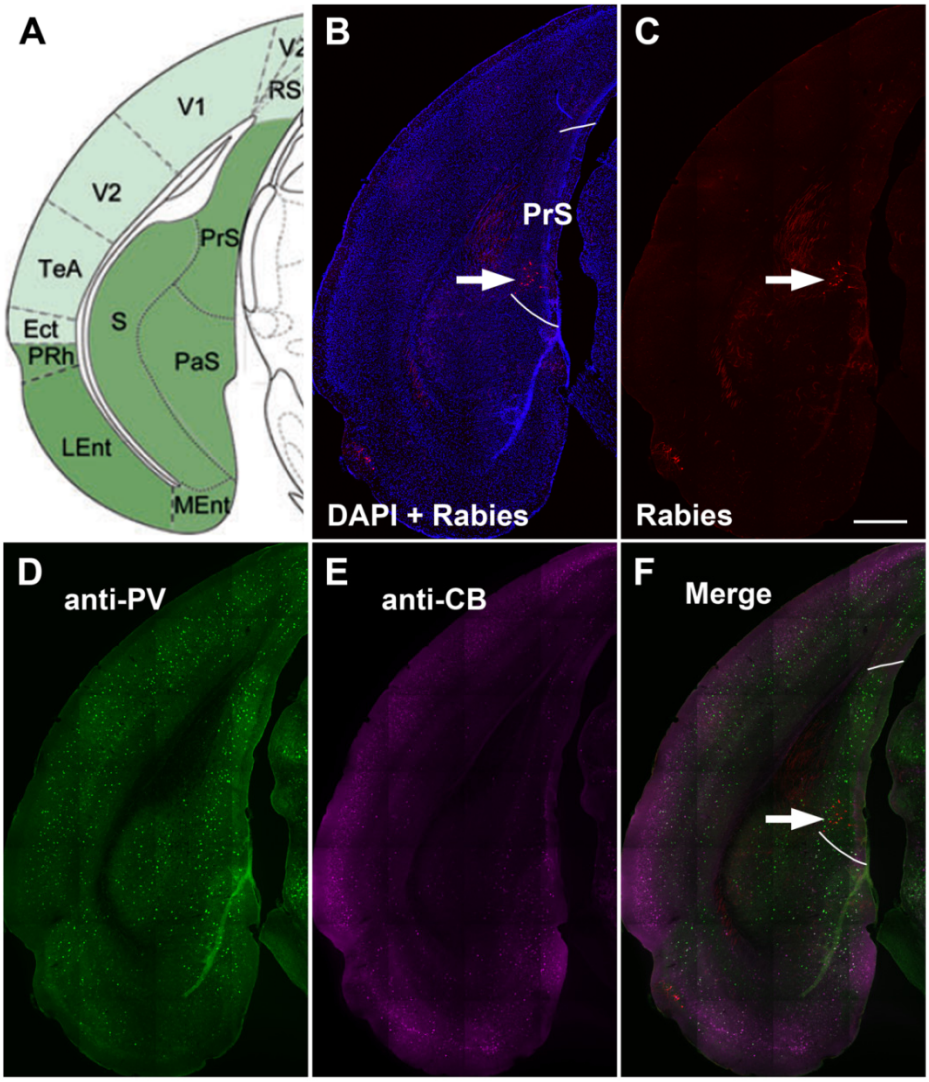

Figure 2.6. There are rabies labeled neurons from presubiculum, confirmed by immunostaining, directly project to hippocampal CA1. (A) An atlas image of a mouse brain coronal section shows the anatomy of presubiculum (PrS). (B) A brain section that is similar to the atlas. There are rabies labeled neurons appear to be in the presubiculum when the viruses were injected into the CA1. DAPI staining is shown in blue. White arrow points to the rabies labeled PrS neurons in red. Two white arcs delineate the region of PrS. (C) Single red channel in B showing rabies labeled neurons in the PrS. Scale bar = 500 μm applies to B-F. (D) Parvalbumin (PV) immunostaining, shown in green, of the same brain section in B. (E) Calbindin-D28k (CB) immunostaining, shown in magenta, of the same brain section in B. (F) A merged image from C-E. White arrow points to the rabies labeled neurons, which locate in the region that has strong PV immunoreactivity and weak calbindin immunoreactivity. Two white arcs delineate the region of PrS according to the PV and calbindin immunoreactivities.

`

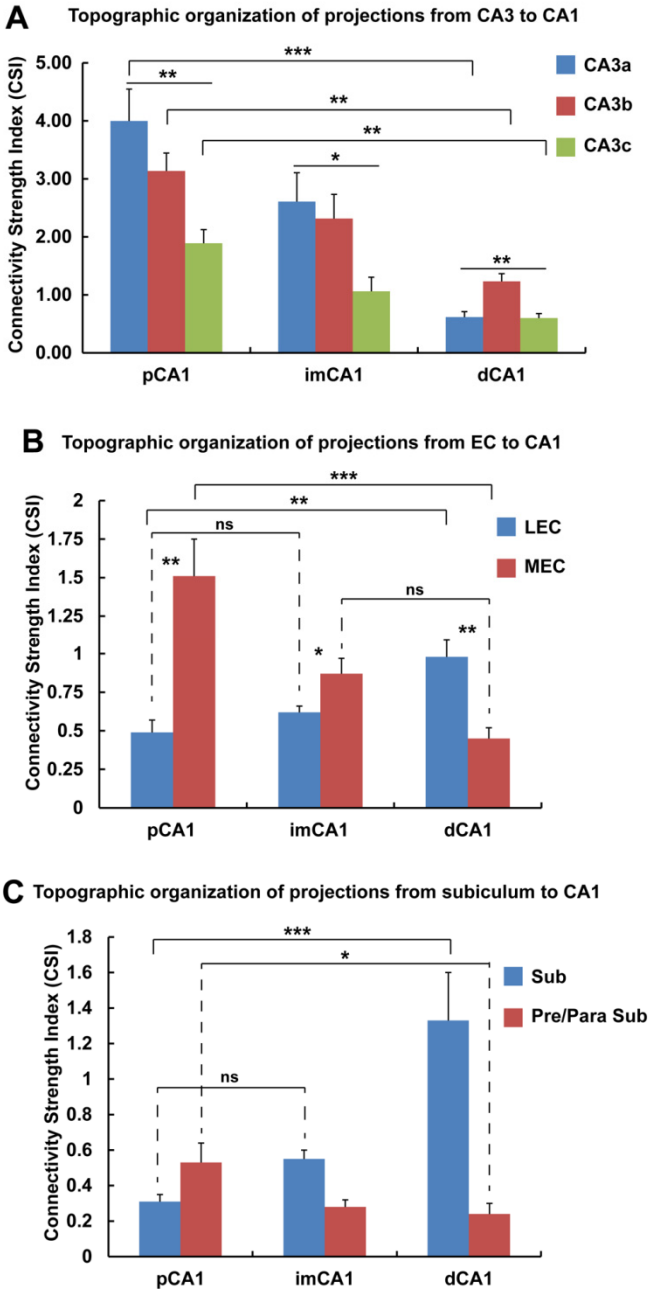

Figure 2.7. Quantitative analysis of intra- and para-hippocampal input connections to different CA1 subfields. (A) A quantitative summary shows input strength differences from a certain CA3 region (CA3a, CA3b, and CA3c) to proximal CA1, intermediate CA1, and distal CA1, respectively. The data are plotted as the connectivity strength index (CSI), which is defined as the number of presynaptic neurons in a specific brain region divide by the number of starter neurons in the injections site. The data also show differences of input connections from three CA3 subfields to a certain CA1 area. Group comparisons were performed by using one-way ANOVA. The data are presented as mean ± SE; *, **, and *** indicate the statistical significance levels of $p < 0.05$, 0.01, and 0.001 respectively. (B) A quantitative summary shows

`

input strength differences from LEC or MEC to proximal CA1, intermediate CA1, and distal CA1, respectively (one-way ANOVA with tukey post-hoc test). The data also show differences of input strength between LEC and MEC to a certain CA1 area (unpaired t-test). The data are presented as mean ± SE; *, **, and *** indicate the statistical significance levels of $p < 0.05$, 0.01, and 0.001 respectively. ns, not significant. (C) A quantitative summary shows input strength differences from subiculum or pre/parasubiculum to proximal CA1, intermediate CA1, and distal CA1, respectively (one-way ANOVA with tukey post-hoc test). The data are presented as mean ± SE; * and *** indicate the statistical significance levels of $p < 0.05$ and 0.001 respectively. ns, not significant.

`

Table 2.1 Quantitative strengths of specific circuit connections to proximal, intermediate, and distal CA1 pyramidal neurons, respectively.

Proximal CA1	CA3a	CA3b	CA3c	LEC	MEC	Sub	Pre/Para Sub
Average CSI	4.00	3.14	1.89	0.49	1.51	0.31	0.53
SE	0.55	0.31	0.23	0.08	0.24	0.04	0.11
N=	6			6		8	
# of starter neurons	Picospritzer inj: 126 ± 17; Iontophresis inj: 21 ± 4						

Intermediate CA1	CA3a	CA3b	CA3c	LEC	MEC	Sub	Pre/Para Sub
Average CSI	2.61	2.32	1.06	0.62	0.87	0.55	0.28
SE	0.50	0.41	0.24	0.04	0.10	0.05	0.04
N=	5			6		7	
# of starter neurons	Picospritzer inj: 136 ± 32; Iontophresis inj: 27 ± 5						

Distal CA1	CA3a	CA3b	CA3c	LEC	MEC	Sub	Pre/Para Sub
Average CSI	0.61	1.23	0.60	0.98	0.45	1.33	0.24
SE	0.10	0.13	0.08	0.11	0.07	0.27	0.06
N=	5			6		7	
# of starter neurons	Picospritzer inj: 80 ± 14; Iontophresis inj: 26 ± 4						

`

REFERNECES

Amaral DG (1993) Emerging principles of intrinsic hippocampal organization. Curr Opin Neurobiol 3:225-229.

Amaral DG, Dolorfo C, Alvarez-Royo P (1991) Organization of CA1 projections to the subiculum: a PHA-L analysis in the rat. Hippocampus 1:415-435.

Amaral DG, Witter MP (1989) The three-dimensional organization of the hippocampal formation: a review of anatomical data. Neuroscience 31:571-591.

Barry C, Lever C, Hayman R, Hartley T, Burton S, O'Keefe J, Jeffery K, Burgess N (2006) The boundary vector cell model of place cell firing and spatial memory. Rev Neurosci 17:71-97.

Berger TW, Swanson GW, Milner TA, Lynch GS, Thompson RF (1980) Reciprocal anatomical connections between hippocampus and subiculum in the rabbit evidence for subicular innervation of regio superior. Brain Res 183:265-276.

Boccara CN, Sargolini F, Thoresen VH, Solstad T, Witter MP, Moser EI, Moser MB (2010) Grid cells in pre- and parasubiculum. Nat Neurosci 13:987-994.

Brivanlou IH, Dantzker JL, Stevens CF, Callaway EM (2004) Topographic specificity of functional connections from hippocampal CA3 to CA1. Proc Natl Acad Sci U S A 101:2560-2565.

Brun VH, Leutgeb S, Wu HQ, Schwarcz R, Witter MP, Moser EI, Moser MB (2008) Impaired spatial representation in CA1 after lesion of direct input from entorhinal cortex. Neuron 57:290-302.

Brun VH, Otnass MK, Molden S, Steffenach HA, Witter MP, Moser MB, Moser EI (2002) Place cells and place recognition maintained by direct entorhinal-hippocampal circuitry. Science 296:2243-2246.

Burke SN, Maurer AP, Nematollahi S, Uprety AR, Wallace JL, Barnes CA (2011) The influence of objects on place field expression and size in distal hippocampal CA1. Hippocampus 21:783-801.

Cappaert NL, Van Strien NM, Witter MP (2015) Hippocampal formation. In: The Rat Nervous System (Fourth Edition) (Paxinos, G., ed), pp 511-573 London: Elsevier.

Craig MT, McBain CJ (2015a) Fast gamma oscillations are generated intrinsically in CA1 without the involvement of fast-spiking basket cells. J Neurosci 35:3616-3624.

Deshmukh SS, Knierim JJ (2011) Representation of non-spatial and spatial information in the lateral entorhinal cortex. Front Behav Neurosci 5:69.

Finch DM, Nowlin NL, Babb TL (1983) Demonstration of axonal projections of neurons in the rat hippocampus and subiculum by intracellular injection of HRP. Brain Res 271:201-216.

Fujimaru Y, Kosaka T (1996) The distribution of two calcium binding proteins, calbindin D-28K and parvalbumin, in the entorhinal cortex of the adult mouse. Neurosci Res 24:329-343.

Fujise N, Hunziker W, Heizmann CW, Kosaka T (1995) Distribution of the calcium binding proteins, calbindin D-28K and parvalbumin, in the subicular complex of the adult mouse. Neurosci Res 22:89-107.

Giocomo LM, Stensola T, Bonnevie T, Van Cauter T, Moser MB, Moser EI (2014) Topography of head direction cells in medial entorhinal cortex. Curr Biol 24:252-262.

Hargreaves EL, Rao G, Lee I, Knierim JJ (2005) Major dissociation between medial and lateral entorhinal input to dorsal hippocampus. Science 308:1792-1794.

`

Harris E, Stewart M (2001) Propagation of synchronous epileptiform events from subiculum backward into area CA1 of rat brain slices. Brain Res 895:41-49.
Henriksen EJ, Colgin LL, Barnes CA, Witter MP, Moser MB, Moser EI (2010) Spatial representation along the proximodistal axis of CA1. Neuron 68:127-137.
Hubel DH, Wiesel TN (1962) Receptive fields, binocular interaction and functional architecture in the cat's visual cortex. J Physiol 160:106-154.
Hubel DH, Wiesel TN (1969) Anatomical demonstration of columns in the monkey striate cortex. Nature 221:747-750.
Igarashi KM (2016) The entorhinal map of space. Brain Res 1637:177-187.
Igarashi KM, Ito HT, Moser EI, Moser MB (2014a) Functional diversity along the transverse axis of hippocampal area CA1. FEBS Lett 588:2470-2476.
Igarashi KM, Lu L, Colgin LL, Moser MB, Moser EI (2014b) Coordination of entorhinal-hippocampal ensemble activity during associative learning. Nature 510:143-147.
Ishizuka N, Weber J, Amaral DG (1990) Organization of intrahippocampal projections originating from CA3 pyramidal cells in the rat. J Comp Neurol 295:580-623.
Jackson J, Amilhon B, Goutagny R, Bott JB, Manseau F, Kortleven C, Bressler SL, Williams S (2014) Reversal of theta rhythm flow through intact hippocampal circuits. Nat Neurosci 17:1362-1370.
Kim SM, Ganguli S, Frank LM (2012) Spatial information outflow from the hippocampal circuit: distributed spatial coding and phase precession in the subiculum. J Neurosci 32:11539-11558.
Kitamura T, Pignatelli M, Suh J, Kohara K, Yoshiki A, Abe K, Tonegawa S (2014) Island cells control temporal association memory. Science 343:896-901.
Kitamura T, Sun C, Martin J, Kitch LJ, Schnitzer MJ, Tonegawa S (2015) Entorhinal Cortical Ocean Cells Encode Specific Contexts and Drive Context-Specific Fear Memory. Neuron 87:1317-1331.
Kohler C (1985) Intrinsic projections of the retrohippocampal region in the rat brain. I. The subicular complex. The Journal of comparative neurology 236:504-522.
Lee H, Wang C, Deshmukh SS, Knierim JJ (2015) Neural Population Evidence of Functional Heterogeneity along the CA3 Transverse Axis: Pattern Completion versus Pattern Separation. Neuron 87:1093-1105.
Lee I, Yoganarasimha D, Rao G, Knierim JJ (2004) Comparison of population coherence of place cells in hippocampal subfields CA1 and CA3. Nature 430:456-459.
Leutgeb S, Leutgeb JK (2007) Pattern separation, pattern completion, and new neuronal codes within a continuous CA3 map. Learn Mem 14:745-757.
Leutgeb S, Leutgeb JK, Treves A, Moser MB, Moser EI (2004) Distinct ensemble codes in hippocampal areas CA3 and CA1. Science 305:1295-1298.
Lever C, Burton S, Jeewajee A, O'Keefe J, Burgess N (2009) Boundary vector cells in the subiculum of the hippocampal formation. J Neurosci 29:9771-9777.
Li XG, Somogyi P, Ylinen A, Buzsaki G (1994) The hippocampal CA3 network: an in vivo intracellular labeling study. The Journal of comparative neurology 339:181-208.
Lorente De Nó R (1934) Studies on the structure of the cerebral cortex. II. Continuation of the study of the ammonic system. Journal für Psychologie und Neurologie 46:113-177.
Lu L, Igarashi KM, Witter MP, Moser EI, Moser MB (2015) Topography of Place Maps along the CA3-to-CA2 Axis of the Hippocampus. Neuron 87:1078-1092.

`

Marrone DF, Satvat E, Odintsova IV, Gheidi A (2014) Dissociation of spatial representations within hippocampal region CA3. Hippocampus 24:1417-1420.
Moser EI, Kropff E, Moser MB (2008) Place cells, grid cells, and the brain's spatial representation system. Annu Rev Neurosci 31:69-89.
Naber PA, Lopes da Silva FH, Witter MP (2001) Reciprocal connections between the entorhinal cortex and hippocampal fields CA1 and the subiculum are in register with the projections from CA1 to the subiculum. Hippocampus 11:99-104.
Nakamura NH, Flasbeck V, Maingret N, Kitsukawa T, Sauvage MM (2013) Proximodistal segregation of nonspatial information in CA3: preferential recruitment of a proximal CA3-distal CA1 network in nonspatial recognition memory. J Neurosci 33:11506-11514.
Patel GH, Kaplan DM, Snyder LH (2014) Topographic organization in the brain: searching for general principles. Trends Cogn Sci 18:351-363.
Penfield W, Boldrey E (1937) Somatic motor and sensory representation in the cerebral cortex of man as studied by electrical stimulation. Brain 60:389-443.
Seidler B, Schmidt A, Mayr U, Nakhai H, Schmid RM, Schneider G, Saur D (2008) A Cre-loxP-based mouse model for conditional somatic gene expression and knockdown in vivo by using avian retroviral vectors. Proc Natl Acad Sci U S A 105:10137-10142.
Shao LR, Dudek FE (2005) Electrophysiological evidence using focal flash photolysis of caged glutamate that CA1 pyramidal cells receive excitatory synaptic input from the subiculum. J Neurophysiol 93:3007-3011.
Sharp PE, Green C (1994) Spatial correlates of firing patterns of single cells in the subiculum of the freely moving rat. J Neurosci 14:2339-2356.
Stensola H, Stensola T, Solstad T, Froland K, Moser MB, Moser EI (2012) The entorhinal grid map is discretized. Nature 492:72-78.
Steward O (1976) Topographic organization of the projections from the entorhinal area to the hippocampal formation of the rat. J Comp Neurol 167:285-314.
Strange BA, Witter MP, Lein ES, Moser EI (2014) Functional organization of the hippocampal longitudinal axis. Nat Rev Neurosci 15:655-669.
Suh J, Rivest AJ, Nakashiba T, Tominaga T, Tonegawa S (2011) Entorhinal cortex layer III input to the hippocampus is crucial for temporal association memory. Science 334:1415-1420.
Sun Y, Nguyen AQ, Nguyen JP, Le L, Saur D, Choi J, Callaway EM, Xu X (2014) Cell-type-specific circuit connectivity of hippocampal CA1 revealed through Cre-dependent rabies tracing. Cell Rep 7:269-280.
Tamamaki N, Nojyo Y (1995) Preservation of topography in the connections between the subiculum, field CA1, and the entorhinal cortex in rats. J Comp Neurol 353:379-390.
Tsien JZ, Chen DF, Gerber D, Tom C, Mercer EH, Anderson DJ, Mayford M, Kandel ER, Tonegawa S (1996) Subregion- and cell type-restricted gene knockout in mouse brain. Cell 87:1317-1326.
Vazdarjanova A, Guzowski JF (2004) Differences in hippocampal neuronal population responses to modifications of an environmental context: evidence for distinct, yet complementary, functions of CA3 and CA1 ensembles. J Neurosci 24:6489-6496.
Wall NR, Wickersham IR, Cetin A, De La Parra M, Callaway EM (2010) Monosynaptic circuit tracing in vivo through Cre-dependent targeting and complementation of modified rabies virus. Proc Natl Acad Sci U S A 107:21848-21853.

`

Wickersham IR, Lyon DC, Barnard RJ, Mori T, Finke S, Conzelmann KK, Young JA, Callaway EM (2007b) Monosynaptic restriction of transsynaptic tracing from single, genetically targeted neurons. Neuron 53:639-647.

Woolsey TA, Van der Loos H (1970) The structural organization of layer IV in the somatosensory region (SI) of mouse cerebral cortex. The description of a cortical field composed of discrete cytoarchitectonic units. Brain Res 17:205-242.

Xu X, Roby KD, Callaway EM (2010) Immunochemical characterization of inhibitory mouse cortical neurons: three chemically distinct classes of inhibitory cells. J Comp Neurol 518:389-404.

Xu X, Sun Y, Holmes TC, Lopez AJ (2016) Noncanonical connections between the subiculum and hippocampal CA1. J Comp Neurol 524:3666-3673.

Zhang SJ, Ye J, Miao C, Tsao A, Cerniauskas I, Ledergerber D, Moser MB, Moser EI (2013) Optogenetic dissection of entorhinal-hippocampal functional connectivity. Science 340:1232627.

`

Chapter 3:

Circuit connections of CA1-projecting and other cell types in the subiculum

`

ABSTRACT

Subicular pyramidal cells, which contain both regular spiking and burst firing neurons, project differentially to their downstream targets. However, the input connection differences of neurons projecting to different brain areas in the subiculum are poorly understood. By using a combinatorial viral tracing strategy, we demonstrated excitatory neurons in the subiculum that project back to CA1 have different input connection pattern compared to other subicular excitatory neurons. Specifically, compared to subicular excitatory neurons in general, CA1-projecting subicular excitatory neurons do not receive input from lateral and medial entorhinal cortex, as well as other parahippocampal cortices. They also receive fewer inputs from CA1 excitatory neurons. However, CA1-projecting subicular excitatory neurons receive more inhibitory inputs from putative CA1 O-LM cells instead. In addition, we also characterized the circuit connections of subicular inhibitory neurons. Although the general connection pattern is similar to excitatory neurons, inputs to subicular inhibitory neurons are much more convergent than the other two neuron types by showing higher connection strengths from CA1 inhibitory neurons, presubiculum, retrosplenial cortex, visual cortex, auditory cortex, and MS-DB. Finally, we mapped the global output projections of the CA1-projecting subicular excitatory neurons. In contrast to the general notion that subicular neurons have a low degree of axonal collateralization, CA1-projecting subicular neurons project extensively to several other brain regions that are known targets for the subiculum. Together, we demonstrate that the CA1-projecting subicular neurons are a distinct group of subicular neurons with unique circuit connection properties compared to other subicular excitatory neurons and inhibitory neurons. Thus, our results further illustrate the heterogeneity of subicular neurons and suggest the differential functions of subicular neurons based on their segregated circuit pathways.

`

INTRODUCTION

The anatomical interface between the Ammon's horn and entorhinal cortex (EC) is the subiculum. Subiculum primarily receives convergent inputs from hippocampal CA1 and relay them to other cortical and subcortical regions, which make it as one of the major output structures of the hippocampus. In addition to CA1, it also receives inputs from EC, retrosplenial cortex, medial septum and diagonal band, amygdala, and thalamus (Witter et al., 1990, Witter, 2006). On the other hand, subfields of the subiculum sends parallel but differential outputs to many other brain regions in a topographic fashion with proximal subiculum projecting to the lateral entorhinal cortex, perirhinal cortex, amygdala, oribitofrontal cortex, nucleus accumbens, etc, while distal subiculum projecting to presubiculum, lateral entorhinal cotex, postrhinal cortex, retrosplenial cortex, and thalamus (Witter et al., 1990, Naber and Witter, 1998, Witter, 2006, Andersen et al., 2007, Kim and Spruston, 2012).

In addition to the differential projections, subicular pyramidal neurons can be categorized into two subpopulations, regular-spiking (RS) and burst-firing (BF) neurons, based on their firing properties (Stewart and Wong, 1993, Taube, 1993, Sharp and Green, 1994, Staff et al., 2000, Kim and Spruston, 2012). Although it is reported that RS cells outnumber BF cells 2:1 across the entire subiculum (Menendez de la Prida et al., 2003, Knopp et al., 2005), BF neurons are concentrated in the distal region of the subiculum while RS neurons are preferentially distributed in the region proximal to the CA1/subiculum border (Staff et al., 2000, Menendez de la Prida et al., 2003). The relationship between the firing properties and the targets of subicular pyramidal neurons has been examined by Kim and Spruston (2012). They reported that neurons projecting to amygdala, lateral entorhinal cortex, nucleus accumbens, and medial/ventral orbitofrontal cortex are located primarily in the proximal subiculum and consist mostly of regular-spiking

`

neurons. In contrast, neurons projecting to medial EC, presubiculum, retrosplenial cortex, and ventromedial hypothalamus are located primarily in the distal subiculum and consist mostly of bursting neurons (Ishizuka, 2001, Kim and Spruston, 2012). However, considering subicular pyramidal cells show a low degree of axonal collateralization and project mostly to only one downstream region (Witter et al., 1990, Naber and Witter, 1998), it is unclear whether neurons projecting to different targets have distinct input connection patterns.

Other than neurons projecting outside the hippocampus, we recently discovered a group of subicular neurons, which contain both excitatory and inhibitory components, project directly back onto the CA1 (Sun et al., 2014). As these CA1-projecting subicular neurons have potential unique functions in learning and memory (Jackson et al., 2014, Craig and McBain, 2015a, Xu et al., 2016), in the present study, we ask a question whether the CA1-projecting subicular neurons, compared to other subicular neurons, form distinct circuit connection patterns. Specifically, by using the newly developed combinatorial viral-genetic tracing, or TRIO technology (Wickersham et al., 2007b, Wall et al., 2010, Gore et al., 2013, Sun et al., 2014, Schwarz et al., 2015), we compared the input connections of CA1-projecting subicular excitatory neurons with the overall subicular excitatory neurons, as well as the subicular inhibitory neurons. Interestingly, we found the input connections of all the three neuron types are different from each other with CA1-projecting subicular excitatory neurons receive no input from parahippocampal cortices. Compared to subicular excitatory neurons, subicular inhibitory neurons receive more inputs from cortical and subcortical regions. In addition, all three neuron types receive differential excitation and inhibition from the CA1. We also characterized the output patterns of CA1-projecting subicular neurons, in contrast to the notion that subicular neurons have very few collaterals, CA1-projecting subicular neurons seems highly collateralized by projecting to

`

multiple brain regions which are known targets of the subiculum. Therefore, by mapping the circuit connections of all three types of subicular neurons, we demonstrated CA1-projecting subicular neurons are a distinct neuronal group in the subiculum with unique circuit connection properties, compared to other subicular excitatory and inhibitory neurons.

MATERIALS AND METHODS

Subjects

All experiments were conducted according to National Institutes of Health guidelines for animal care and use and were approved by the Institutional Animal Care and Use Committee of the University of California, Irvine. Although the genetically modified rabies viruses used for the proposed experiments are deletion-mutant rabies and are based on a vaccine strain (SAD-B19), they still pose a limited potential health risk with the helper virus. All personnel working with the rabies are therefore vaccinated and experiments are conducted under biosafety level (BSL) 2 conditions with a protocol approved by the institutional biosafety committee.

To achieve Cre-directed, cell type specific expression of TVA receptors in the subiculum, we used a LSL-R26$^{Tva\text{-}lacZ}$ mouse line conditionally expressing TVA receptor (avian retroviral receptor, tumor virus A) in a Cre-recombinase-dependent manner (Seidler et al., 2008); the LSL-R26$^{Tva\text{-}lacZ}$ mouse line was cross-bred with Camk2a-Cre (T29) mouse line (Tsien et al., 1996) to target subicular excitatory neurons, and Gad2-Cre mouse line to target subicular inhibitory neurons (Taniguchi et al., 2011). We termed the double transgenic mice as Camk2a-Cre; TVA, and GAD-Cre; TVA in which Cre-expressing cells also express TVA to restrict initial infection of EnvA-SADΔG rabies virus. For the input and output mapping of CA1-projecting subicular neurons, wild type C57BL/6 mice were used for the experiment. The mice of 8-12 weeks old (either sex) were used for experiments and had free access to food and water in their home-cages

`

before and after surgeries.

Viral injections for neural circuit tracing

To perform stereotaxic viral injections into the brain, mice were anesthesitized under 1.5% isoflurane for 10 minutes with a 0.8 L/min oxygen flow rate using an isoflurane table top unit (HME109, Highland Medical Equipment). Mice were then placed in a rodent stereotax (Leica Angle Two™ for mouse) with continuous 1% isoflurane anesthesia with the head secured. A small incision was made in the head, the skin reflected, and the skull exposed to show the landmarks of bregma and lambda, and desired injection sites. A three-axis micromanipulator guided by a digital atlas was used to determine coordinates for the bregma and lambda. The injection site was calculated relative to these landmarks, using canonical coordinates. The following injection coordinates targeting different brain regions were used (all values given relative to the bregma), intermediate CA1: anteroposterior (AP) −1.94 mm, lateromedial (ML) -1.40 mm; dorsoventral (DV) −1.35 mm; Subiculum: AP -3.40 mm, ML -1.96 mm, DV -1.67 mm. A small drill hole was made in the skull over the injection site, exposing the pia surface. A pulled glass pipette (tip diameter, ≈30 μm) was loaded with virus and then lowered into the brain with the appropriate coordinates. A Picospritzer (General Valve, Hollis, NH) was used to pulse virus into the brain. For the input mapping experiments of the subicular excitatory and inhibitory neurons, a total of 0.1 μl of the helper virus (AAV8-EF1a-FLEX-HB, ∼2 × 10^{11} genome units per ml; H: histone GFP; B: rabies B19 glycoprotein) (Addgene, Plasmid 37452) was injected into the subiculum of Camk2a-Cre;TVA and GAD-Cre; TVA mice, respectively, at a rate of 20 - 30 nl/min with 10 ms pulse duration. To prevent backflow of virus, the pipette remained in the brain for 5 min after completion of the injection. Once the injection pipette was withdrawn, the mouse was removed from the stereotax, and the incision was closed with either wound clips or

`

tissue adhesive (3M Vetbond, St. Paul, MN). Mice were taken back and recovered in their home cages. After 3 weeks of the AAV injection which allowed for the infected neurons to express high contents of RGs and GFP, the pseudotyped, RG-deleted rabies virus (EnVA-SADΔG-mCherry rabies, 0.2 μl, ~2×10^9 infectious units per ml) was injected into the same location of the previous injection. The rabies virus was allowed to replicate and retrogradely spread from targeted Cre+ cell types to directly connected presynaptic cells for 9 days before the animals were perfused for tissue processing. Since it has been estimated that rabies virus requires only 24 h to cross a synapse (Ugolini, 2008), the rabies infection time would be sufficient for crossing sparse and weak synaptic contacts, which is confirmed by our results.

To map the input connections of CA1-projecting subicular neurons, 0.4 μl of CAV2-Cre virus (~3×10^{12} infectious units per ml) was delivered into the intermediate CA1 region of the wild type C57BL/6 mouse in order to target the CA1-projecting subicular neurons. CAV2-Cre is able to retrogradely transport into the subiculum and express Cre restricted in the CA1-projecting subicular neurons. Then AAV8-EF1a-FLEX-HTB (~2×10^{11} genome units per ml; H: histone GFP; T: TVA: B: rabies B19 glycoprotein) was delivered into the subiculum at the same surgery session. Three weeks later, 0.2 μl of EnVA-SADΔG-mCherry rabies was injected into the same subiculum location. In order to verify the efficiency and specificity of the CAV2-Cre, we also injected the CAV2-Cre virus (0.4 μl) into CA1 of the Ai9 tdTomato reporter line (Madisen et al., 2010). The Ai9 animals are perfused for tissue processing 3 weeks after the injections.

To map the output projections of the CA1-projecting subicular neurons, the same CAV2-Cre virus was delivered into the intermediate CA1 region. Two weeks after the CAV2-Cre injections, 0.5ul Cre-dependent, tdTomato expressing herpes simplex virus H129ΔTK-TT (Lo and Anderson, 2011) was injected into the subiculum. The H129 virus was allowed to replicate

`

and anterogradely spread from targeted Cre+ cell types to directly connected postsynaptic cells for 72 hours before the animals were perfused for tissue processing.

Histology and immunohistochemistry

The mice were transcardially perfused with 5 ml of phosphate buffered saline (PBS), followed by 25 ml PBS containing 4% paraformaldehyde. The brains were removed and left in 4% paraformaldehyde overnight, then transferred into 30% sucrose in PBS in the next day. The brain is sectioned coronally in 30 μm thickness on a freezing microtome (Leica SM2010R, Germany). Every one out of 3 sections was mounted for examination and quantification of starter cells and their presynaptic cells in different brain structures. For the CA1-projecting subicular neurons input connection mapping cases, selected sections were stained with a GFP antibody to amplify GFP signal resulting from the helper AAV expression for dependable identification of starter cells. As mCherry expression is strong in rabies labeled cell, we did not perform immunostaining against mCherry. For GFP staining, a chicken anti-GFP primary antibody (Aves Labs, 1:500 dilution) followed with an Alexa Fluor (AF) 488-conjugated donkey anti-chicken secondary antibody (Jackson ImmunoResearch, 1:200 dilution) applied to the sections. To immunochemically identify neuronal cells, NeuN immunostaining was used with a mouse anti-NeuN primary antibody (Millipore, 1:100) followed with an AF488 -conjugated donkey anti-mouse secondary antibody (Jackson ImmunoResearch, 1:200). To immunochemically identify GABAergic cells, GABA immunostaining was performed with a rabbit anti-GABA primary antibody (Sigma-Aldrich, 1:1000) followed with an AF488 or AF647-conjugated donkey anti-rabbit secondary antibody (Jackson ImmunoResearch, 1:200 dilution). For the H129 experiment, we performed dsRed staining to amplify the mCherry signal with a rabbit anti-dsRed antibody (Clontech, 1:250 dilution) followed with an Cy3-conjugated

`

donkey anti-rabbit secondary antibody (Jackson ImmunoResearch, 1:200 dilution). Sections were counter-stained with 10 μM DAPI, then mounted and cover-slipped.

Image data acquisition and analysis

Brain slice images were acquired by using an automated slide scanning and analysis software (Metamorph, Inc) in a high-capacity computer coupled with a fluorescent BX61 Olympus microscope and a high-sensitive Hamamatsu CCD camera, under a 10X objective we were able to obtain sufficient-resolution images suitable for all subsequent computer-based analyses. Image stitching, overlaying, cell counting and further imaging analysis were completed by using Metamorph imaging and analysis tools. In addition, we also imaged labeled cells in selected sections with a confocal microscope (LSM 700/780, Carl Zeiss Microscopy, Nussloch, Germany) coupled with z-stack and tile scanning features under a 20X objective lens.. Image stitching, overlaying, maximum projections and export were performed by using the ZEN software analysis tools.

Quantitative examinations across the series of sections were conducted for complete and unbiased analyses of rabies-mediated, direct synaptic connections to targeted Cre-defined cell types by using either Metamorph or Adobe Photoshop software (CS4 extended version, Adobe Systems, San Jose, CA). Quantifications and analysis of H129 mediated projections were measured by using automatic threshold counting provided by the Adobe Photoshop software.

Statistical Analysis

Data were presented as mean ± SE. For statistical comparisons between groups, the data were checked for normality distribution and equal variance. If the criteria where met, a t-test was performed to compare two groups; when the criteria were not met, a Mann–Whitney U-test was used. For statistical comparisons across more than two groups, One-Way ANOVA with a

`

tukey post hoc test was used for group comparisons. In all experiments, the level of statistical significance was defined as $p < 0.05$.

RESULTS

Targeting CA1-projecting subicular excitatory neurons by using a retrograde axonal transport CAV2-Cre virus.

Canine adenovirus type 2 (CAV2) is a type of strong neurotropic virus with low cytotoxicity and high-level of retrograde transport (Kremer et al., 2000, Soudais et al., 2001, Peltekian et al., 2002). Cre expressing CAV2 virus (CAV2-Cre; Fig. 3.1 A) has been widely used for targeting projection specific neural circuits in the neuroscience research (Carter et al., 2013, Junyent and Kremer, 2015, Schwarz et al., 2015). CAV2-Cre can efficiently infect neurons in vivo and activates transgene expression in local and long-range connected populations of neurons in a Cre-dependent manner with transgenic animals or other genetically modified viruses. Taking advantage of its retrograde labeling in neurons, we use the CAV2-Cre to target the CA1-projecting subicular neurons.

To characterize the viral spread and the retrograde axonal transport of the CAV2-Cre, we injected the CAV2-Cre into hippocampal CA1 of the Ai9 reporter mice (Fig. 3.1 B). As a result of the CAV2 local infection, introducing Cre recombinase activates the tdTomato expression in the CA1 neurons around the injection site, with a viral spread ~200-300 μm, in the Ai9 mouse (Fig. 3.1 C). Interestingly, tdTomato expressions are exclusively restricted to the CA1 pyramidal cell layer, which indicate the CAV2-Cre primarily infect the CA1 excitatory pyramidal neurons (Fig. 3.1 C). We then characterized the retrograde axonal transport properties of the CAV2-Cre. All known projections from the CA3, entorhinal cortex, and MS-DB to CA1 are labeled with tdTomato (data not shown). More importantly, we found a significant number of neurons are

`

labeled in the subiculum indicating the CAV2-Cre effectively labels the CA1-projecting subicular neurons by its retrograde transport (Fig. 3.1 D). As it has been shown that the CA1-projecting subicular neurons contain both excitatory and inhibitory components (Sun et al., 2014), we performed GABA staining in selected subiculum sections in order to see if CAV2-Cre shows similar viral tropism in the subiculum as in CA1. As expected, tdTomato-labeled CA1-projecting subicular neurons are predominantly excitatory as none of them showing positive for GABA staining (Fig 3.1 E).

Because experiments in the rest of the study target the CA1-projecting subicular neurons by a combinatorial using of the CAV2-Cre with a Cre-dependent AAV virus, we further examined the CAV2 labeling efficiency and tropism by injecting the CAV2-Cre in the CA1 and a Cre-dependent, mCherry-expressing AAV virus (AAV-DIO-hM4D-mCherry) in the subiculum simultaneously into the wild type C57BL/6 mice. CA1-projecting subicular neurons are labeled with mCherry at a density of ~65 cells/mm^2 (Fig. 3.1 F, G, and K; N=4). Compared to the densities of total subicular neurons (2433 cells/mm^2; N=4) characterized by NeuN staining (Fig. 3.1 H) and total subicular inhibitory neurons (144 cells/mm^2; N=4) characterized by GABA staining (Fig. 3.1 I), CAV2-labeled CA1-projecting subicular neurons accounts for 2.7% ± 0.1% (mean ± SE) of the overall population of subicular neurons. In addition, similar to our findings above, CA1-projecting subicular neurons targeted by the combinatorial viral strategy are preferentially excitatory neurons that confirmed by GABA staining (Fig. 3.1 G-J). Overall, 98% (N=4) of labeled CA1-projecting subicular neurons are GABA negative. Thus, we conclude that CAV2-Cre primarily targets the excitatory neurons in CA1 and subiculum due to its viral tropism. Therefore, CAV2-Cre effectively and specifically targets the CA1-projecting subicular excitatory neurons.

`

Input connections of CA1-projecting subicular excitatory neurons compared to the overall subicular excitatory neurons and inhibitory neurons.

Although the anatomical projections of subicular neurons have been extensively studied, the cell type-specific and projection specific input connections to subicular neurons have yet been systematically characterized. As recent discoveries showing the subiculum to CA1 back-projections may play very important roles in cortical oscillations (Jackson et al., 2014, Sun et al., 2014, Craig and McBain, 2015a, Xu et al., 2016), we would like to see if the circuit connections of these CA1-projecting subicular neurons are different from other subicular excitatory or inhibitory neurons. Taking advantage of the combinatorial viral genetic approach with the CAV2-Cre and Cre-dependent rabies tracing (Sun et al., 2014, Schwarz et al., 2015, Sun et al., 2017), we are able to target the CA1-projecting subicular excitatory neurons and map their direct input connections in a cell-type as well as a projection specific manner (Fig. 3.2 E). More specifically, CAV2-Cre was injected into the hippocampal CA1 of the wild type C57BL/6 mice, meanwhile, a Cre-dependent helper AAV (AAV-DIO-HTB; H: histone GFP, T: TVA, B: rabies B19 glycoprotein) was injected into the subiculum (Fig. 3.2 E). After the Cre specifically expresses in the CA1-projecting subicular excitatory neurons via the retrograde CAV2-Cre, EnvA receptor (TVA) and rabies glycoprotein (RG) will be expressed in the same group of neurons via the helper AAV. This starter population is then selectively infected with an EnvA-pseudotyped, RG-deleted rabies virus (EnvA-SADΔG-mCherry). Together, this conditional intersection results in transcomplementation and monosynaptic retrograde spread of the rabies virus to presynaptic neurons of the starter population (Fig. 3.2 E). In addition, to target subicular excitatory and inhibitory neurons, we crossed the Camk2a-Cre and the Gad2-Cre mouse lines with a Cre-dependent TVA expressing LSL-R26$^{Tva\text{-}lacZ}$ mouse line, and term them as Camk2a-

`

Cre; TVA and GAD-Cre; TVA lines, respectively. A Cre-dependent AAV helper virus (AAV-DIO-HB; H: histone GFP, B: rabies B19 glycoprotein) and EnvA-SADΔG-mCherry are then delivered into the subiculum of the Camk2a-Cre; TVA and GAD-Cre; TVA mice with a three-week interval in order to map the direct input connections to the Cre defined, TVA-expressing cell types (Fig. 3.2 A and C). In all three neuron types we targeted, the starter neurons in subiculum sections can be unambiguously identified by their GFP and mCherry expression from the helper AAV and ΔG-mCherry rabies genomes, respectively (Fig. 3.2 B, D, and F).

In terms of their extrinsic inputs, all three subicular cell types receive a great majority of inputs from hippocampal CA1 (Fig. 3.3 C, D, K, L, R, and S), but they appear to differ quantitatively as assessed by the % of total labeled neurons providing extrinsic inputs to the subiculum, as well as the connectivity strength index (CSI) defined as the ratio of the number of presynaptic neurons labeled in a specific brain structure divide by the number of starter neurons (Fig. 3.4). The putative CA1 excitatory input accounts for 86.7 ± 1.6%, 45.2 ± 1.6% and 60.3 ± 4.4% of the total inputs, respectively, to overall subicular excitatory neurons, inhibitory neurons, and CA1-projecting subicular excitatory neurons (Fig. 3.4; Table 3.1). Subicular excitatory neurons receive little inputs from CA1 inhibitory neurons (CSI: 0.9 ± 0.22), in contrast, CA1-projecting subicular excitatory neurons and subicular inhibitory neurons receive a significant number of inhibitory inputs from putative O-LM cells in the stratum oriens (CSI: 4 ± 0.44 and 8.2 ± 1.12, respectively; Fig. 3.3 R, S, and L). In addition, subicular inhibitory neurons also receive the inhibition from CA1 s.r. and s.l.m. layers (CSI: 1.19 ± 0.21 and 1.99 ± 0.51, respectively; Fig. 3.3 L; Fig. 3.4). Interestingly, all the incoming CA1 inhibitory inputs arise from the hippocampus towards more temporal levels (Fig. 3.3 C, D, K, L, Q, and R). Compared to subicular excitatory neurons, CA1-projecting subicular excitatory neurons also receive

`

relatively strong inputs from visual cortex (1.3 ± 0.3% vs 13.2 ± 2.1 %; Fig 3.3 E and U). However, they receive no input from temporal association cortex, perirhinal cortex, and entorhinal cortex (Fig. 3.3 H and W; Fig. 3.4; Table 3.1). This indicates that CA1-projecting subicular neurons can modulate CA1 circuit activity without direct entorhinal cortical inputs. In comparison to the two types of excitatory neurons, the circuit connections of subicular inhibitory neurons are much more convergent by showing higher CSI from various of the brain regions including presubiculum, retrosplenial cortex, visual cortex, auditory cortex, temporal association cortex, perirhinal cortex, MS-DB, and Thalamus (Fig. 3.3 and 3.4; Table 3.1). Together, all three type of subicular neurons display connection patterns from similar brain regions. However, they are quite different in terms of the connection strengths. Namely, subicular inhibitory neurons show a much higher convergent input connection pattern compared to excitatory neurons. More importantly, CA1-projecting subicular excitatory neurons have a distinct circuit organization compared to the overall subicular excitatory neurons and inhibitory neurons.

Global output projections of CA1-projecting subicular excitatory neurons.

By using the CAV2-Cre combined with a Cre-dependent, tdTomato-expressing anterograde-directed herpes simplex virus (H129ΔTK-tdTomato)(Lo and Anderson, 2011), we are able to map the output projections of CA1-projecting subicular excitatory neurons (Fig. 3.5 A-B). The H129ΔTK-tdTomato is able to transport to the connected postsynaptic neurons and illuminate them with tdTomato. In addition to the confirmed projections to CA1 (Fig. 3.5 E), CA1-projecting subicular excitatory neurons also project to a number of brain regions including orbital prefrontal cortex, MS-DB, thalamus, visual cortex, retrosplenial cortex, perirhinal, ectorhinal, and temporal association cortices (Fig. 3.5 C-H). They also show very strong projections to both lateral and medial entorhinal cortex (Fig. 3.5 I; Table 3.2). Interestingly, we

`

found the input and projection patterns seem complementary in some brain regions. For example, CA1-projecting subicular neurons receive input from retrosplenial granular cortex (RSG), while they tend to project to the retrosplenial agranular cortex (RSA) (Fig. 3.3V and 3.5G). In addition, subicular neurons receive thalamic inputs from the anteroventral region. In contrast, they project to ventrolateral thalamus instead (Fig. 3.3 B, J, and 3.5 E). This complementary input-output connection pattern suggests the segregated information processing in the cortical networks.

DISCUSSION

In the present study, we mapped the whole brain circuit connections of CA1-projecting subicular excitatory neurons, overall subicular excitatory neurons, and subicular inhibitory neurons by using the combinatorial viral genetic tracing. Our data have shown the circuit connections of three subicular neuronal types are different from each other, particularly in their connection strengths. One striking difference between the subicular excitatory neurons and the other two neuron types are CA1-projecting subicular excitatory neurons and subicular inhibitory neurons receive a significant amount of inputs from CA1 inhibitory neurons, most of which are putative O-LM cells in the oriens layer. This is consistent with previous studies using slice or juxtacellular recording-labeling showing the long-range hippocampal GABAergic projection neurons, mostly somatostatin+, from the CA1 oriens layer innervating the subiculum, presubiculum, retrosplenial cortex, and septum (Losonczy et al., 2002, Jinno et al., 2007, Jinno, 2009). Our data even move this finding forward by showing these oriens GABAergic projection neurons primarily innervate the subicular inhibitory neurons and a subset of subicular excitatory neurons, namely the CA1-projecting subicular excitatory neurons. Functionally, as these subiculum-projecting CA1 GABAergic neurons show a theta phase precession which fire particularly at or after the trough of the theta cycle, and strongly increase their firing frequency

`

during the sharp wave-associated ripple oscillations, they may preset the subiculum before the arrival of CA1 excitations (Jinno et al., 2007) and coordinate a compress of CA1 signals in a highly informative way before sending to other downstream brain regions (Kim et al., 2012). This is consistent with our observations that subicular excitatory neurons receive highly convergent inputs from CA1. On the other hand, CA1-projecting subicular neurons may play critical roles in providing feedback signals to set the timing of the CA1 information flow in order to ensure the correct signal transformation (Deadwyler and Hampson, 2004). This is supported by a recent study showing hippocampal theta network activity can flow 'in reverse' from the subiculum to CA1 and CA3 to actively modulate spike timing and local network rhythms in these sub-regions (Jackson et al., 2014). Our current study focuses on the excitatory CA1-projecting subicular neurons. However, a more recent slice physiology study suggests inhibitory CA1-projecting subicular neurons may also play important roles in modulating the hippocampal rhythmic activates by showing disconnecting the subiculum increased pharmacologically induced gamma frequencies in rat CA1 (Craig and McBain, 2015a). It was proposed that this is perhaps due to removal of an inhibitory feedback mechanism from the subiculum to CA1. In fact, intrinsically generated fast and slow gamma oscillations as well as the aforementioned back-propagating theta oscillations within the subiculum imply the inhibitory mechanism likely have a greater contribution to the coordination between the CA1 and subiculum (Jackson et al., 2011, Jackson et al., 2014). Nevertheless, it needs further investigation whether subiculum to CA1 projections indeed modulate hippocampal network activities.

The subiculum contains several functional cell types, although few in number, including place cells, head-direction cells, and boundary vector cells (Sharp and Green, 1994, O'Mara et al., 2001, Lever et al., 2009). More recently, it has been shown that a subpopulation of subicular

`

neurons tuned to the axis of travel (Olson et al., 2017). However, in addition to the much less convergent inputs from CA1, CA1-projecting subicular excitatory neurons do not receive input from the entorhinal cortex. This suggests the CA1-projecting subicular excitatory neurons may be independent to the entorhinal inputs and show less spatial tuning properties. Nevertheless, as both the CA1-projecting subicular neurons and boundary vector cells are concentrated in the proximal subiculum, it is worthwhile to see if the CA1-projecting subicular neurons show any spatial related properties. Furthermore, it is also unclear whether the subiculum to CA1 back-projections modulate the spatial tuning properties of CA1 place cells. On the other side, as we have demonstrated the subiculum to CA1 back-projections innervate the distal CA1 more than the proximal (chapter 2), CA1-projecting subicular neurons likely have impact on processing non-spatial information, such as objects, items, and odor signals (Henriksen et al., 2010, Burke et al., 2011, Deshmukh and Knierim, 2011, Nakamura et al., 2013, Igarashi et al., 2014a, Igarashi et al., 2014b).

Our data surprisingly showed significant direct visual cortical projections to subicular inhibitory neurons. This is partly supported by the previous studies shown that there are reciprocal connections between the visual cortex and pre/parasubiculum (Vogt and Miller, 1983, Coogan and Burkhalter, 1993). In addition, anterograde tracing experiments performed in the primary visual area from Allen Mouse Brain Connectivity Atlas also show axon fibers in the subiculum (Oh et al., 2014). However, the inputs from visual cortex to subicular inhibitory neurons shown by us are much higher than the previous reports. It is unlikely due to the potential leak through (virus back flow) during the virus injection, as our control experiment (without helper AAV injection) shows minimal direct rabies infection in the visual cortex. In addition, we

`

cannot rule out the possibility that the virus spread into the distal subiculum that close to the presubiculum, which receives greater inputs from the visual cortex.

Our H129 results have shown that CA1-projecting subicular neurons also project to several other brain regions. This seems contradictory to the earlier anatomical studies shown that subicular neurons have very few axonal collaterals and send parallel projections to different brain regions (Donovan and Wyss, 1983, Naber and Witter, 1998, Witter, 2006, Kim and Spruston, 2012). However, study has also shown around 30% of subicular neurons project to more than one downstream targets (Swanson et al., 1981). Moreover, by using intracellular injection of HRP, Finch et al., 1983 reported a case of a single subicular pyramidal cell with 4 major efferent branches targeting 3 different brain regions (Finch et al., 1983). Despite the limited combinations of subiculum targets that were tested in the previous studies, it is likely to be true that most of the subicular neurons only project to one downstream target. However, based on our observation, CA1-projecting subicular neurons only account for 3% of total neurons in the subiculum. As a unique neuronal group in the subiculum, it is possible that the CA1-projecting subicular neurons are highly collateralized, which is different from other subicular neurons. In addition, the CA1-projecting subicular neurons mainly arise from the proximal subiculum (Fig 3.1 D), this is in accordance with the previous study showing neurons in the proximal subiculum have much greater axonal collateralization than the distal (Donovan and Wyss, 1983). One of the major limitations of this anterograde tracing is the H129 virus can cross multiple synapses as time goes by (Lo and Anderson, 2011). However, as we strictly controlled the post-injection time and all the labeled brain regions are known targets for the subiculum, this discrepancy is unlikely due to the technical issue of the virus infection.

`

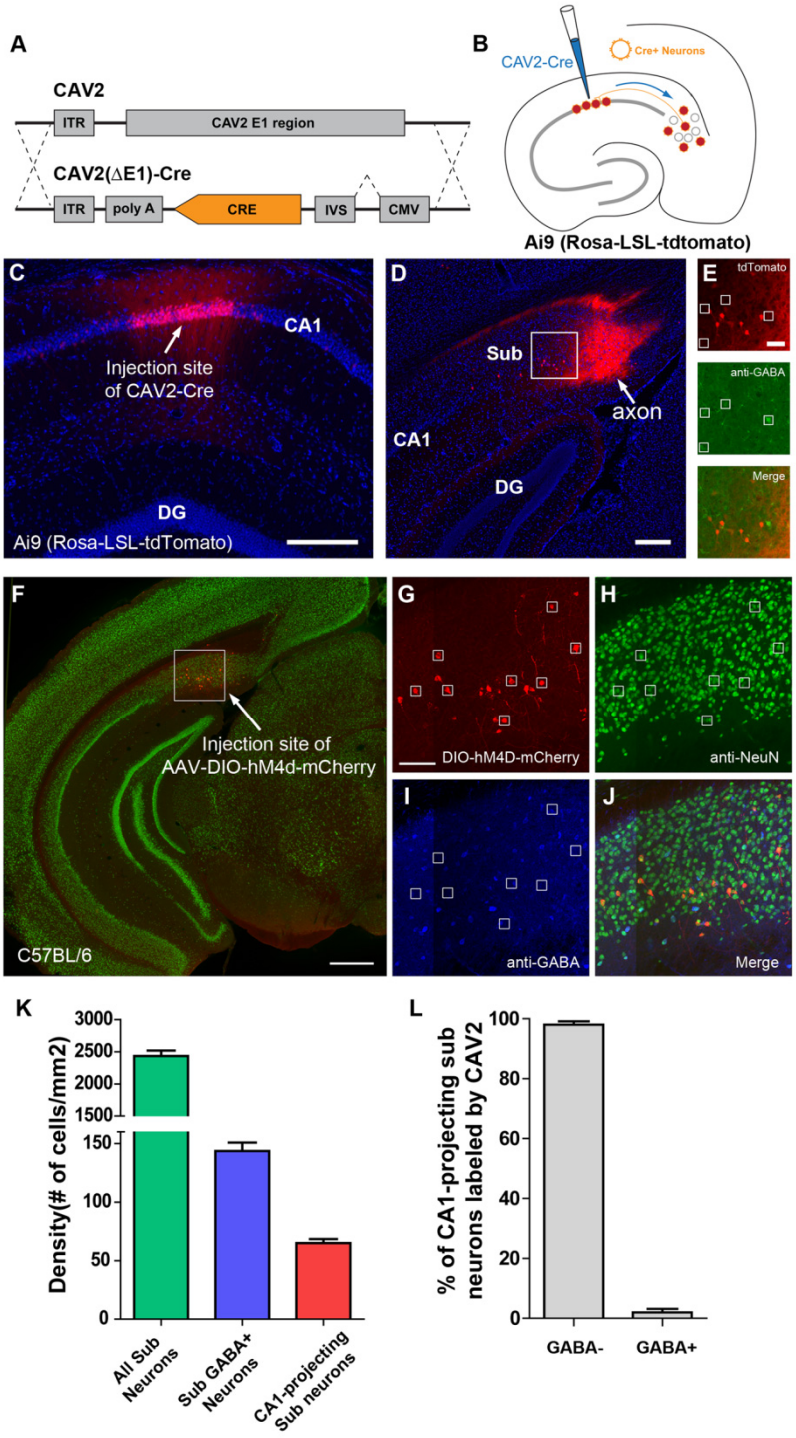

Figure 3.1. Selective targeting of CA1-projecting excitatory subicular neurons by canine adenovirus 2 (CAV2)-mediated retrograde Cre expression. (A) Schematic of E1-deleted CAV2 viral vector expressing Cre recombinase. (B) Schematic illustration of CAV2-Cre injection in the CA1, in the meantime, CA1-projecting subicular neurons are labeled by the

`

retrograde transport of the CAV2-Cre in the Ai9 reporter mouse. (C) An example image of the CAV2-Cre injection site in dorsal CA1 with a viral spread of 300-500 μm. tdTomato expression, shown in red, can be seen in the local infected neurons restricted to the pyramidal cell layer. DAPI is shown in blue. Scale bar = 200 μm. (D) An example of tdTomato labeled CA1-projecting subicular neurons after the CAV2-Cre transport retrogradely from CA1 to the subiculum. Scale bar = 200 μm. (E) An enlarged view of the white square area in D with GABA immunostaining. The top panel shows CAV2-Cre labeled, tdTomato expressing CA1-projecting subicular neurons. The panel in the middle shows GABA staining in green. The bottom panel shows the overlay image. The small white boxes indicate GABA immunopositive neurons are tdTomato negative. It turns out the CAV2-Cre infected CA1-projecting subicular neurons are devoid of GABA. Scale bar = 50 μm. (F) Tag the CA1-projecting subicular neurons in the wild type animal by injecting CAV2-Cre in the CA1 (not shown), while delivering a Cre-depedent, mChreey-expressing AAV virus (AAV2-DIO-hM4d-mCherry) into the subiculum. The mCherry expressing CA1-projecting subicular neurons are shown in red. NeuN staining is shown in green. Scale bar = 500 μm. (G-J) An enlarged view of the white square area in F with GABA and NeuN immunostaining. Scale bar = 100 μm (G) shows the mCherry-expressing CA1-projecting subicular neurons in red. (H) shows the NeuN staining in green. (I) shows the GABA staining in blue. (J) shows the overlay image. Small white boxes indicate CA1-projecting subicular neurons are positive for NeuN staining but negative for GABA staining. (K) Cell density quantification of overall subicular neurons (NeuN stained neurons), GABA+ subicular neurons, and CA1-projecting subicular neurons. By comparing total NeuN positive neurons in the subiculum, the CAV2-labeled subset (per one injection) of CA1-projecting neurons accounts for 2.7% ± 0.1% (mean ± SE, pooled from 4 cases) of the overall population of subicular neurons. (L) Essentially all CA1-projecting subicular neurons are excitatory neurons. Based on the measurements of 241 CAV2-labled subicular neurons from 4 different mice, 98% of them are GABA negative.

`

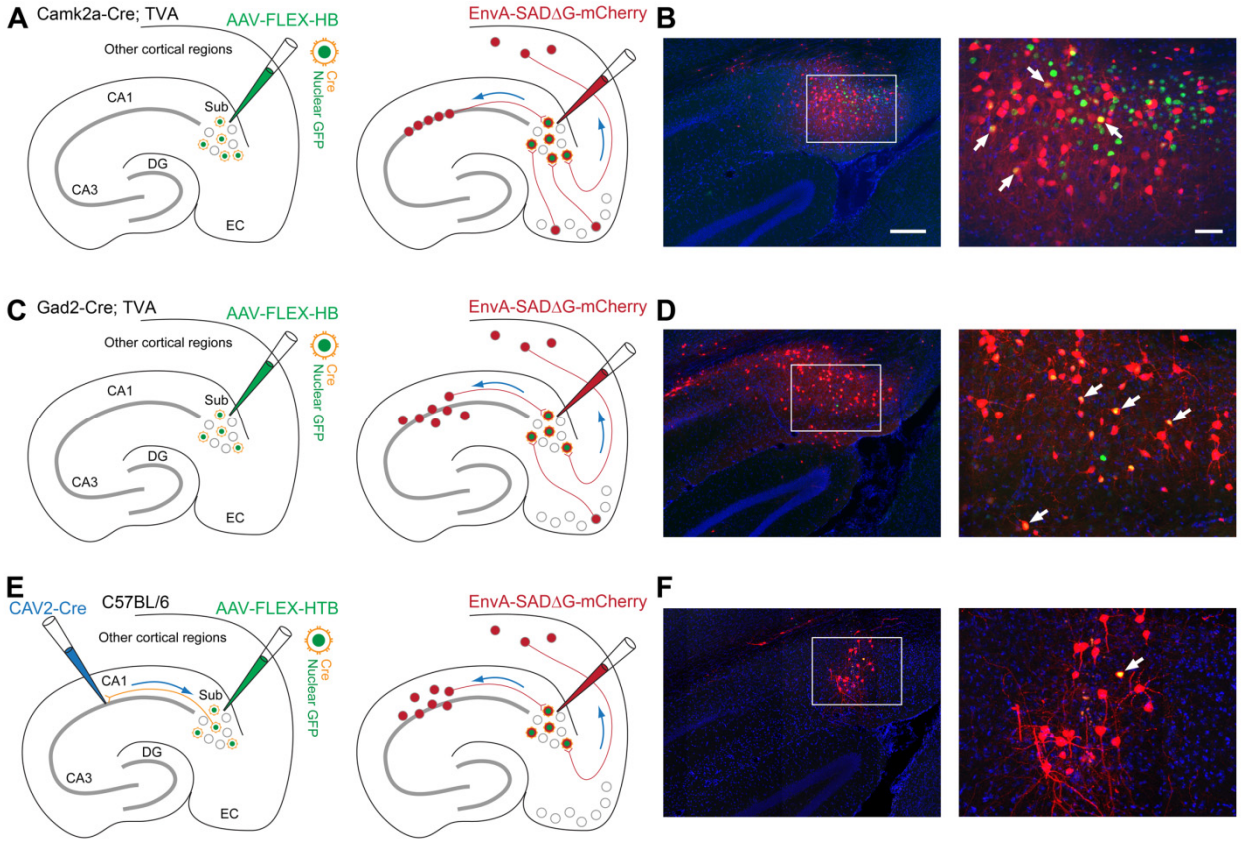

Fig. 3.2. Experiment design and viral injection sites of mapping circuit connections to specific subicular neuron types. (A) Schematic illustration of using Cre dependent helper AAV (AAV-FLEX-HB; H: histone GFP; B: rabies B19 glycoprotein) and genetically modified pseudotyped rabies (EnvA-SADΔG-mCherry) in the Camk2a-Cre; TVA mouse to perform the input connection mapping in subicular excitatory neurons. At three weeks following the AAV injection, the genetically modified rabies is injected for monosynaptic tracing of direct inputs to targeted cells. (B). A section image of the viral injection site targeting subicular excitatory neurons. Panel on the right shows the enlarged view of the white square area highlighted on the left panel. Example starter neurons in the subiculum are pointed by white arrows with both dsRed expression from the rabies genome and nuclear GFP expression from the helper AAV genome. Scale bar on the left = 200 μm; scale bar on the right = 50 μm apply to all corresponding panels in B, D, and F. (C) Organized similar to A, schematic illustration of using Cre dependent helper AAV and genetically modified pseudotyped rabies in the GAD-Cre; TVA mouse to perform the input connection mapping in subicular inhibitory neurons. (D) Organized similar to B, white arrows point to the example starter neurons of subicular inhibitory neurons with both rabies dsRed and AAV GFP expressions. (E) Schematic illustration of the combinatorial use of CAV2-Cre and Cre dependent helper AAV (AAV-FLEX-HTB; H: histone GFP; T: TVA; B: rabies B19 glycoprotein) to target CA1-projecting subicular excitatory

`

neurons, and genetically modified pseudotyped rabies in the wild type C57 mouse. (F) Shows a section image of the rabies tracing injection site with a starter CA1-projecting subicular neuron pointing by a white arrow.

`

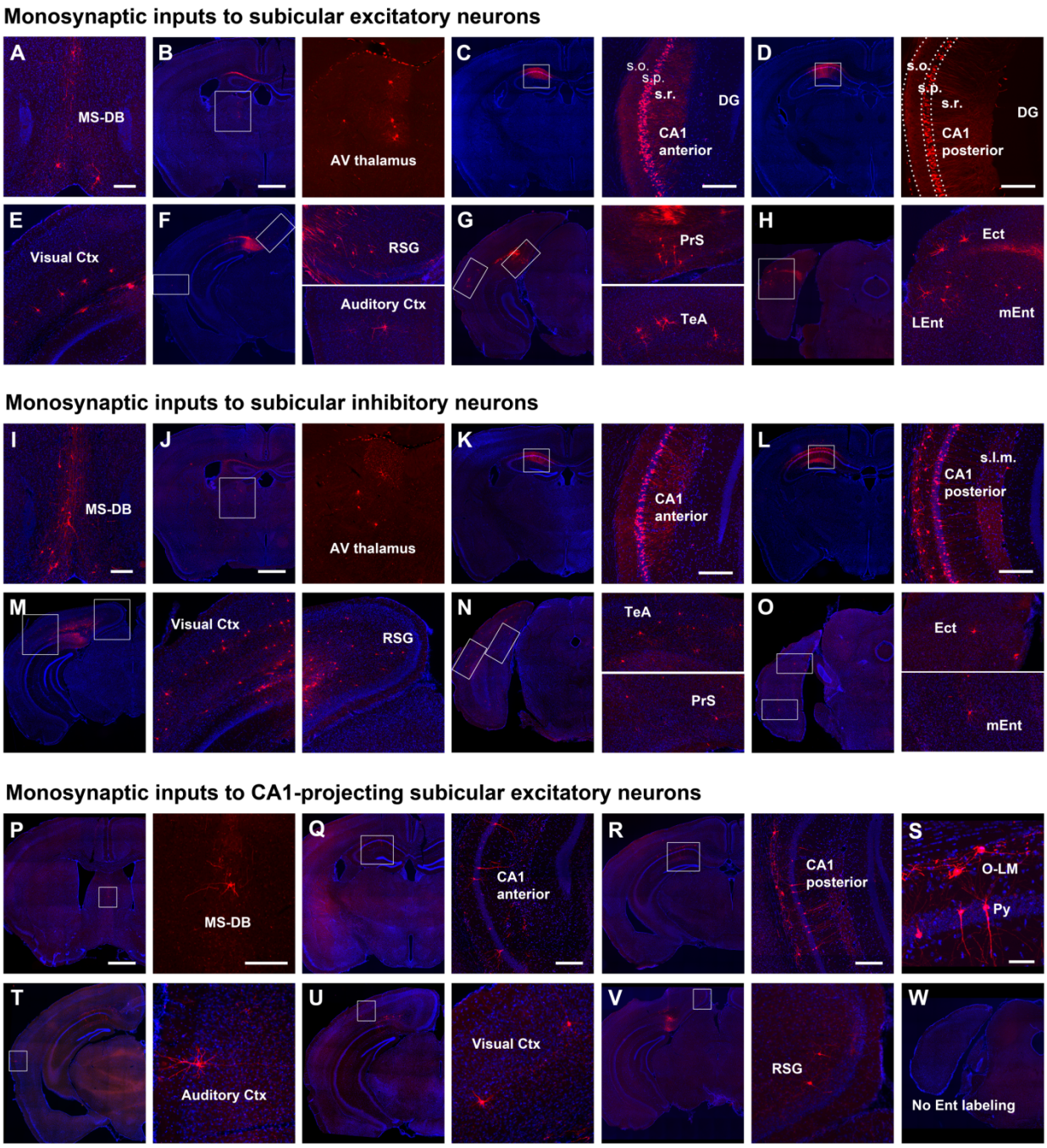

Fig. 3.3. Whole-brain wide circuit inputs to specific subicular neuron types. Panels on the top section show the circuit connections to subicular excitatory neurons targeted by the Camk2a-Cre; TVA mouse. Rabies labeled neurons are shown in red; DAPI staining is shown in blue. (A) An example of rabies labeled presynaptic neurons in the medial septum and diagonal band (MS-DB). Scale bar = 200 μm applies to A, E, and the zoom in panels in B, F, G, and H. (B) Rabies labeled neurons in the anteroventral thalamic nucleus (AV thalamus). The right panel shows a zoom in view of the white square area on the left panel. Scale bar on the left panel = 1mm

`

applies to all the zoom out panels in B, C, D, F, G, and H. (C) Rabies labeled neurons in the CA1 pyramidal cell layer close to the septal end of the hippocampus. Scale bar on the right panel = 200 μm. s.o. stratum oriens; s.p. stratum pyramidale; s.r. stratum radiatum. (D) Rabies labeled neurons in the CA1 pyramidal cell layer towards a little bit temporal hippocampus compared to C. Scale bar on the right panel = 200 μm. (E) Rabies labels neurons in the primary visual cortex. (F) Rabies labeled neurons in the retrosplenial granular cortex (RSG) and auditory cortex. The top right panel shows a zoom in view of the white square indicating the RSG on top of the left panel. The bottom right panel shows a zoom in view of the white square indicating the auditory cortex on bottom of the left panel. (G) Organized similar to F showing rabies labeled neurons in the presubiculum (PrS) and temporal association cortex (TeA). (H) Rabies labeled neurons in the ectorhinal cortex (Ect), lateral entorhinal cortex (LEnt), and medial entorhinal cortex (mEnt). Panels in the middle section, organized similar to the top section, show the circuit connections to subicular inhibitory neurons targeted by the GAD-Cre; TVA mouse. (I) Rabies labeled presynaptic neurons in MS-DB. Scale bar = 200 μm applies to I and the zoom in panels in J, M, N, and O. (J) Rabies labeled neurons in thalamus. Scale bar on the left panel = 1mm applies to all the zoom out panels in J, K, L, M, N, and O. (K) Rabies labeled neurons in the CA1 pyramidal cell layer close to the septal end of the hippocampus. Scale bar on the right panel = 200 μm. (L) Rabies labeled neurons in the CA1 pyramidale as well as the orien and lacunosum moleculare layers towards a little bit temporal hippocampus compared to K. s.l.m. stratum lacunosum moleculare. Scale bar on the right panel = 200 μm. (M) Rabies labeled neurons in the RSG and visual cortex. The panel on right shows a zoom in view of the white square indicating the RSG on top of the left panel. The panel in the middle shows a zoom in view of the white square indicating the visual cortex on bottom of the left panel. (N) Rabies labeled neurons in PrS and TeA. (O) Rabies labeled neurons in Ect and Ent. Panels on the bottom section show the circuit connections to CA1-projecting subicular excitatory neurons targeted by a combinatorial viral tracing. (P) Rabies labeled presynaptic neurons in MS-DB. Scale bar on the left panel = 1mm applies to all the zoom out panels in this section. Scale bar on the right panel = 200 μm applies to the zoom in panels in P, T, U, V, and W. (Q) Rabies labeled neurons in the CA1 close to the septal end of the hippocampus. Scale bar on the right panel = 200 μm. (R) Rabies labeled neurons in the CA1 towards a little bit temporal hippocampus compared to Q. (S) A high power confocal image of rabies labeled neurons from posterior CA1. There are putative O-LM cells in the s.o. layer and pyramidal cells in the s.p. layer based on the cell morphology. Scale bar = 50 μm. (T) Rabies labeled neurons in auditory cortex. (U) Rabies labeled neurons in visual cortex. (V) Rabies labeled neurons in RSG. (W) There are no labeled neurons from the parahippocampal cortices, especially the entorhinal cortex.

`

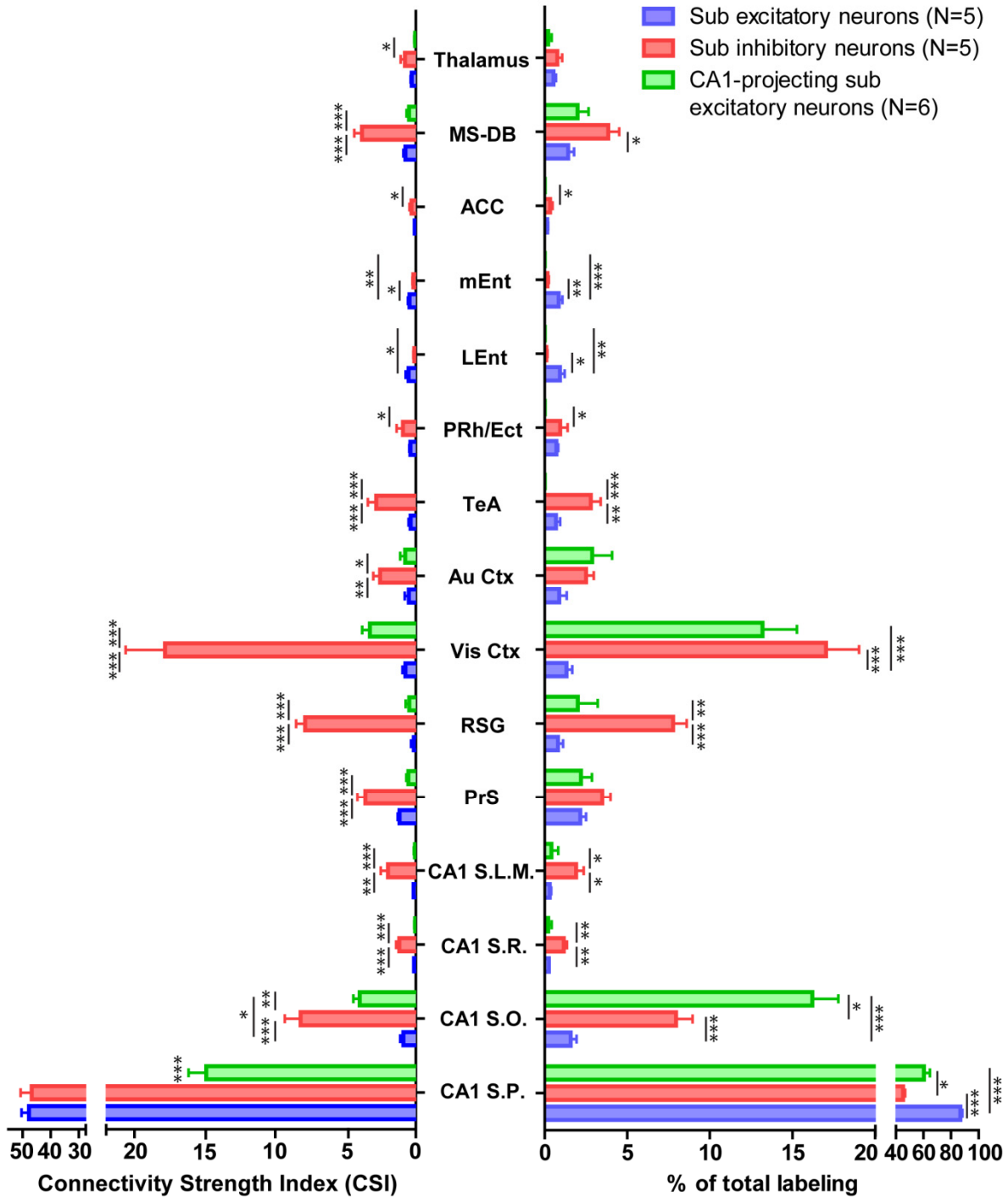

Fig. 3.4. Quantitative analysis of the input connection patterns to three different subicular neuron types. Comparison of specific circuit connection strengths to overall excitatory and inhibitory subicular neurons (N = 5 for each) and CA1-projecting excitatory subicular neurons (N = 6). Data on the left are plotted as the connectivity strength index (CSI) for each specified brain structure. The CSI is defined as the ratio of the number of presynaptic neurons labeled in a

`

specific brain structure divide by the number of starter neurons. Data on the right are plotted as the % of total labeled neurons for a specified brain structure. The % of total labeled neurons is calculated as the percentage of the number of labeled presynaptic neurons in a specified brain structure versus the overall total presynaptic neuron count in each case. Data present as mean ± SE. One-way ANOVA and post hoc Tukey's multiple comparison tested the significance within each input region. *P < 0.05; **P < 0.01; ***P < 0.001. ACC: anterior cingular cortex.

`

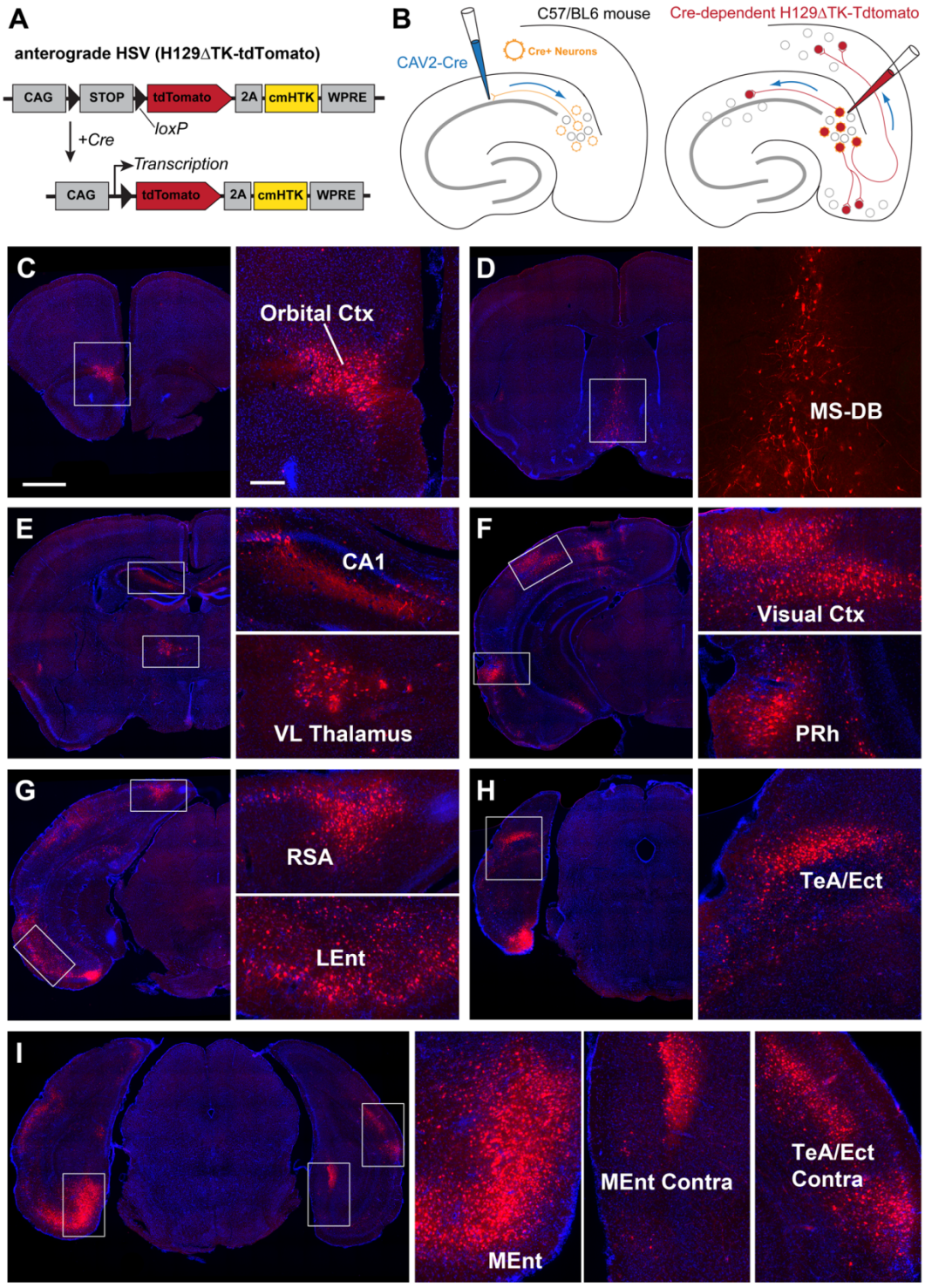

Figure 3.5. Global output projections of CA1-projecting subicular excitatory neurons. (A) Schematic illustration of an anterograde transneuronal HSV strain, the H129ΔTK-tdTomato. (B) Retrograde CAV2-Cre based strategy for mapping output connections of CA1-projecting subicular excitatory neurons. (C-I) Organized similar to Fig. 3.3. (C) Direct postsynaptic labeling in the frontal orbital cortex. Scale bar on the left = 1mm applies to all zoom out panels. Scale bar

`

on the right = 200 μm applies to all zoom in panels. (D) Postsynaptic labeling in the MS-DB. (E) Example images of direct postsynaptic labeling in hippocampal CA1 and ventrolateral thalamic nucleus (VL thalamus) (F) Postsynaptic labeling in visual cortex and perirhinal cortex. (G) Postsynaptic labeling of retrosplenial agranular cortex (RSA) and lateral entorhinal cotex. (H-I) Bilateral postsynaptic labeling in temporal association/ectorhinal (TEA/Ect) cortex, and medial entorhinal cortex.

Table 3.1 Quantitative strengths of specific circuit connections to subicular excitatory neurons, subicular inhibitory neurons, and CA1-projecting subicular neurons, respectively.

Sub Excitatory neurons	CA1 S.P.	CA1 S.O.	CA1 S.R.	CA1 S.L.M.	PrS	RSG	Vis Ctx	Au Ctx	TeA	PRh/Ect	LEnt	mEnt	ACC	MS-DBB	Thalamus
Average CSI	47.72	0.90	0.14	0.17	1.16	0.46	0.74	0.51	0.38	0.39	0.53	0.46	0.09	0.75	0.30
SE	2.69	0.22	0.02	0.05	0.13	0.19	0.22	0.29	0.15	0.08	0.20	0.11	0.03	0.15	0.08
Average percentage	86.71	1.58	0.26	0.31	2.16	0.81	1.32	0.88	0.68	0.71	0.92	0.85	0.16	1.42	0.54
SE	1.56	0.36	0.03	0.09	0.35	0.30	0.35	0.46	0.26	0.12	0.30	0.22	0.06	21.34	0.15
# of starter neurons	50 ± 8				Total labeled neurons			2681 ± 372				N=5			

Sub Inhibitory neurons	CA1 S.P.	CA1 S.O.	CA1 S.R.	CA1 S.L.M.	PrS	RSG	Vis Ctx	Au Ctx	TeA	PRh/Ect	LEnt	mEnt	ACC	MS-DBB	Thalamus
Average CSI	46.74	8.20	1.19	1.99	3.60	7.88	17.83	2.55	2.83	0.93	0.12	0.18	0.32	3.83	0.78
SE	3.97	1.12	0.21	0.51	0.56	0.64	2.79	0.48	0.58	0.45	0.07	0.07	0.14	0.56	0.30
Average percentage	45.21	7.96	1.16	1.91	3.49	7.78	17.03	2.51	2.79	0.94	0.11	0.18	0.33	3.85	0.77
SE	1.56	0.99	0.19	0.46	0.50	0.81	1.99	0.47	0.60	0.45	0.07	0.07	0.15	0.66	0.29
# of starter neurons	24 ± 2				Total labeled neurons			2432 ± 148				N=5			

CA1-proj sub neurons	CA1 S.P.	CA1 S.O.	CA1 S.R.	CA1 S.L.M.	PrS	RSG	Vis Ctx	Au Ctx	TeA	PRh/Ect	LEnt	mEnt	ACC	MS-DBB	Thalamus
Average CSI	14.90	4.00	0.06	0.08	0.54	0.47	3.27	0.76	0.00	0.00	0.00	0.00	0.00	0.49	0.06
SE	1.25	0.44	0.06	0.08	0.15	0.26	0.55	0.36	0.00	0.00	0.00	0.00	0.00	0.17	0.06
Average percentage	60.28	16.19	0.21	0.41	2.20	2.01	13.18	2.88	0.00	0.00	0.00	0.00	0.00	1.99	0.21
SE	4.41	1.58	0.21	0.41	0.67	1.20	2.08	1.21	0.00	0.00	0.00	0.00	0.00	0.66	0.21
# of starter neurons	3.2 ± 0.6				Total labeled neurons			77 ± 13				N=6			

`

Table 3.2. Relative abundance of neurons postsynaptic to CA1-projecting subicular neurons revealed by H129ΔTK-tdTomato anterograde tracing

Ipsilateral		Contralateral	
Regions	Labeling	Regions	Labeling
Orbital Ctx	++	PFC/PrL	+
PFC/PrL	+	Pir Ctx	+
MS-DB	+++	VL Thalamus	+
VCl	+	CA1	+
Pir Ctx	++	CA2	++
NAc	+++	CA3	++
Re Thalamus	+	Visual Ctx	++
VL Thalamus	++	Auditory Ctx	++
AHP	+	TeA	+++
CA1	++	PRh/Ect	++
CA2	+	Lent	+++
CA3	+	mEnt	++++
PrS	++		
RSG	+++		
Visual Ctx	+++		
Auditory Ctx	+		
TeA	+++		
PRh/Ect	+++		
LEnt	++++	N=3	
mEnt	++++		

`

REFERENCES

Andersen P, Morris RM, Amaral D, Bliss T, O'Keefe J (2007) The hippocampus book. Oxford ; New York: Oxford University Press.

Burke SN, Maurer AP, Nematollahi S, Uprety AR, Wallace JL, Barnes CA (2011) The influence of objects on place field expression and size in distal hippocampal CA1. Hippocampus 21:783-801.

Carter ME, Soden ME, Zweifel LS, Palmiter RD (2013) Genetic identification of a neural circuit that suppresses appetite. Nature 503:111-114.

Coogan TA, Burkhalter A (1993) Hierarchical organization of areas in rat visual cortex. J Neurosci 13:3749-3772.

Craig MT, McBain CJ (2015a) Fast gamma oscillations are generated intrinsically in CA1 without the involvement of fast-spiking basket cells. J Neurosci 35:3616-3624.

Deadwyler SA, Hampson RE (2004) Differential but complementary mnemonic functions of the hippocampus and subiculum. Neuron 42:465-476.

Deshmukh SS, Knierim JJ (2011) Representation of non-spatial and spatial information in the lateral entorhinal cortex. Front Behav Neurosci 5:69.

Donovan MK, Wyss JM (1983) Evidence for some collateralization between cortical and diencephalic efferent axons of the rat subicular cortex. Brain Res 259:181-192.

Finch DM, Nowlin NL, Babb TL (1983) Demonstration of axonal projections of neurons in the rat hippocampus and subiculum by intracellular injection of HRP. Brain Res 271:201-216.

Gore BB, Soden ME, Zweifel LS (2013) Manipulating gene expression in projection-specific neuronal populations using combinatorial viral approaches. Curr Protoc Neurosci 4:4 35 31-34 35 20.

Henriksen EJ, Colgin LL, Barnes CA, Witter MP, Moser MB, Moser EI (2010) Spatial representation along the proximodistal axis of CA1. Neuron 68:127-137.

Igarashi KM, Ito HT, Moser EI, Moser MB (2014a) Functional diversity along the transverse axis of hippocampal area CA1. FEBS Lett 588:2470-2476.

Igarashi KM, Lu L, Colgin LL, Moser MB, Moser EI (2014b) Coordination of entorhinal-hippocampal ensemble activity during associative learning. Nature 510:143-147.

Ishizuka N (2001) Laminar organization of the pyramidal cell layer of the subiculum in the rat. The Journal of comparative neurology 435:89-110.

Jackson J, Amilhon B, Goutagny R, Bott JB, Manseau F, Kortleven C, Bressler SL, Williams S (2014) Reversal of theta rhythm flow through intact hippocampal circuits. Nat Neurosci 17:1362-1370.

Jackson J, Goutagny R, Williams S (2011) Fast and slow gamma rhythms are intrinsically and independently generated in the subiculum. J Neurosci 31:12104-12117.

Jinno S (2009) Structural organization of long-range GABAergic projection system of the hippocampus. Front Neuroanat 3:13.

Jinno S, Klausberger T, Marton LF, Dalezios Y, Roberts JD, Fuentealba P, Bushong EA, Henze D, Buzsaki G, Somogyi P (2007) Neuronal diversity in GABAergic long-range projections from the hippocampus. J Neurosci 27:8790-8804.

Junyent F, Kremer EJ (2015) CAV-2--why a canine virus is a neurobiologist's best friend. Curr Opin Pharmacol 24:86-93.

`

Kim SM, Ganguli S, Frank LM (2012) Spatial information outflow from the hippocampal circuit: distributed spatial coding and phase precession in the subiculum. J Neurosci 32:11539-11558.

Kim Y, Spruston N (2012) Target-specific output patterns are predicted by the distribution of regular-spiking and bursting pyramidal neurons in the subiculum. Hippocampus 22:693-706.

Knopp A, Kivi A, Wozny C, Heinemann U, Behr J (2005) Cellular and network properties of the subiculum in the pilocarpine model of temporal lobe epilepsy. J Comp Neurol 483:476-488.

Kremer EJ, Boutin S, Chillon M, Danos O (2000) Canine adenovirus vectors: an alternative for adenovirus-mediated gene transfer. J Virol 74:505-512.

Lever C, Burton S, Jeewajee A, O'Keefe J, Burgess N (2009) Boundary vector cells in the subiculum of the hippocampal formation. J Neurosci 29:9771-9777.

Lo L, Anderson DJ (2011) A Cre-dependent, anterograde transsynaptic viral tracer for mapping output pathways of genetically marked neurons. Neuron 72:938-950.

Losonczy A, Zhang L, Shigemoto R, Somogyi P, Nusser Z (2002) Cell type dependence and variability in the short-term plasticity of EPSCs in identified mouse hippocampal interneurones. J Physiol 542:193-210.

Madisen L, Zwingman TA, Sunkin SM, Oh SW, Zariwala HA, Gu H, Ng LL, Palmiter RD, Hawrylycz MJ, Jones AR, Lein ES, Zeng H (2010) A robust and high-throughput Cre reporting and characterization system for the whole mouse brain. Nat Neurosci 13:133-140.

Menendez de la Prida L, Suarez F, Pozo MA (2003) Electrophysiological and morphological diversity of neurons from the rat subicular complex in vitro. Hippocampus 13:728-744.

Naber PA, Witter MP (1998) Subicular efferents are organized mostly as parallel projections: a double-labeling, retrograde-tracing study in the rat. The Journal of comparative neurology 393:284-297.

Nakamura NH, Flasbeck V, Maingret N, Kitsukawa T, Sauvage MM (2013) Proximodistal segregation of nonspatial information in CA3: preferential recruitment of a proximal CA3-distal CA1 network in nonspatial recognition memory. J Neurosci 33:11506-11514.

O'Mara SM, Commins S, Anderson M, Gigg J (2001) The subiculum: a review of form, physiology and function. Prog Neurobiol 64:129-155.

Oh SW, Harris JA, Ng L, Winslow B, Cain N, Mihalas S, Wang Q, Lau C, Kuan L, Henry AM, Mortrud MT, Ouellette B, Nguyen TN, Sorensen SA, Slaughterbeck CR, Wakeman W, Li Y, Feng D, Ho A, Nicholas E, Hirokawa KE, Bohn P, Joines KM, Peng H, Hawrylycz MJ, Phillips JW, Hohmann JG, Wohnoutka P, Gerfen CR, Koch C, Bernard A, Dang C, Jones AR, Zeng H (2014) A mesoscale connectome of the mouse brain. Nature 508:207-214.

Olson JM, Tongprasearth K, Nitz DA (2017) Subiculum neurons map the current axis of travel. Nat Neurosci 20:170-172.

Peltekian E, Garcia L, Danos O (2002) Neurotropism and retrograde axonal transport of a canine adenoviral vector: a tool for targeting key structures undergoing neurodegenerative processes. Mol Ther 5:25-32.

Schwarz LA, Miyamichi K, Gao XJ, Beier KT, Weissbourd B, DeLoach KE, Ren J, Ibanes S, Malenka RC, Kremer EJ, Luo L (2015) Viral-genetic tracing of the input-output organization of a central noradrenaline circuit. Nature 524:88-92.

`

Seidler B, Schmidt A, Mayr U, Nakhai H, Schmid RM, Schneider G, Saur D (2008) A Cre-loxP-based mouse model for conditional somatic gene expression and knockdown in vivo by using avian retroviral vectors. Proc Natl Acad Sci U S A 105:10137-10142.

Sharp PE, Green C (1994) Spatial correlates of firing patterns of single cells in the subiculum of the freely moving rat. J Neurosci 14:2339-2356.

Soudais C, Laplace-Builhe C, Kissa K, Kremer EJ (2001) Preferential transduction of neurons by canine adenovirus vectors and their efficient retrograde transport in vivo. FASEB J 15:2283-2285.

Staff NP, Jung HY, Thiagarajan T, Yao M, Spruston N (2000) Resting and active properties of pyramidal neurons in subiculum and CA1 of rat hippocampus. J Neurophysiol 84:2398-2408.

Stewart M, Wong RK (1993) Intrinsic properties and evoked responses of guinea pig subicular neurons in vitro. J Neurophysiol 70:232-245.

Sun Y, Grieco SF, Holmes TC, Xu X (2017) Local and Long-Range Circuit Connections to Hilar Mossy Cells in the Dentate Gyrus. eNeuro 4.

Sun Y, Nguyen AQ, Nguyen JP, Le L, Saur D, Choi J, Callaway EM, Xu X (2014) Cell-type-specific circuit connectivity of hippocampal CA1 revealed through Cre-dependent rabies tracing. Cell Rep 7:269-280.

Swanson LW, Sawchenko PE, Cowan WM (1981) Evidence for collateral projections by neurons in Ammon's horn, the dentate gyrus, and the subiculum: a multiple retrograde labeling study in the rat. J Neurosci 1:548-559.

Taniguchi H, He M, Wu P, Kim S, Paik R, Sugino K, Kvitsiani D, Fu Y, Lu J, Lin Y, Miyoshi G, Shima Y, Fishell G, Nelson SB, Huang ZJ (2011) A resource of Cre driver lines for genetic targeting of GABAergic neurons in cerebral cortex. Neuron 71:995-1013.

Taube JS (1993) Electrophysiological properties of neurons in the rat subiculum in vitro. Exp Brain Res 96:304-318.

Tsien JZ, Chen DF, Gerber D, Tom C, Mercer EH, Anderson DJ, Mayford M, Kandel ER, Tonegawa S (1996) Subregion- and cell type-restricted gene knockout in mouse brain. Cell 87:1317-1326.

Vogt BA, Miller MW (1983) Cortical connections between rat cingulate cortex and visual, motor, and postsubicular cortices. J Comp Neurol 216:192-210.

Wall NR, Wickersham IR, Cetin A, De La Parra M, Callaway EM (2010) Monosynaptic circuit tracing in vivo through Cre-dependent targeting and complementation of modified rabies virus. Proc Natl Acad Sci U S A 107:21848-21853.

Wickersham IR, Lyon DC, Barnard RJ, Mori T, Finke S, Conzelmann KK, Young JA, Callaway EM (2007b) Monosynaptic restriction of transsynaptic tracing from single, genetically targeted neurons. Neuron 53:639-647.

Witter MP (2006) Connections of the subiculum of the rat: topography in relation to columnar and laminar organization. Behav Brain Res 174:251-264.

Witter MP, Ostendorf RH, Groenewegen HJ (1990) Heterogeneity in the Dorsal Subiculum of the Rat. Distinct Neuronal Zones Project to Different Cortical and Subcortical Targets. Eur J Neurosci 2:718-725.

Xu X, Sun Y, Holmes TC, Lopez AJ (2016) Noncanonical connections between the subiculum and hippocampal CA1. J Comp Neurol 524:3666-3673.

`

Chapter 4:

Functional implications of the subiculum to CA1 back-projections in spatial learning and memory

`

ABSTRACT

The hippocampal formation is traditionally viewed as having a feed-forward, unidirectional circuit organization which promotes propagation of excitatory processes. While the substantial forward projection from hippocampal CA1 to the subiculum has been very well established, accumulating evidence supports the existence of a significant back-projection pathway comprised of both excitatory and inhibitory elements from the subiculum to CA1. Furthermore, recent physiological evidence suggests such a back projection could serve to modulate information processing in hippocampal CA1. To better understand the circuit mechanism and function of this pathway, in the present study, we investigated the roles that subiculum-CA1 projections may play in hippocampus-associated learning and memory behaviors through targeted inactivation of CA1-projecting subicular excitatory neurons. DREADDs mediated inactivation impairs the long-term memory formation of location-dependent object recognition. However, the novel object recognition remains intact. Together, our data have shown the subiculum to CA1 back-projection pathway is essential for proper long-term object location memory formation, and further suggest this pathway may have critical roles in the hippocampal-related functions.

`

INTRODUCTION

Perhaps the most prominent cognitive feature of the hippocampus is its role in spatial navigation since the discovery of hippocampal place cells (O'Keefe and Dostrovsky, 1971, O'Keefe, 1976). As a major output structure of the hippocampus, subiculum receives its predominant input from CA1 and projects to numerous downstream cortical and subcortical brain regions that are critical for learning and memory related functions (Witter et al., 1990, Amaral et al., 1991, Sharp and Green, 1994, Witter, 2006). Although the place fields are not as sharp as CA1 place cells, subicular neurons do show clear spatial firing patterns with high firing rates at some localized regions (Sharp and Green, 1994). However, in contrast to CA1 place cells, subicular neurons show stable place fields with less remapping across different environments (Sharp, 1997, Knierim, 2006). In addition, subicular neurons are also tuned to other navigation related properties including movement speed (Martin and Ono, 2000, Anderson and O'Mara, 2004), head-directions (Sharp and Green, 1994), environmental boundaries (Lever et al., 2009), and the axis of travel (Olson et al., 2017). On the neuronal population level, subiculum is able to intrinsically generate both fast and slow gamma oscillations, which are essential for memory encoding and retrieval (Jackson et al., 2011). Neurons in the subiculum also show strong phase procession to gamma oscillations as well as sharp-wave associated ripples (Jackson et al., 2011, Bohm et al., 2015).

It has been suggested the subiculum and CA1 work in a timely concerted while complementary manner to encode the memory (Hampson and Deadwyler, 2003, Deadwyler and Hampson, 2004), and transform the sparse encoded CA1 representations into a highly informative distributed representations to communicate with other brain regions (Kim et al., 2012). In the meantime, most of the studies considered the CA1 to subiculum projections as a

`

unidirectional, feedforward circuit connection and highlighted the influences from CA1 to the subiculum, but not the other way around. However, accumulating evidence starts to challenge the traditional view of the unidirectional connection between hippocampal CA1 and the subiculum (Xu et al., 2016). Recent physiological evidence has shown that the subiculum generated theta oscillations can flow "in reverse" to CA1 and CA3 to actively modulate spike timing and local network rhythms of the hippocampus (Jackson et al., 2014). Additionally, disconnecting the subiculum also increased the peak frequency of gamma oscillations in CA1 (Craig and McBain, 2015a). Therefore, the backward functional impact of the subiculum on the "upstream" CA1 is likely stronger than what we anticipated before. In accordance with these findings, we recently discovered a select group of subicular neurons, including both excitatory and inhibitory components, directly project back onto hippocampal CA1 (Sun et al., 2014). This back-projection pathway may provide an underlying circuit mechanism to the backward functions of the subiculum to CA1 (Craig and McBain, 2015b, Xu et al., 2016). Thus, in order to understand the functional role of the subiculum to CA1 back-projections, in the present study, we specifically target the excitatory CA1-projecting subicular neurons by using a combinatorial viral-genetic strategy (Gore et al., 2013, Schwarz et al., 2015) and manipulate their activity via the Designer Receptors Exclusively Activated by Designer Drugs (DREADDs) (Sternson and Roth, 2014, Sun et al., 2016). We found that inactivation of CA1-projecting subicular excitatory neurons results in impairment of the long-term memory formation for location-dependent object recognition (LOR), but not novel object recognition (NOR). Together, our data demonstrate that the subiculum to CA1 back-projections are necessary for the acquisition/consolidation of the object location memory.

`

MATERIALS AND METHODS

Subjects

C57BL/6J mice (male) purchased from the Jackson Laboratory were used for the behavior experiments. Mice were 8 - 12 wk of age at the time of the experiment and had free access to food and water in their home-cages. Lights were maintained on a 12-h light/12-h dark cycle, with all behavioral testing carried out during the light portion of the cycle. All experiments were conducted according to National Institutes of Health guidelines for animal care and use and were approved by the Institutional Animal Care and Use Committee of the University of California, Irvine.

Viral injections

To specifically target the CA1-projecting subicular excitatory neurons, 0.3μl of CAV2-Cre virus (~3×10^{12} infectious units per ml) was bilaterally delivered into the intermediate CA1 region (AP −1.94 mm, ML ±1.40 mm; DV −1.35 mm) of the wild type C57BL/6J mice. CAV2-Cre is able to retrogradely transport into the subiculum and express Cre specifically in the CA1-projecting subicular excitatory neurons (Fig. 3.1 F-J). In order to inactivate the CA1-projecting subicular neurons, 0.2-0.3 μl of AAV2-DIO-hM4D-mCherry (3.7×10^{12} genome units per ml; UNC Vector Core) was delivered into the subiculum bilaterally (AP -3.40 mm, ML ±1.96 mm, DV -1.67 mm) at the same surgery session. Mice were then allowed to recover in their home cages for three weeks before the training session.

Novel object recognition and location-dependent object recognition assays

The novel object recognition (NOR) and location-dependent object recognition (LOR) assays used in this study were described previously (Stefanko et al., 2009, Haettig et al., 2013, Wang et al., 2015). All mice were handled 2 min/day for 6 days and were habituated to the

`

experimental apparatus 6 min/day for 3 consecutive days without objects. The experimental apparatus is a rectangular open field (20×40×20 cm, manufactured by carpentry facility, University of California, Irvine). 45 min before training, mice were intraperitoneally injected with clozapine-N-oxide (CNO, 1.4 mg/kg) or saline for the inactivation group or control group, respectively. During the training phase, mice were placed in the experimental apparatus with 2 identical objects (For NOR: PVC male pipe adapter, white, 1.5 inch x 2.2 inch; PVC female hose mender, green, 1.4 inch x 2.2 inch; For LOR: shrub spray, black, 1.25 inch x 2.5 inch) and allowed to explore for 10 minutes. Exploration was defined as occurring when an animal faced an object by 1 inch or less or when any part of the animal body touched the object, except for the tail. The objects were thoroughly cleaned with 70% ethanol and dried between trials. 24 hours later, mice were given a retention test. For the NOR retention test, mice were allowed to explore the experimental apparatus for 5 minutes with a novel object introduced and replaced one of the objects in the training. For the LOR retention test, mice were allowed to explore the experimental apparatus for 5 minutes with one of the objects (same as in the training) moved to a novel location. Duration and the number of times that the mice explored familiar or novel object were recorded individually. The relative exploration time was recorded and expressed by a discrimination index: (Tnovel − Tfamiliar)/ (Tnovel + Tfamiliar)×100%. Tests were video recorded and analyzed by ANY-MAZE software (Stoelting Co.).

Histology and image data acquisition

The mice were transcardially perfused with 5 ml of phosphate buffered saline (PBS), followed by 25 ml PBS containing 4% paraformaldehyde. The brains were removed and left in 4% paraformaldehyde overnight, then transferred into 30% sucrose in PBS the next day. The brain was then sectioned coronally at a 30 μm thickness on a freezing microtome (Leica

`

SM2010R, Germany). Every third section was mounted for examination and quantification of the starter cells and their presynaptic cells in different brain structures. As the mCherry expression was strong in AAV infected cells, we did not perform immunostaining against mCherry. Sections were counter-stained with 10 μM DAPI, then mounted and cover-slipped with a Vectashield antifade mounting medium (Vector Laboratories, Burlingame, CA). Using Automated Slide Scanning and Analysis software (Metamorph Inc., Nashville, TN) in a high-capacity computer with a fluorescent BX61/BX63 Olympus microscope and a high-sensitive Hamamatsu CCD camera, we were able to obtain sufficient-resolution images suitable for all subsequent computer-based analyses under a 10x objective. Image stitching, overlaying, cell counting and further imaging analysis were completed using the MetaMorph imaging and analysis software or Adobe Photoshop CS4 extended version (Adobe Systems, San Jose, CA) analysis tools.

Statistical analysis

Data were presented as mean ± SE. For statistical comparisons between groups, the data were checked for normality distribution and equal variance. If the criteria were met, a t-test was performed to compare two groups; when the criteria were not met, a Mann–Whitney U-test was used. In all experiments, the level of statistical significance was defined as $p < 0.05$.

RESULTS

In order to target and inactivate the subiculum to CA1 back-projecting pathway specifically, we employed a combinatorial viral strategy by using both CAV2-Cre (canine adenovirus type 2) and AAV-DIO-hM4D-mCherry (Gore et al., 2013, Schwarz et al., 2015). The CAV2-Cre that injected into the hippocampal CA1 can retrogradely transport to the subiculum via the incoming axon terminals from the subiculum to CA1. Cre recombinase is then expressed

`

specifically in the CA1-projecting subicular neurons (Fig. 4.1 A). Furthermore, Cre targeted CA1-projecting subicular neurons express the hM4D receptor and mCherry fluorescent protein via a delivery of the Cre-dependent, AAV-DIO-hM4d-mCherry virus into the subiculum (Fig. 4.1 A, B, and Fig. 3.1 F). In addition, we unexpectedly found that most of the targeted CA1-projecting subicular neurons are non-GABAergic excitatory cells due to the potential viral tropism of CAV2 (Fig. 3.1; see chapter 3 for more details). All the viral injections were made bilaterally, and we validated through histology that there is no expression of the AAV virus in brain regions outside the subiculum complex (Fig. 4.1 C). Therefore, we are able to specifically inhibit the neuronal activity of CA1-projecting subicular excitatory neurons for behavioral experiments *in vivo*.

It has been previously shown that inactivating either CA1 excitatory neurons or inhibitory neurons disrupt the long-term memory formation of location-dependent object recognition (Haettig et al., 2013). In order to investigate whether CA1-projecting subicular neurons are required for object location memory, we performed the same task by inactivating the CA1-projecting subicular excitatory neurons via an inhibitory DREADDs, hM4D (Armbruster et al., 2007, Krashes et al., 2011, Sun et al., 2016). The location-dependent object recognition task is based on an animal's innate preference for novelty. During the training session, two identical objects are presented 10 min to the animal for free exploring. This will give the animal a robust long-term memory in the normal situation (Stefanko et al., 2009, Haettig et al., 2013, Vogel-Ciernia and Wood, 2014). Long-term memory of the animal is then tested 24 hours after the training with one object moved to a novel location (Fig. 4.1 D). If the animal remembers the location of the objects in the training session, then it will preferentially explore the familiar object in the novel location during the testing, which gives rise to a higher discrimination index

`

(as described in the methods). In order to inactivate the subiculum to CA1 back-projections, clozapine-N-oxide (CNO), the ligand of the hM4D receptor, was administered through a single dose intraperitoneal injection 45 min prior to the training (Fig. 4.1 D and E). Since the effect of CNO in the neuronal tissue can last up to 12 hours *in vivo* (Alexander et al., 2009, Wess et al., 2013, Miao et al., 2015), this pre-training delivery of CNO likely affect the memory acquisition and consolidation period, but not the retrieval which test 24 hours after the training (Haettig et al., 2013). In the location-dependent object recognition, CNO-injected mice showed no object preference during the testing compared to the saline control, which means the animals' long-term memory formation are impaired upon the inactivation of CA1-projecting subicular excitatory neurons (Fig. 4.1 D). There are no differences in total exploration time between groups during training ($p = 0.91$) or testing ($p = 0.11$; Fig. 4.1 D and Table 4.1). These results suggest that CA1-projecting subicular excitatory neurons are necessary for long-term, location-dependent object recognition memory formation.

In addition to the object location memory, we would also like to know whether CA1-projecting subicular neurons are required in novel object recognition, which is supposed to be a hippocampus independent task based on our behavior paradigm (Mumby, 2001, Balderas et al., 2008, Piterkin et al., 2008, Stefanko et al., 2009, Vogel-Ciernia and Wood, 2014). Similar to the object location test, two identical objects are presented 10 min to the animal for free exploring in the object recognition task. Instead of moving the familiar object to a novel location, one object is replaced with a novel, distinct object at the same location for long-term memory testing 24 hours after the training (Wang et al., 2015). As expected, we found no significant differences between the CNO group and the saline group in this task. This result suggests that the CA1-

`

projecting subicular neurons are not involved in the long-term memory formation of novel object recognition task.

DISCUSSION

In the present study, by using the combinatorial viral strategy coupled with the DREADDs system, we specifically inactivated the excitatory subiculum to CA1 back-projecting pathway of behaving mice to examine their functional roles in the memory acquisition/consolidation of location-dependent object recognition as well as novel object recognition. We found silencing CA1-projecting subicular neurons impairs the long-term memory formation of object location task. However, the object recognition memory remains intact. Our findings provide important functional understanding for the role of subiculum and CA1 in the long-term memory formation.

One outstanding question raised from our data is does the subiculum contribute to the object location memory per se or via an indirect effect through the back-projections to hippocampal CA1. Subiculum can contribute to spatial navigation via its spatially tuned functional cell types including place cells, head-direction cells, boundary vector cells, and a more recently described axis tuned cells (Sharp and Green, 1994, Sharp, 1997, Anderson and O'Mara, 2004, Lever et al., 2009, O'Mara et al., 2009, Olson et al., 2017). Inactivating subicular neurons may result in the disruption of place field properties in the subiculum. It is still unclear whether the CA1-projecting subicular neurons show any of the spatial related tuning. However, our anatomical data suggest the CA1-projecting subicular neurons may not be spatially selective, as they do not receive input from entorhinal cortex and less convergent input from CA1 (see chapter 3). On the other hand, in a Delayed-Nonmatch-to-Sample (DNMS) task, inactivating subicular neurons with baclofen specifically impairs the behavioral performance at short delays.

`

More interestingly, inactivation of subicular cells also significantly reduced the firing of CA1 trial-type cells (Hampson and Deadwyler, 2003). Considering the canonical feedforward information flow of the subiculum has to cross multiple synapses in order to go back to the CA1, the results above matches our data that subicular neurons may provide functional influence to the activity of CA1 neurons through the direct backward innervations. Thus, the memory impairment of the location-dependent object recognition shown in our data might be a direct result of disrupting the neuronal activities of hippocampal CA1 (Hampson and Deadwyler, 2003, Deadwyler and Hampson, 2004). Therefore, it is very important to know whether the CA1-projecting subicular neurons show any functional properties in the learning and memory task or whether they contribute to the CA1 place cell activities (Xu et al., 2016).

On the neuronal network level, CA1 fast gamma oscillation has been demonstrated to promote encoding of novel object-place associated memory (Zheng et al., 2016). In accordance with our data, as the peak frequency of CA1 gamma oscillation can be modulated by the subiculum (Craig and McBain, 2015a) plus subiculum generated theta oscillations can flow backward to actively modulate the CA1 neuronal activities (Jackson et al., 2014), the memory impairment induced by the inactivation of CA1-projecting subicular neurons are presumably a result of a network change of hippocampal CA1 rhythms modulated by the subiculum. However, it would be very interesting to know if these back-projections amplify or dampen large network synchronies within and between these two regions in the hippocampal formation (Xu et al., 2016).

The subiculum receives direct projections from perirhinal cortex (Naber et al., 1999, Witter et al., 2000), which is considered as the most critical region for object recognition (Eichenbaum et al., 2007). In line with this anatomical evidence, it has been shown that during

`

the object recognition task, subicular neurons participate in recognition-related coding by increasing the theta power when encounters a novel object in the same environment (Chang and Huerta, 2012). Our data show here that manipulating CA1-projecting subicular neurons does not affect the object recognition memory. This is consistent with our anatomical finding that CA1-projecting subicular neurons do not receive direct input from perirhinal cortex (see chapter 3).

It has been shown that the hippocampal neurons are not only code for the spatial information, but also code for non-spatial information including objects, faces, odors, sounds, etc. (Fried et al., 1997, Sakurai, 2002, Igarashi et al., 2014b, Aronov et al., 2017). A more recent study start to unveil that a single hippocampal neuron is able to encode multiple entities of a behavior task (Aronov et al., 2017). Therefore, it is also possible for the CA1-projecting subicular neurons provide task-relevant spatial as well as non-spatial information at the same time for the object recognition memory formation.

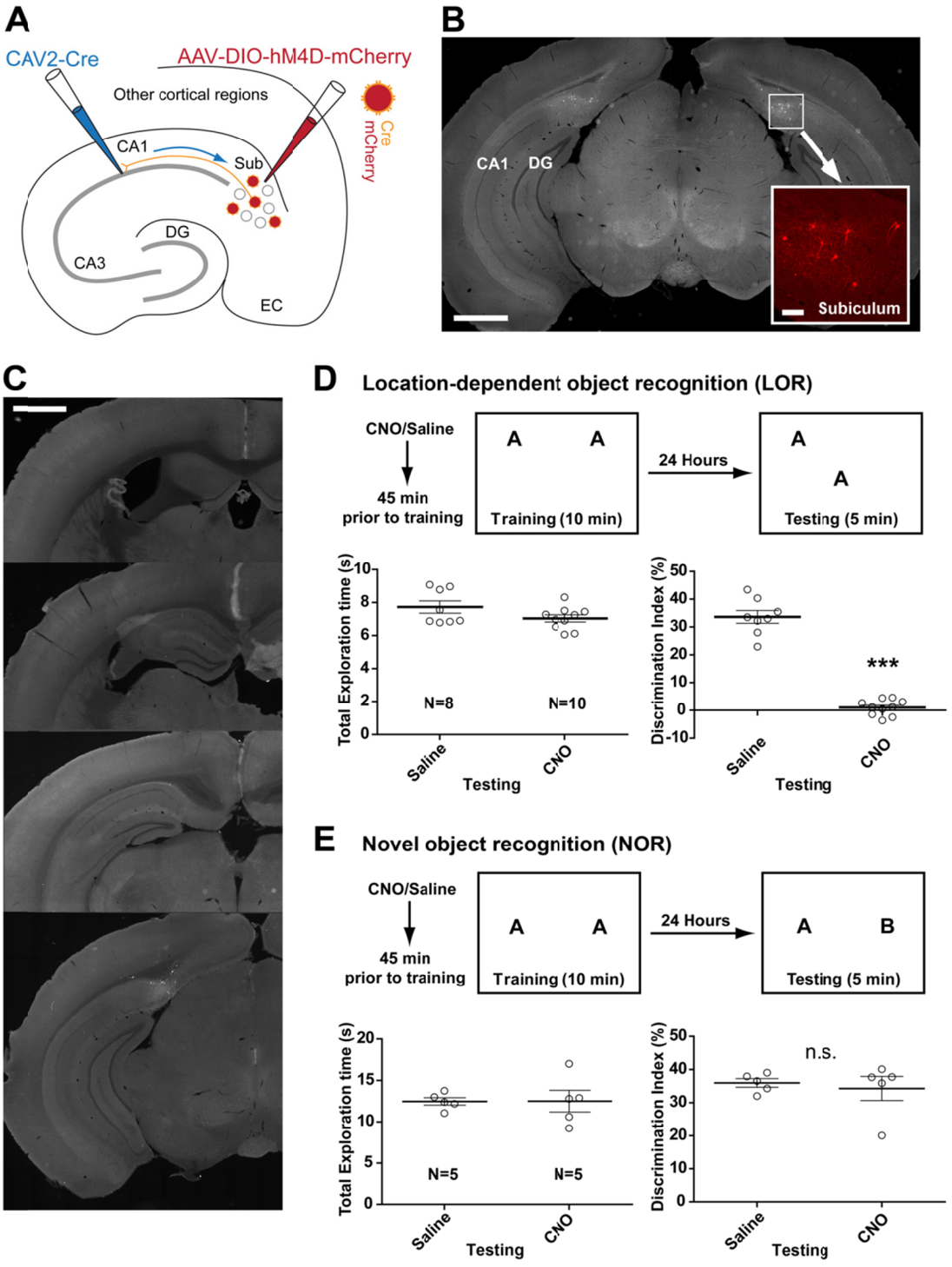

Figure 4.1. Subiculum to CA1 projections are required for location-dependent object recognition task, but not novel object recognition task. (A) Schematic illustration of targeting CA1-projecting subicular excitatory neurons by using a combinatorial viral strategy with CAV2-Cre injected in CA1 and AAV-DIO-hM4D-mCherry injected in the subiculum. (B) A coronal

`

brain section shows the AAV infection around the subiculum injection site bilaterally. The bright white dots are neurons expressing hM4D-mCherry. Scale bar = 1 mm. The panel on the bottom right shows a zoom in view of the white square in B. mCherry expressing CA1-projecting subicular neurons are shown in red, scale bar = 100 μm. (C) A series of coronal brain sections from the anterior to posterior verify there is no leaky expression of AAV outside the subiculum. Scale bar = 1mm. (D) Experiment procedure and result of location-dependent object recognition task upon the inactivation of CA1-projecting subicular excitatory neurons. Schematic diagram showing on top describes the object location recognition task. Letters A in the boxes indicate positioning of the objects. In each experiment, mice were handled and habituated to the context prior to a 10-min training. The animals received a single dose i.p. injection of 1.4mg/kg CNO or saline 45 min prior to training. The graph on the left shows the animal total exploration time during the testing session. The graph on the right shows the animal discrimination index in testing. Mice that received CNO show no preference for the moved object in contrast to the saline treated mice. Data are presented as mean ± SE. *** $p < 0.001$ (t-test). (E) Experiment procedure and result of novel object recognition task upon the inactivation of CA1-projecting subicular excitatory neurons. Schematic diagram showing on top describes the object location recognition task. Letters A and B in the boxes indicate distinct objects. In each experiment, mice were handled and habituated to the context prior to a 10-min training. The animals received a single dose i.p. injection of 1.4mg/kg CNO or saline 45 min prior to training. The graph on the left shows the animal total exploration time during the testing session. The graph on the right shows the animal discrimination index in testing. Mice that received CNO show preference for the novel object similar to the saline treated mice. Data are presented as mean ± SE. n.s. not significant (t-test). For more information, see Table 4.1

`

Table 4.1. Training and Testing data for LOR and NOR Experiments

LOR	Training		Testing	
	Saline	CNO	Saline	CNO
Total Time (s)	20.83	20.67	7.73	7.04
SE	1.03	0.99	0.37	0.22
Dis Index	0.51	-0.88	33.63	1.00
SE	2.24	1.04	2.14	0.89

NOR	Training		Testing	
	Saline	CNO	Saline	CNO
Total Time (s)	21.27	21.69	12.48	12.51
SE	1.16	1.72	0.45	1.32
Dis Index	-0.91	1.02	35.98	33.87
SE	2.24	0.72	2.24	4.05

`

REFERENCES

Alexander GM, Rogan SC, Abbas AI, Armbruster BN, Pei Y, Allen JA, Nonneman RJ, Hartmann J, Moy SS, Nicolelis MA, McNamara JO, Roth BL (2009) Remote control of neuronal activity in transgenic mice expressing evolved G protein-coupled receptors. Neuron 63:27-39.

Amaral DG, Dolorfo C, Alvarez-Royo P (1991) Organization of CA1 projections to the subiculum: a PHA-L analysis in the rat. Hippocampus 1:415-435.

Anderson MI, O'Mara SM (2004) Responses of dorsal subicular neurons of rats during object exploration in an extended environment. Exp Brain Res 159:519-529.

Armbruster BN, Li X, Pausch MH, Herlitze S, Roth BL (2007) Evolving the lock to fit the key to create a family of G protein-coupled receptors potently activated by an inert ligand. Proc Natl Acad Sci U S A 104:5163-5168.

Aronov D, Nevers R, Tank DW (2017) Mapping of a non-spatial dimension by the hippocampal-entorhinal circuit. Nature 543:719-722.

Balderas I, Rodriguez-Ortiz CJ, Salgado-Tonda P, Chavez-Hurtado J, McGaugh JL, Bermudez-Rattoni F (2008) The consolidation of object and context recognition memory involve different regions of the temporal lobe. Learn Mem 15:618-624.

Bohm C, Peng Y, Maier N, Winterer J, Poulet JF, Geiger JR, Schmitz D (2015) Functional Diversity of Subicular Principal Cells during Hippocampal Ripples. J Neurosci 35:13608-13618.

Chang EH, Huerta PT (2012) Neurophysiological correlates of object recognition in the dorsal subiculum. Front Behav Neurosci 6:46.

Craig MT, McBain CJ (2015a) Fast gamma oscillations are generated intrinsically in CA1 without the involvement of fast-spiking basket cells. J Neurosci 35:3616-3624.

Craig MT, McBain CJ (2015b) Navigating the circuitry of the brain's GPS system: Future challenges for neurophysiologists. Hippocampus 25:736-743.

Deadwyler SA, Hampson RE (2004) Differential but complementary mnemonic functions of the hippocampus and subiculum. Neuron 42:465-476.

Eichenbaum H, Yonelinas AP, Ranganath C (2007) The medial temporal lobe and recognition memory. Annu Rev Neurosci 30:123-152.

Fried I, MacDonald KA, Wilson CL (1997) Single neuron activity in human hippocampus and amygdala during recognition of faces and objects. Neuron 18:753-765.

Gore BB, Soden ME, Zweifel LS (2013) Manipulating gene expression in projection-specific neuronal populations using combinatorial viral approaches. Curr Protoc Neurosci 4:4 35 31-34 35 20.

Haettig J, Sun Y, Wood MA, Xu X (2013) Cell-type specific inactivation of hippocampal CA1 disrupts location-dependent object recognition in the mouse. Learn Mem 20:139-146.

Hampson RE, Deadwyler SA (2003) Temporal firing characteristics and the strategic role of subicular neurons in short-term memory. Hippocampus 13:529-541.

Igarashi KM, Lu L, Colgin LL, Moser MB, Moser EI (2014b) Coordination of entorhinal-hippocampal ensemble activity during associative learning. Nature 510:143-147.

Jackson J, Amilhon B, Goutagny R, Bott JB, Manseau F, Kortleven C, Bressler SL, Williams S (2014) Reversal of theta rhythm flow through intact hippocampal circuits. Nat Neurosci 17:1362-1370.

`

Jackson J, Goutagny R, Williams S (2011) Fast and slow gamma rhythms are intrinsically and independently generated in the subiculum. J Neurosci 31:12104-12117.
Kim SM, Ganguli S, Frank LM (2012) Spatial information outflow from the hippocampal circuit: distributed spatial coding and phase precession in the subiculum. J Neurosci 32:11539-11558.
Knierim JJ (2006) Neural representations of location outside the hippocampus. Learn Mem 13:405-415.
Krashes MJ, Koda S, Ye C, Rogan SC, Adams AC, Cusher DS, Maratos-Flier E, Roth BL, Lowell BB (2011) Rapid, reversible activation of AgRP neurons drives feeding behavior in mice. J Clin Invest 121:1424-1428.
Lever C, Burton S, Jeewajee A, O'Keefe J, Burgess N (2009) Boundary vector cells in the subiculum of the hippocampal formation. J Neurosci 29:9771-9777.
Martin PD, Ono T (2000) Effects of reward anticipation, reward presentation, and spatial parameters on the firing of single neurons recorded in the subiculum and nucleus accumbens of freely moving rats. Behav Brain Res 116:23-38.
Miao C, Cao Q, Ito HT, Yamahachi H, Witter MP, Moser MB, Moser EI (2015) Hippocampal Remapping after Partial Inactivation of the Medial Entorhinal Cortex. Neuron 88:590-603.
Mumby DG (2001) Perspectives on object-recognition memory following hippocampal damage: lessons from studies in rats. Behav Brain Res 127:159-181.
Naber PA, Witter MP, Lopez da Silva FH (1999) Perirhinal cortex input to the hippocampus in the rat: evidence for parallel pathways, both direct and indirect. A combined physiological and anatomical study. Eur J Neurosci 11:4119-4133.
O'Keefe J (1976) Place units in the hippocampus of the freely moving rat. Exp Neurol 51:78-109.
O'Keefe J, Dostrovsky J (1971) The hippocampus as a spatial map. Preliminary evidence from unit activity in the freely-moving rat. Brain Res 34:171-175.
O'Mara SM, Sanchez-Vives MV, Brotons-Mas JR, O'Hare E (2009) Roles for the subiculum in spatial information processing, memory, motivation and the temporal control of behaviour. Prog Neuropsychopharmacol Biol Psychiatry 33:782-790.
Olson JM, Tongprasearth K, Nitz DA (2017) Subiculum neurons map the current axis of travel. Nat Neurosci 20:170-172.
Piterkin P, Cole E, Cossette MP, Gaskin S, Mumby DG (2008) A limited role for the hippocampus in the modulation of novel-object preference by contextual cues. Learn Mem 15:785-791.
Sakurai Y (2002) Coding of auditory temporal and pitch information by hippocampal individual cells and cell assemblies in the rat. Neuroscience 115:1153-1163.
Schwarz LA, Miyamichi K, Gao XJ, Beier KT, Weissbourd B, DeLoach KE, Ren J, Ibanes S, Malenka RC, Kremer EJ, Luo L (2015) Viral-genetic tracing of the input-output organization of a central noradrenaline circuit. Nature 524:88-92.
Sharp PE (1997) Subicular cells generate similar spatial firing patterns in two geometrically and visually distinctive environments: comparison with hippocampal place cells. Behav Brain Res 85:71-92.
Sharp PE, Green C (1994) Spatial correlates of firing patterns of single cells in the subiculum of the freely moving rat. J Neurosci 14:2339-2356.

`

Stefanko DP, Barrett RM, Ly AR, Reolon GK, Wood MA (2009) Modulation of long-term memory for object recognition via HDAC inhibition. Proc Natl Acad Sci U S A 106:9447-9452.

Sternson SM, Roth BL (2014) Chemogenetic tools to interrogate brain functions. Annu Rev Neurosci 37:387-407.

Sun Y, Ikrar T, Davis MF, Gong N, Zheng X, Luo ZD, Lai C, Mei L, Holmes TC, Gandhi SP, Xu X (2016) Neuregulin-1/ErbB4 Signaling Regulates Visual Cortical Plasticity. Neuron 92:160-173.

Sun Y, Nguyen AQ, Nguyen JP, Le L, Saur D, Choi J, Callaway EM, Xu X (2014) Cell-type-specific circuit connectivity of hippocampal CA1 revealed through Cre-dependent rabies tracing. Cell Rep 7:269-280.

Vogel-Ciernia A, Wood MA (2014) Examining object location and object recognition memory in mice. Curr Protoc Neurosci 69:8 31 31-17.

Wang L, Alachkar A, Sanathara N, Belluzzi JD, Wang Z, Civelli O (2015) A Methionine-Induced Animal Model of Schizophrenia: Face and Predictive Validity. Int J Neuropsychopharmacol 18.

Wess J, Nakajima K, Jain S (2013) Novel designer receptors to probe GPCR signaling and physiology. Trends Pharmacol Sci 34:385-392.

Witter MP (2006) Connections of the subiculum of the rat: topography in relation to columnar and laminar organization. Behav Brain Res 174:251-264.

Witter MP, Naber PA, van Haeften T, Machielsen WC, Rombouts SA, Barkhof F, Scheltens P, Lopes da Silva FH (2000) Cortico-hippocampal communication by way of parallel parahippocampal-subicular pathways. Hippocampus 10:398-410.

Witter MP, Ostendorf RH, Groenewegen HJ (1990) Heterogeneity in the Dorsal Subiculum of the Rat. Distinct Neuronal Zones Project to Different Cortical and Subcortical Targets. Eur J Neurosci 2:718-725.

Xu X, Sun Y, Holmes TC, Lopez AJ (2016) Noncanonical connections between the subiculum and hippocampal CA1. J Comp Neurol 524:3666-3673.

Zheng C, Bieri KW, Hwaun E, Colgin LL (2016) Fast Gamma Rhythms in the Hippocampus Promote Encoding of Novel Object-Place Pairings. eNeuro 3.

`

Chapter 5:

Conclusions and future directions

`

My dissertation includes a series of extensive and coherent studies that I have conducted for our improved understanding of canonical and non-canonical circuit organization and function of hippocampal CA1 and the subiculum. We started to map local and long-range circuit connections to specific excitatory and inhibitory CA1 cell types using monosynaptic rabies tracing and LSPS based circuit mapping (Chapter 1). Our results uncovered distinct connectivity patterns and input strengths between CA1 excitatory and specific inhibitory neurons, and strongly support that PV inhibitory neurons, and SOM inhibitory neurons mediate local feedforward vs feedback inhibition to differentially regulate the activity of local excitatory neurons. In addition, we identified a novel back-projection arising from the subiculum that directly innervates hippocampal CA1 neurons. This subicular back-projection contains both excitatory and inhibitory components that innervate both CA1 pyramidal cells and interneurons. We then continued to map topographic organization of canonical and non-canonical circuit inputs to hippocampal CA1 through monosynaptic rabies tracing (Chapter 2). The results extended our previous finding of non-canonical subiculum inputs to CA1 by showing distal CA1 receives stronger subicular inputs than proximal CA1. Pre- and para-subiculum also project to CA1 directly with proximal CA1 receiving stronger inputs than intermediate CA1 and distal CA1. The subiculum has long been considered as a major output structure of the hippocampal formation and it is well positioned to mediate circuit interactions between the hippocampal and neocortical systems. The concept of bidirectional connections between the subiculum and CA1 derived from our studies requires an update of the general notion that the subiculum is commonly regarded as an output structure of the hippocampal formation and not as an input structure. Feedback connections provide the means for modulating activity by immediately preceding events in contrast to strictly feedforward circuitry. Our discovery suggests previously

`

unconsidered functional roles for direct subicular modulation of hippocampal CA1 circuit activity. The subiculum to CA1 back-projection pathway is direct and local, thus potentially faster and more powerful than distant feedback loops via hippocampal-cortical connections.

To further understand the circuit organization of CA1 projecting subicular neurons, we mapped and compared circuit connections of overall subicular excitatory neurons, inhibitory neurons, and CA1-projecting subicular excitatory neurons (Chapter 3). Compared to overall subicular excitatory neurons, CA1-projecting subicular excitatory neurons receive much less input from CA1 excitatory pyramidal cells, but they receive more input from CA1 GABAergic inhibitory neurons. Additionally, CA1-projecting subicular neurons do not receive input from perirhinal cortex and entorhinal cortex. These data support that CA1-projecting subicular neurons are a unique subset of subicular neurons with their local and distant inputs underlying their direct feedback modulation of hippocampal CA1 activity. In conjunction with behavior analysis and genetically targeted neuronal inactivation, our preliminary behavior experiments validate the functional significance of CA1-projecting subicular neurons (Chapter 4). DREADDS-mediated inactivation of CA1-projecting subicular neurons impairs object location memory performance, indicating that the subicular back-projection is critically implicated in hippocampus-associated spatial memory. Together, my dissertation research has provided novel anatomical and functional insights on cell-type specific neural circuits of hippocampal CA1 and the subiculum.

My studies have focused on the circuit connections and function of the dorsal hippocampus. It has been known that gene expression patterns and the function of the ventral hippocampus are quite different from the dorsal hippocampus (Fanselow and Dong, 2010). Thus, it would be important to study circuit connection differences between the dorsal and ventral

`

hippocampus. Recently improved rabies tracing with the optimized rabies glycoprotein (oG) (Kim et al., 2016) or the CVS-N2c rabies strain (Reardon et al., 2016) should be adopted in future studies for more efficient retrograde labeling of presynaptic inputs. This technical improvement can partly overcome the issue of incomplete presynaptic labeling using our current method (Callaway and Luo, 2015), which can provide a more precise comparison of circuit inputs.

To further understand the functional roles of CA1-projecting subicular neurons, It would be interesting to examine whether CA1-projecting subicular neurons show spatial modulation or task-specific activities (Lever et al., 2009, Olson et al., 2017), and study how CA1-projecting subicular neurons modulate CA1 place cell activities and ensemble representation of the environment. New and emerging technologies such as GCaMP6-mediated calcium imaging via miniaturized fluorescence microscopes in freely behaving animals could help to resolve these questions (Ziv et al., 2013, Cai et al., 2016). Another related question is whether subicular back-projections contribute to large-scale network activities of hippocampus (Jackson et al., 2014, Craig and McBain, 2015). As both excitatory and inhibitory subicular neurons project to CA1, we need to determine how the projections as a whole amplify or dampen the hippocampal network oscillations. Furthermore, it would also be worthwhile to dissect the projections and examine how specific excitatory and inhibitory components differentially contribute to hippocampal network oscillations and ensemble representations, respectively.

Compared to CA1, the subiculum is an under-investigated brain structure. It would also be interesting to look at the circuit organization and function of subicular neurons that project to other cortical and subcortical regions (Kim and Spruston, 2012), including the subicular neurons projecting to EC, PFC, or retrosplenial cortex. This would help us to understand how the

`

information transferred from the hippocampus are distributed and relayed to different brain regions to subserve animal's learning and memory behavior.

As it is closely relevant to our work, I would like to quote Dr. Menno Witter to conclude my dissertation, "Now, it is time to move forward to abandon the classic hierarchical view and to encompass the many parallel and converging routes present in the region and the importance of feedback and feed-forward balance" (Witter et al., 2014).

`

REFERENCES

Cai DJ, Aharoni D, Shuman T, Shobe J, Biane J, Song W, Wei B, Veshkini M, La-Vu M, Lou J, Flores SE, Kim I, Sano Y, Zhou M, Baumgaertel K, Lavi A, Kamata M, Tuszynski M, Mayford M, Golshani P, Silva AJ (2016) A shared neural ensemble links distinct contextual memories encoded close in time. Nature 534:115-118.

Callaway EM, Luo L (2015) Monosynaptic Circuit Tracing with Glycoprotein-Deleted Rabies Viruses. J Neurosci 35:8979-8985.

Craig MT, McBain CJ (2015) Fast gamma oscillations are generated intrinsically in CA1 without the involvement of fast-spiking basket cells. J Neurosci 35:3616-3624.

Fanselow MS, Dong HW (2010) Are the dorsal and ventral hippocampus functionally distinct structures? Neuron 65:7-19.

Jackson J, Amilhon B, Goutagny R, Bott JB, Manseau F, Kortleven C, Bressler SL, Williams S (2014) Reversal of theta rhythm flow through intact hippocampal circuits. Nat Neurosci 17:1362-1370.

Kim EJ, Jacobs MW, Ito-Cole T, Callaway EM (2016) Improved Monosynaptic Neural Circuit Tracing Using Engineered Rabies Virus Glycoproteins. Cell Rep.

Kim Y, Spruston N (2012) Target-specific output patterns are predicted by the distribution of regular-spiking and bursting pyramidal neurons in the subiculum. Hippocampus 22:693-706.

Lever C, Burton S, Jeewajee A, O'Keefe J, Burgess N (2009) Boundary vector cells in the subiculum of the hippocampal formation. J Neurosci 29:9771-9777.

Olson JM, Tongprasearth K, Nitz DA (2017) Subiculum neurons map the current axis of travel. Nat Neurosci 20:170-172.

Reardon TR, Murray AJ, Turi GF, Wirblich C, Croce KR, Schnell MJ, Jessell TM, Losonczy A (2016) Rabies Virus CVS-N2c(DeltaG) Strain Enhances Retrograde Synaptic Transfer and Neuronal Viability. Neuron 89:711-724.

Witter MP, Canto CB, Couey JJ, Koganezawa N, O'Reilly KC (2014) Architecture of spatial circuits in the hippocampal region. Philos Trans R Soc Lond B Biol Sci 369:20120515.

Ziv Y, Burns LD, Cocker ED, Hamel EO, Ghosh KK, Kitch LJ, El Gamal A, Schnitzer MJ (2013) Long-term dynamics of CA1 hippocampal place codes. Nat Neurosci 16:264-266.